Characterization of a ^{4}He Scintillation Detector and its Applications in Nuclear Material Assay

by

Oskar Fick Searfus

A dissertation submitted in partial fulfillment
of the requirements for the degree of
Doctor of Philosophy
(Nuclear Engineering and Radiological Sciences)
in the University of Michigan
2024

Doctoral Committee:

Professor Igor Jovanovic, Chair
Professor Christine Aidala
Dr. Peter Marleau, Sandia National Laboratories
Professor Sara Pozzi

Oskar Fick Searfus
osearfus@umich.edu
ORCID iD: 0000-0001-6203-5346

Dedication

For my Dad

Acknowledgments

I want to first thank my advisor, Professor Igor Jovanovic. The opportunities and successes I had during my time at Michigan were only possible with your encouragement, advice, and insights, which I will always value. I would also like to thank the members of my committee: Professor Sara Pozzi, Professor Christine Aidala, and Dr. Peter Marleau. Pete, thank you for your mentorship these past two years, for supporting and advocating for my research, and for the many, many R&A reviews you've done for me.

The only reason I became interested in radiation detection research, which led me to study at Michigan, was my first internship at Sandia while I was an undergraduate student. For this, I need to thank Dr. Jeffrey Martin for hiring me and being my first mentor, and Dr. Richard Harrison for involving me in some incredible experimental opportunities, giving me the experience I needed to succeed in grad school.

Many others have supported me in this journey, in collaboration and consultation. In particular I want to thank in no particular order: Jordan Carnahan, Jeremy Osborn, Scott Kiff, David Reyna, Melinda Sweany, Heather Reedy, and Eva Uribe, all of Sandia National Laboratories; Jesson Hutchinson and Vlad Henzl, of Los Alamos National Laboratory; Louise Evans, Richard Reed, Karen Hogue, and Bob McElroy, all of Oak Ridge National Laboratories; and Madeline Lockhart, of North Carolina State University.

My time at Michigan would not have been the same without my friends and classmates in NERS, as well as students from other universities I've been privileged to meet. I especially want to thank Lonnie Garrett, who joined ANSG at the same time and waded through the most intense first semester of grad school with me (during COVID, too!), and has been a reliable friend ever since. Thank you to Kris Ogren, who patiently spent many hours helping me take my first steps in ROOT and C++, even while he was very busy writing his thesis. Thanks also to Colton Graham, who subsequently helped me with many silly ROOT mistakes. I want to thank Ethan Klein, who made all of our conferences so much more fun, and who could always commiserate with me about certain bureaucracies. I also want to acknowledge all of the other members of the

ANSG detection group, past and present, whose lively exchanges in our lab meetings have contributed immeasurably to my learning.

Very importantly, I want to thank all of my friends and family for their constant support. To my partner, Anuj, thank you for always having my back and making time for me, even though you've had more than a full plate yourself. You make the bad days good, and you inspire me every day. I would be remiss not to acknowledge my number one canine coworker, Sophie, who has given me such comfort and joy these past four years.

I have been supported by several grants and fellowships, which have financed both my education and my research at Michigan. Thank you to both the Rackham Merit Fellowship and the Nuclear Nonproliferation International Safeguards Fellowship Program, sponsored by the National Nuclear Security Administration (NNSA) Office of International Nuclear Safeguards. Thank you to the NNSA Office of Defense Nuclear Nonproliferation Research and Development, which sponsored the work in Ch. 5, and also provided support under the consortium for Monitoring Technology and Verification for the entirety of this work. Thank you to the Department of Homeland Security Countering Weapons of Mass Destruction Office for their support of the work in Ch. 4 and 6. Sandia National Laboratories is a multimission laboratory managed and operated by National Technology Engineering Solutions of Sandia, LLC, a wholly owned subsidiary of Honeywell International Inc., for the U.S. Department of Energy's National Nuclear Security Administration under contract DE NA0003525.

Table of Contents

List of Figures

List of Tables

Abstract

Helium-4-based scintillation detectors have been developed as a γ-insensitive alternative to organic scintillators for fast neutron detection and spectroscopy. While these detectors hold significant promise for applications in extreme environments where organic scintillators are not suitable, there has been relatively little scholarship on their fundamental characteristics and applications.

The only commercially available ^{4}He-based detector is the Arktis S670. This detector has a unique construction, containing three optically segmented regions, each providing four signal outputs. An algorithm was developed to condense these four outputs into a single data list, showing an improved time resolution compared to a separate analysis of the outputs, and an energy calibration using monoenergetic 2.45 MeV and 14.1 MeV neutrons was demonstrated.

Another experiment was performed to characterize the response of the ^{4}He detector to monoenergetic nuclear recoils up to 9 MeV. The ^{4}He detector was positioned in the center of a semicircular array of organic scintillation detectors operated in coincidence, in conjunction with monoenergetic neutron sources. The measured detector response provides evidence for scintillation linearity and was used to develop an energy resolution function applicable to this energy range, enabling high-fidelity detector simulation for future applications.

Precise knowledge of the temporal output profile of a pulsed neutron generator is beneficial for several neutron active interrogation techniques. Using the ^{4}He detector,

the primary temporal profile of a short-pulsed deuterium-tritium neutron generator was isolated from scattered and induced contaminants by spectral thresholding. This method can be used to continuously monitor the pulse characteristics and quality for various neutron active interrogation techniques.

The production of ^{233}U poses unique challenges for nuclear safeguards, as it is associated with an extreme γ ray environment from ^{232}U contamination, as well as more conservative accountability requirements than for ^{235}U. The ^{4}He detector and an array of ^{3}He detectors were used to demonstrate three advanced neutron signatures of ^{233}U in oxide. These measurements provide a benchmark for future nondestructive assay instrumentation development and demonstrate a set of key neutron signatures to be leveraged for nuclear safeguards in the thorium fuel cycle.

The use of photon active interrogation for the detection of special nuclear material has held significant promise; however, neutrons produced by photonuclear reactions in the accelerator target, collimator, and environment can obscure the fission neutron signal. High-pressure ^{4}He-based scintillation detectors are well-suited to photon active interrogation, as they can measure the fast neutron spectrum, but show little response to gamma rays. A photon active interrogation system utilizing a ^{4}He scintillation detector and a 9 MeV linac-bremsstrahlung X-ray source was experimentally evaluated. It was shown to be capable of detecting photofission neutrons from ^{238}U based on their clear spectral separation from (γ,n) neutrons produced in lead, a common shielding material.

This collection of research serves to deepen the understanding of ^{4}He-based detector characteristics and pioneer some of their promising applications in nuclear safeguards and security. While additional work remains to develop the demonstrated applications into operational systems, this work has significantly broadened the plausible application space for ^{4}He scintillation detectors.

Chapter 1

Neutron Sources and Detection

1.1. Nuclear Energy and Atomic Weapons

A hallmark of the fields of nuclear physics and engineering has always been the staggering pace of discovery and development, particularly in the mid-1900s. The discovery of the neutron by James Chadwick in 1932 [1] was followed by the discovery of neutron-induced nuclear fission by Hahn, Frisch, and Meitner only 6 years later [2]–[4], which was in turn followed by the first operational nuclear weapon 7 years later in the Manhattan Project. Nuclear energy and technology were primary drivers of geopolitical dynamics in the 20^{th} century, and continue to shape the global landscape today. On one hand, civilian nuclear power generation has served as an important and reliable source of low-carbon energy to meet the needs of an increasingly developed world, and the production of medical isotopes has revolutionized cancer treatments and medical imaging. On the other hand, the growth of nuclear weapons programs introduced the first truly existential threat to humanity.

Nuclear energy is the single largest source of carbon-free energy in the world [5]. The worldwide capacity for nuclear energy generation is expected to increase by up to 42% by 2030 and double by 2050 compared to current capacity [6], making nuclear energy a

critical element of global plans to meet international climate goals and curb the worst effects of climate change. While several countries have scaled back or eliminated their nuclear energy portfolios in the aftermath of the Fukushima Daiichi accident in 2011 [7], many others, particularly in the developing world, are scaling up their nuclear capacity as a means to achieve economic prosperity: India, for example, has an ambitious national nuclear power program which aims to be domestically self-sufficient using thorium fuel cycles [8], and is expected to triple its nuclear energy capacity as a share of its total energy production [9].

At the same time, nuclear weapons pose as great a risk as ever to modern civilization. The nuclear arms control treaties of the Cold War era and its immediate aftermath which led many to hope for the possibility of nuclear disarmament have been all but eliminated, with the United States withdrawing from the Intermediate-Range Nuclear Forces (INF) treaty in 2019 and Russia suspending its obligations under the New START treaty in early 2023 [10]. Without any clear path for current nuclear-armed states to disarm, it is critical to prevent additional states from developing nuclear weapons. The primary international framework to prevent nuclear proliferation and ensure that civilian nuclear power programs remain in peaceful use is the Treaty on the Nonproliferation of Nuclear Weapons (NPT), which has been in force since 1970 [11]. This treaty established an international nuclear safeguards regime, in which signatory non-nuclear weapon states must submit their nuclear facilities for independent inspection, carried out by the International Atomic Energy Agency (IAEA). The goal of these inspections is to verify declared nuclear material inventories and facility designs as evidence of signatory states' compliance with the NPT. Furthermore, Additional Protocols (AP) [12] have gone into effect in the majority of signatory states, in which the IAEA is granted unscheduled complimentary access (CA) to declared facilities as well as undeclared facilities, further

deterring nuclear proliferation. Nondestructive assay (NDA) techniques based on the detection of γ rays and neutrons from nuclear materials, performed by inspectors during facility visits, are critical for the IAEA to verify compliance with the NPT in a timely fashion.

1.2. Characteristics of Neutrons

Neutron radiation has fundamentally distinct characteristics from other common forms of nuclear radiation (*i.e.*, α, β, and γ radiation) in that neutrons interact only with the nuclei of atoms, as opposed to the electrons. In effect, due to the minuscule size of nuclei, this means that neutrons can travel a comparatively great distance through matter without interaction. As a result, neutrons are difficult to shield against, and their detection is complex relative to other radiations.

1.2.1. Neutron production mechanisms

Neutrons are emitted in the decay of highly excited nuclei, in which the nuclear excitation energy exceeds the binding energy of the last neutron to the nucleus [13]. These highly excited nuclei may be the products of nuclear fission, fusion, or some other transmutation reaction.

In the case of fission, the vast majority of neutrons are emitted by the fission fragments between 10^{-18} and 10^{-13} s after the fission occurs and are considered "prompt" [14]. A small fraction of fission neutrons, however, are emitted with the β decay of fission fragments in the seconds to minutes following fission and are considered "β-delayed" neutrons.

In nuclear fusion, two light nuclei are fused into a heavier compound nucleus, which

de-excites by the emission of a particle. In the most widely studied fusion reactions, this particle is usually a neutron. Fusion neutrons are commonly produced in neutron generators, which are small linear accelerators in which projectile ions are accelerated and bombard a surface containing the target nucleus. Neutron generators typically utilize either the $^{2}H(^{2}H,n)^{3}He$ or $^{3}H(^{2}H,n)^{4}He$ reactions, and less frequently the $^{7}Li(^{1}H,n)^{7}Be$ reaction [15]. An illustration of the deuterium-tritium (D-T) fusion reaction is shown in Figure 1.1

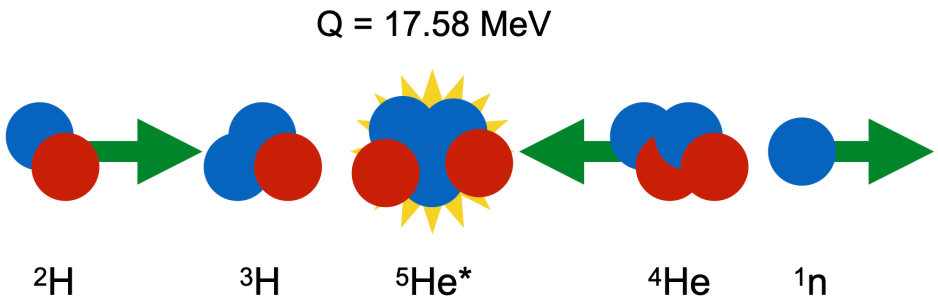

Figure 1.1: Conceptual illustration of the D-T fusion reaction, a common source of neutrons.

Some other important neutron-production mechanisms include (α,n) and (γ,n) reactions. (α,n) reactions occur when an α-emitting radioisotope is mixed or collocated with certain low-Z isotopes, where the high-energy α particle has sufficient kinetic energy to surpass the Coulomb barrier of the target isotope. The α particle is absorbed and an excited compound nucleus forms, which then de-excites by neutron emission. Similarly, (γ,n) reactions take place when a γ ray with energy greater than the neutron separation energy is absorbed by a nucleus, which de-excites by neutron emission. In contrast to (α,n) reactions, (γ,n) reactions can occur in both low- and high-Z materials, as γ rays do not experience the Coulombic repulsion which prevents radioisotope α particles from approaching high-Z nuclei.

Neutrons can also be produced in inverse β-decay reactions, in which an electron antineutrino is absorbed by a proton, which then emits a positron and transforms into a neutron. Notably, this reaction led to the direct detection of the antineutrino [16] and remains the primary mechanism for antineutrino detection.

1.2.2. Fast Neutron Interactions

All neutrons are "born" fast–that is, with high energy. Fast neutrons are typically considered to be those with > 1 keV of kinetic energy, and most neutron sources produce neutrons with an average energy of > 1 MeV. Fast neutrons characteristically have small interaction cross sections and primarily interact via elastic or inelastic scattering on nuclei. In elastic scattering, the neutron transfers a portion of its energy to the nucleus, determined by the scattering angle and target nucleus mass such that kinetic energy and momentum are conserved. The maximum neutron fractional energy loss in a single collision by elastic scattering is

$$\Delta E = 1 - \left(\frac{A-1}{A+1}\right)^2, \tag{1.1}$$

where A is the atomic mass number. As a result, neutrons lose much more energy in collisions with light nuclei, (*e.g.*, up to 100% on ^{1}H) than on heavy nuclei, (*e.g.*, up to 1.7% on ^{238}U).

Conversely, inelastic scattering results in some portion of the neutron kinetic energy being converted to excitation of the target nucleus, which then de-excites by emission of one or more γ rays or by internal conversion.

At sufficiently high energies, fast neutrons can also induce reactions that lead to the emission of nucleons from the target nucleus [17]. The most common of these reactions

are (n,2n), (n,p), and (n,α) reactions [18]. These reactions are typically endothermic, such that there is a minimum neutron energy required for the reaction to proceed.

Notably, some heavy nuclei ($Z \geq 90$) can undergo fission after absorption of a fast neutron. These isotopes are generally referred to as *fissionable* if a fast neutron (<10 MeV) supplies sufficient energy to the compound nucleus to surpass the fission barrier and include ^{232}Th, ^{233}U, ^{235}U, ^{237}Np, ^{238}U, and ^{239}Pu.

1.2.3. Slow Neutrons

After a number of scattering interactions, neutrons eventually slow down and reach thermal equilibrium with their environment and have energy given by the Maxwellian distribution:

$$\phi(E) = \frac{2\pi}{(\pi kT)^{3/2}} \sqrt{\frac{2}{m_n}} E \mathrm{e}^{-\frac{E}{kT}}, \tag{1.2}$$

where k is the Boltzmann constant, T is the absolute temperature, and m_n is the neutron mass.

With a few important exceptions, interactions of *thermal* neutrons are limited to elastic scattering as described above, or by radiative capture, *i.e.*, (n,γ) reactions. In (n,γ) reactions, the neutron is absorbed, and an excited compound nucleus forms, which then de-excites by emitting a γ ray. Since thermal neutrons have little kinetic energy, the excitation energy in the compound nucleus arises from the excess binding energy that the neutron supplies to the nucleus via the strong force. In comparison to fast neutrons, many thermal neutron cross-sections are exceptionally large: ^{113}Cd, for example, has a (n,γ) cross-section of over 10000 barns for thermal neutrons [19]. As a result, thermal neutrons can be more easily shielded than their fast counterparts.

Several isotopes can undergo other reactions and emit charged particles after absorb-

ing thermal neutrons, with large cross sections:

$$^{3}\mathrm{He} \ + \ \mathrm{n}_{th} \ \rightarrow \ ^{1}\mathrm{H} \ + \ ^{3}\mathrm{H} \ + \ 0.764 \text{ MeV} \tag{1.3}$$

$$^{6}\mathrm{Li} \ + \ \mathrm{n}_{th} \ \rightarrow \ ^{4}\mathrm{He} \ + \ ^{3}\mathrm{H} \ + \ 4.78 \text{ MeV} \tag{1.4}$$

$$^{10}\mathrm{B} \ + \ \mathrm{n}_{th} \ \rightarrow \ \begin{cases} ^{4}\mathrm{He} \ + \ ^{7}\mathrm{Li} \ + \ 2.792 \text{ MeV } (6\%) \\ ^{4}\mathrm{He} \ + \ ^{7}\mathrm{Li}^{*} \ + \ 2.310 \text{ MeV } (94\%) \end{cases} \tag{1.5}$$

These reactions are widely utilized for both neutron detection and shielding.

There is also a select subset of the fissionable isotopes that can undergo fission after absorbing a thermal neutron: ^{233}U, ^{235}U, and ^{239}Pu are *fissile* isotopes, and are the most important isotopes both for nuclear energy production and nuclear weapons.

1.3. Nuclear Materials

The term *nuclear material* typically refers to any form of thorium, uranium, or plutonium, and is essentially synonymous with *fissionable* material, *i.e.*, material that can undergo fission after absorption of a fast neutron. In the context of nuclear fuel cycles and nuclear safeguards, nuclear material is usually further classified as either *source* material or *special fissionable* material, also referred to as *special nuclear material* (SNM). Source materials include those materials which, through either enrichment or irradiation, are used to obtain SNM. SNM can be used to construct nuclear weapons, so its detection and verification are tantamount for many applications ranging from arms control to homeland security to international nuclear safeguards.

1.3.1. Highly Enriched Uranium

Uranium occurs naturally in the Earth's crust, which contains three of its isotopes: ^{234}U, ^{235}U, and ^{238}U. The natural abundances and half-lives of these isotopes are shown in Table 1.1. ^{238}U is fissionable, while ^{235}U is the only naturally occurring fissile isotope in the Earth's crust. If by some means the proportion of ^{235}U is increased in some quantity of uranium, it is considered *enriched*. If uranium is enriched above 20%, it is referred to as *highly enriched uranium* (HEU), which is suitable for the production of nuclear weapons and is commonly used in naval propulsion reactors [20]. On the other hand, uranium enriched to less than 20% is *low enriched uranium* (LEU), commonly used for civilian nuclear power and research reactors.

Table 1.1: Natural abundances and half-lives for isotopes of uranium [21]. Abundances are given by weight.

Isotope	^{234}U	^{235}U	^{238}U
Abundance	0.005%	0.720%	99.275%
Half-life (y)	2.46×10^5	7.04×10^8	4.47×10^9

Separation of uranium isotopes is challenging since ^{235}U and ^{238}U have effectively the same chemical properties; nonetheless, several methods have been developed to enrich uranium. The first technique to successfully enrich macroscopic quantities of uranium was the electromagnetic method developed during the Manhattan Project [22]. It was effectively a production-scale cyclotron, dubbed the Calutron. In this method, uranium is ionized and accelerated through some high-voltage potential into a strong magnetic field which deflects the ions, as shown in Figure 1.2. The magnetic field produces the same Lorentz force on both uranium isotopes, but since ^{238}U has a larger mass and

therefore more inertia, it is deflected less than ^{235}U. The effect of this is to produce two ion streams that can be collected separately. While the electromagnetic method has a high separation factor, (*i.e.*, isotopes can be fully separated in a single pass), this method is extremely energy intensive and difficult to scale to large production rates.

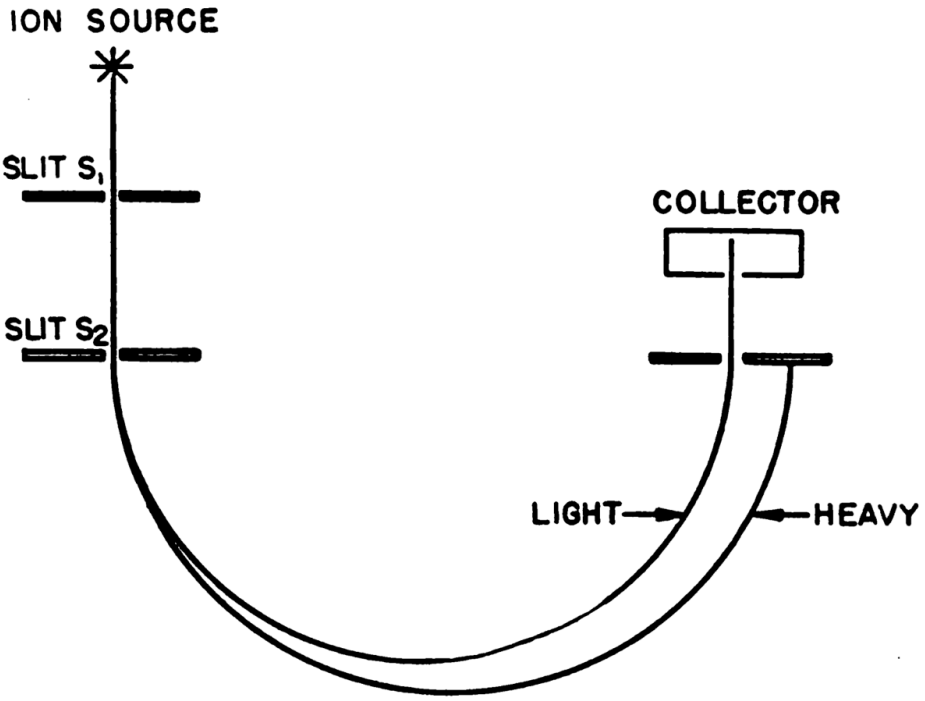

Figure 1.2: Conceptual illustration of the Calutron isotope separator, from Ref. [22].

The next technique developed was gaseous diffusion, which remained the dominant isotope separation technique for the majority of the 20th century. In gaseous diffusion, high-pressure UF_6 gas is passed across a porous membrane. Since $^{235}UF_6$ molecules are lighter, at a given temperature their speed is greater than $^{238}UF_6$, and therefore they collide with the membrane more frequently. As a result, $^{235}UF_6$ is preferentially passed through the membrane. While gaseous diffusion is relatively easy to scale, it is also extremely energy intensive: The Paducah Gaseous Diffusion Plant consumed

approximately 3000 MW of electricity at its peak, enough to power Washington, DC [23].

Currently, the widest-spread technology for uranium enrichment is the gas centrifuge. Simply put, UF_6 gas is injected into cylinders that spin at a high rate, pushing the heavier $^{238}UF_6$ to the outer radius while the lighter $^{235}UF_6$ moves to the center. The gas centrifuge uses less than 10% of the energy for the same separative work when compared to gaseous diffusion [24].

For both the gaseous diffusion and the centrifuge technology, the maximum differential enrichment that can be achieved by a single node, (*i.e.*, a single membrane or centrifuge) is quite small compared to the enrichment desired for either civilian power production or weapons production. As a result, these enrichment facilities usually take the form of large cascades, consisting of thousands of nodes.

1.3.2. Plutonium

Unlike uranium, plutonium isotopes do not naturally occur in any appreciable quantity in the Earth's crust and must be artificially produced via nuclear reactions. This is usually done in nuclear reactors by the irradiation of ^{238}U with neutrons:

$$^{238}\mathrm{U} + \mathrm{n} \rightarrow {}^{239}\mathrm{U} \xrightarrow[23\ \mathrm{min}]{\beta^-} {}^{239}\mathrm{Np} \xrightarrow[2.4\ \mathrm{day}]{\beta^-} {}^{239}\mathrm{Pu}. \tag{1.6}$$

Since thermal neutron reactors can operate with natural uranium fuel if deuterium or graphite are used as the moderator, it is possible to produce plutonium without any uranium enrichment capability. Once plutonium is produced, it is relatively simple to chemically separate from the uranium feed material when compared to the process of uranium enrichment. However, if plutonium is left in the reactor for a significant period of time, the desired ^{239}Pu will continue to absorb neutrons, leading either to fission or to

the production of higher Pu isotopes. The build-in of ^{240}Pu is of special importance, as this isotope has a significant rate of spontaneous fission and dramatically increases the neutron background of the resultant plutonium. While this is of minimal consequence for plutonium intended for use in a reactor, plutonium containing high concentrations of ^{240}Pu is unsuitable for use in nuclear weapons: the probability of a predetonation or "fizzle" before the fissile material fully assembles is directly related to the neutron background. Consequently, reactors used primarily for weapons-grade plutonium (WGPu) production are designed to allow for frequent or continuous refueling, such that the plutonium can be removed before ^{240}Pu builds in.

1.3.3. Uranium-233

Similarly to ^{239}Pu, ^{233}U is not naturally occurring on Earth, and is produced via neutron absorption on ^{232}Th in nuclear reactors:

$$^{232}\mathrm{Th} + \mathrm{n} \rightarrow {}^{233}\mathrm{Th} \xrightarrow[22\ \mathrm{min}]{\beta^-} {}^{233}\mathrm{Pa} \xrightarrow[27\ \mathrm{day}]{\beta^-} {}^{233}\mathrm{U}. \tag{1.7}$$

^{233}U can also be chemically separated from thorium feed relatively easily. Like plutonium, higher uranium isotopes can build in with prolonged irradiation; however, neither ^{234}U nor ^{235}U are associated with increased neutron background and do not fundamentally hinder the weaponization potential of the resultant ^{233}U. While neutron backgrounds are not a concern, trace quantities of ^{232}U can accumulate from (n,2n) reactions on ^{232}Th, ^{233}Pa, and ^{233}U. ^{232}U has a half-life of only 68.9 years and serially decays to ^{208}Tl, which emits a 2.6 MeV γ ray. This γ ray is very difficult to shield due to its high energy and introduces a major biological hazard to most ^{233}U-bearing materials.

1.4. Neutron Detection

Many approaches to neutron detection have been developed for broad applications from reactor instrumentation and oil well logging to nuclear security and safeguards, and all share a common principle: the neutron is "converted" into a charged particle, whose ionization, scintillation, or Cherenkov emission is measured. This can be accomplished with a wide range of detector media by either neutron absorption or scattering.

1.4.1. Slow neutron detection

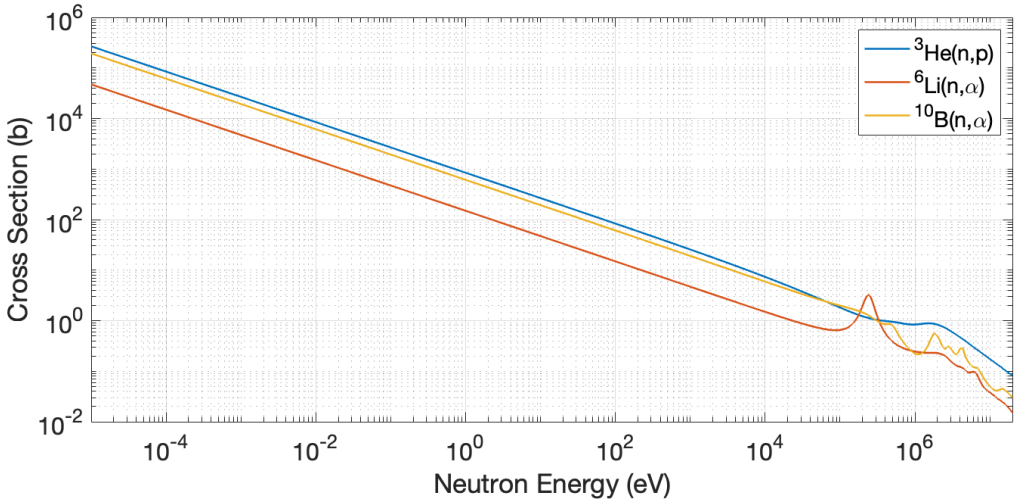

Figure 1.3: Neutron cross sections for the ^{3}He(n,p), ^{6}Li(n,α), and ^{10}B(n,α) reactions [19].

In the vast majority of thermal neutron detectors, ^{3}He, ^{6}Li, or ^{10}B are included in the detector active volume, utilizing the reactions in Eqs. (1.3–1.5), whose cross-sections are compared in Figure 1.3. These reactions are desirable because they produce heavy charged particles with high energy, creating an unambiguous signal that can be discriminated from γ rays, especially in gaseous detectors. The most common thermal

neutron detector is the ^{3}He proportional counter [25]. These detectors have a number of advantages: helium is a good proportional gas and is environmentally benign, the detectors can be pressurized up to 10 atm or higher to increase sensitivity [26], and ^{3}He has the largest neutron absorption cross section among the candidate isotopes. On the other hand, ^{3}He is difficult to obtain, as it is a minuscule fraction of naturally occurring helium, and most of it is derived from the decay of ^{3}H in nuclear weapons stockpiles.

Boron is utilized in BF_3 proportional counters, which are very similar in design to ^{3}He detectors. However, BF_3 tubes are often considered a second choice to ^{3}He tubes since BF_3 is a toxic gas. The BF_3 performs well as a proportional gas only up to about 1 atm, and the ^{10}B thermal neutron absorption cross-section is 28% smaller than that of ^{3}He, therefore ^{3}He detectors typically have superior intrinsic efficiency. Furthermore, BF_3 detectors typically have a shorter operational lifetime, as dissociation of BF_3 molecules can contaminate the anode and cathode [27]. Many of these drawbacks are mitigated in boron-lined proportional counters, in which a thin layer of boron is deposited upon the inner surface of the tube, and an ordinary proportional gas is utilized. However, since the neutron absorption reaction occurs in a solid layer, only the energy of a reaction product that escapes the layer can be deposited in the proportional gas. This effect manifests in the energy deposition spectrum as the sum of two quasi-rectangular continua, from 0 to the maximum particle energy [28]–[30]. Since a portion of this spectrum at low energy overlaps with the γ-ray response in gaseous detectors, a portion of the neutron sensitivity typically must be discarded in pulse-height discrimination of γ rays.

Lithium does not have any stable gaseous compounds that could be used as a proportional gas, so detectors utilizing the ^{6}Li(n,α) reaction are limited to either liquid or solid phase. Most commonly, ^{6}Li is incorporated into a scintillator, which emits light in response to the reaction products depositing their energy. While the energy

released in this reaction, 4.78 MeV, is large compared to most γ-ray energies, scintillation detectors do not have the same intrinsic γ-ray rejection capabilities as their gaseous counterparts: typically, scintillator dimensions are larger than the range of high-energy electrons which may be produced in γ-ray interactions, so it is possible for γ rays to deposit their full energy. ^{6}LiI(Eu) is the most common scintillator for thermal neutron detection, with similar scintillation characteristics to NaI(Tl) albeit with poorer energy resolution [31]. A number of other ^{6}Li-bearing scintillators have been developed, such as doped organics [32] and glass scintillators [33], the latter often taking the form of scintillating fibers [34].

1.4.2. Fast neutron detection

The detection of fast neutrons is characteristically more complex than thermal neutron detection, as fast neutrons have smaller interaction cross-sections and experience a greater variety of interaction mechanisms.

The simplest means to detect fast neutrons is to slow down, or moderate, the neutrons to low energy such that they can be detected using one of the methods described in the previous section. High-density polyethylene (HDPE) is the most common neutron moderator for detector applications, while water and paraffin wax are used less frequently. These materials share the property of high hydrogen density, as ^{1}H is the nuclide to which a neutron can transfer its entire energy in a single collision and has an acceptable cross-section. While the two-step process of moderating a fast neutron followed by the detection of the subsequent thermal neutron is effective and can yield high efficiencies, much of the temporal and energy information contained in the initial fast neutron is lost: the process of neutron moderation and diffusion toward the detector

can take on the order of 10 to 100 µs [35], and the neutron's kinetic energy is deposited in the moderator where it cannot be directly measured.

One approach to reconstructing the fast neutron spectrum while using thermal neutron detectors is to compare the response of identical detectors within moderating spheres of various radii [36]. The principle of this approach is there is a distinct optimal moderator thickness for a given neutron energy; generally, higher-energy neutrons require a larger moderator volume to be efficiently moderated, however, with too much moderator, the neutrons are scattered away from the detector or otherwise captured parasitically outside the detector. So, the detector response from each moderator radius can inform the relative contribution of a different portion of the neutron spectrum to the overall count rate. This is characteristically an integrating measurement, as it is not possible to extract information on the energy of any particular neutron, but rather the neutron spectrum in aggregate.

Another method to measure the neutron spectrum is to use one of the neutron absorption reactions in Eqs. (1.3–1.5) and measure the energy deposited in excess of the reaction Q-value, as this is equivalent to the incident neutron energy. As shown in Figure 1.3, the cross-sections for these reactions are several orders of magnitude lower for fast neutrons than for thermal neutrons, so detecting fast neutrons directly in this way typically has much poorer efficiency than if the neutrons are moderated before detection. The preferred reaction among these for this method is the ^{3}He(n,p) reaction, as it has the largest cross-section for MeV-scale neutrons and the lowest reaction Q-value. Analysis of the ^{3}He detector spectrum in response to fast neutrons is often complex, as there are components related to the far more probable capture of slow neutrons and elastic scattering of fast neutrons in addition to the desired capture of incident fast neutrons [37].

At sufficiently high energies, fast neutrons can also be directly measured via elastic scattering on some light nuclei, typically ^{1}H, ^{2}H, or ^{4}He. The most common application of this nuclear recoil-based approach is the use of organic scintillators to measure high-energy recoil protons that result from fast neutron scattering on hydrogen. In organic scintillators, information on the neutron energy is preserved, as the magnitude of the scintillation pulse is related to the proton's recoil energy. The neutron's time signature is also preserved, as the neutron is directly measured such that there is no detection delay due to moderation, and organic scintillators have exceptionally short decay constants typically on the order of ns. Because organic scintillators most commonly take the form of a crystal, plastic, glass, or liquid, the relatively small cross-section for fast neutron scattering is compensated by high density when compared to gaseous detectors, and reasonably high detection efficiency can be achieved [38].

Condensed matter detectors have a significantly higher sensitivity to γ rays than their gaseous counterparts, thus it is of critical importance to discriminate γ rays from recoil protons in these detectors. Organic scintillators often have the capability for pulse-shape discrimination (PSD), in which the fraction of the scintillation light in the pulse tail can determine whether a scintillation event is due to a γ ray or recoil proton. This distinction is possible due to the delayed fluorescence phenomenon, as long-lived triplet states diffuse and can recombine to form a singlet state, which subsequently fluoresces [39]. Protons have a higher stopping power than electrons such that their track density and therefore triplet state density is much higher, which leads to a relative increase in the delayed fluorescence phenomenon for protons. The delayed fluorescence process has a characteristically longer decay compared to prompt fluorescence, so typically the ratio of light emitted in the tail of the pulse compared to the pulse as a whole is used as a metric for PSD. The prominence of delayed fluorescence varies significantly for different

organic scintillator materials, leading to a hierarchy of PSD performance, with crystals like *trans*-stilbene and liquid scintillators performing better than plastic scintillators [40]. With the widespread availability of waveform digitizers, PSD is now typically performed by digital waveform analysis, in which different time regions of the scintillation pulse are separately integrated and compared [41].

The applications of organic scintillators are numerous and diverse. Precise measurements of fast neutron spectra have been routinely performed using organic scintillators and the time-of-flight (TOF) technique [42]–[44], the results of which can be used to develop a detector response matrix for deconvolution of measured proton recoil spectra and reconstruction of the incident neutron spectrum without TOF [45], [46]. Due to the fast timing characteristic of organic scintillators, TOF measurements have also been applied to the development of neutron scatter cameras, in which the measured recoil proton energy is measured in one organic scintillator cell and the exiting neutron energy is estimated by its TOF to determine the neutron's angle of incidence [47]–[51].

Neutron absorption agents such as ^{6}Li and ^{10}B are often added to organic scintillator matrices to construct a *capture-gated neutron spectrometer* [52]–[55]. If a neutron loses all of its energy via elastic scattering in the detector, it will diffuse and may be captured at a delay after the initial recoil scintillation pulse. In requiring that proton recoil events be followed in a short coincidence window by a capture event, neutrons that only deposit a fraction of their energy in the detector can be discriminated to improve the neutron spectroscopy capability of the detector [56], [57].

Several organic scintillators have been developed in which the ordinary ^{1}H is replaced with deuterium, ^{2}H [58]–[61]. While the maximum energy transfer from a neutron to a deuteron is lower than for ^{1}H, these detectors have some unique features that make them preferable over ordinary organic scintillators for some applications. Since ^{2}H is heavier

than ^{1}H, its stopping power is higher, such that its track has higher density, leading to improved PSD, even though this also leads to lower light output [62]. Furthermore, while ^{1}H has an isotropic scattering cross-section at most fast neutron energies which leads to a quasi-rectangular spectral response to monoenergetic neutrons, ^{2}H has a highly anisotropic response such that clear peaks form at the maximum energy deposition. This effect improves the spectral unfolding performance, so deuterated detectors are often preferred for this application [63].

Neutron detection in organic scintillators faces a major limitation when the γ-ray exposure rate is high. Although PSD typically performs well at low to moderate γ ray rates, its performance degrades as the incidence of pulse pile-up increases. While pile-up can degrade the performance of any radiation detector, it has a particularly strong impact on PSD since the background discrimination is based on the quality of the pulse tail. In a piled-up pulse, the excess amplitude in the first pulse tail due to the second pulse manifests as the misclassification of γ-ray pulses as neutrons. The effect of pulse pile-up can be mitigated by the use of γ-ray shielding [64], or by relatively complex pulse-shape analysis algorithms [65], [66].

1.5. Useful Neutron Signatures for Nuclear Nonproliferation and Security

All SNM isotopes are radioactive and thus all emit some form of radiation spontaneously. For nuclear material nondestructive assay (NDA), it is often preferable to measure the γ-ray spectra of these isotopes, which are readily measurable with inorganic scintillators and high-purity germanium (HPGe) detectors. For example, uranium enrichment can

be measured by taking the ratio of the 185.7-keV γ ray associated with ^{235}U to the 1001-keV γ ray associated with the decay of ^{238}U (with the assumption of equilibrium with its daughter ^{234m}Pa) [67]. However, γ-based NDA methods are very sensitive to the validity of significant assumptions on the material composition, thickness, shielding, and backgrounds. Furthermore, certain shielding and background conditions preclude the use of γ-based methods altogether. In these cases, neutron signatures can be used to perform NDA on nuclear materials. All nuclear material nuclides are also associated with neutron signatures, which can be emitted passively or as the result of induced fission. Neutrons are generally much more penetrating than γ rays, so are less susceptible to the effects of external and self-shielding. A summary of the passive γ-ray and neutron emissions from select uranium and plutonium isotopes is shown in Table 1.2.

Table 1.2: Summary of primary passive signatures respective activities of selected uranium and plutonium isotopes [68]. $A_{(\alpha,n)}$ is given for dioxides, (*i.e.*, UO_2, PuO_2)

		($s^{-1}g^{-1}$)		
Isotope	Principal E_γ (keV)	A_γ	$A_{n,\,SF}$	$A_{(\alpha,n)}$
^{233}U	317.2	8.3×10^4	$< 4 \times 10^{-4}$	4.7
^{234}U	120.9	5.4×10^5	7.6×10^{-3}	3.0
^{235}U	185.7	4.3×10^4	1.1×10^{-5}	7.2×10^{-4}
^{238}U	1001	75	1.4×10^{-2}	8.5×10^{-5}
^{239}Pu	413.7	3.5×10^4	2.3×10^{-2}	42
^{240}Pu	642.5	1.1×10^3	9.9×10^2	1.5×10^2

1.5.1. Total Neutron Counting

The simplest form of neutron-based NDA is total neutron counting. Moderated thermal neutron detectors are typically used for this measurement. Total neutron counting is often best applied in scenarios where sensitivity to very small or well-shielded neutron sources is needed, such as in portal monitors [69] or for measurement of plutonium hold-up in fuel cycle facilities [70]. While these detectors can determine the presence of neutrons, very little additional quantitative information can be gained on the neutron source.

1.5.2. Neutron Multiplicity

A primary signature of fission, either spontaneous or induced, is the multiplicity of neutrons that are emitted effectively instantaneously. Neutrons emitted in the same fission event are correlated in time, distinguishing them from (α,n) and active interrogation neutrons, which are emitted as single neutrons and uncorrelated in time [71]. The most common detector systems to measure neutron multiplicity are called *well counters*, which are large drums whose walls contain concentric rings of ^{3}He detectors embedded in HDPE. This geometry is desirable, as nuclear material placed in the center of the well has nearly 4π solid angle coverage by the detectors. The *active well coincidence counter* (AWCC) is one such well counter in which two americium-lithium (AmLi) (α,n) neutron sources are placed in the end caps of the well to induce fission in the object being measured [72]. The overall detection rate of neutrons from induced fission in the detectors is usually much smaller than the rate due to the AmLi sources themselves, so it is necessary to use the rate of multiplets (primarily doubles and triples, *i.e.*, two or three neutrons detected in a coincidence gate) to achieve a favorable signal-to-noise

ratio (SNR). The AWCC is the most common neutron-based NDA method for nuclear safeguards and is primarily employed for the measurement of uranium, whereas passive coincidence counting is used more frequently for the measurement of plutonium.

In multiplicity counters based on neutron moderation and absorption, the time from neutron emission to detection takes the form of an exponential distribution with a significant mean or "die-away time" on the order of 50 µs. As a result, a large coincidence gate must be used. The magnitude of the uncorrelated background which must be subtracted from the signal is approximately proportional to the width of this gate, so a system with a smaller die-away time is highly desirable. Fast neutron multiplicity counters are under development for this purpose based on organic scintillators, as these detectors have negligible intrinsic die-away time, and the coincidence gate width can be set based on the neutron TOF, which is typically less than 20 ns, representing a three-order of magnitude reduction in the uncorrelated background [73]. Major challenges in the deployment of these systems arise due to pulse pile-up degradation of PSD as previously discussed and in the background induced by neutron *cross-talk*, in which a neutron scatters and is detected in multiple detectors [74].

1.5.3. Neutron Spectra

Fission neutrons also have a distinct energy spectrum from other common sources of neutrons. Fast neutron spectroscopy based on organic scintillators has been demonstrated for discrimination of spontaneous fission and (α,n) neutrons in plutonium samples [75] and to detect induced-fission neutrons above the spectral end point of a D-D neutron generator [76].

Neutron resonance transmission analysis (NRTA) is a powerful technique that can

measure the transmission of a white (*i.e.*, broad and structure-free) epithermal neutron source through an item of interest to determine its isotopic composition. SNM isotopes have unique neutron cross-section resonance structures in the epithermal (1–100 eV) region, such that a neutron's transmission through the object has a strong dependence on its energy. The transmitted neutron spectrum is measured via TOF, usually with a ^{6}Li scintillator. NRTA has been demonstrated for the detection of depleted uranium [77] and for the detection of plutonium in spent nuclear fuel [78]. Since resonance cross-sections are often extremely large, NRTA methods are insensitive to the areal density of thick objects (*i.e.*, thickness in excess of several mean free paths), and are better suited to thin targets.

1.5.4. Differential Die-Away

If a pulsed neutron generator is used to induce fission in nuclear material, it is possible to detect high-energy fission neutrons even after the generator is turned off. In many cases, this signal is primarily driven by thermal neutrons, which can linger in the environment for µs to ms [79] and diffuse back to the fissile material to induce fission. If fast neutron detectors are used, this measurement of fission neutrons emitted after the pulse exhibits excellent SNR [80].

In multiplying fissile assemblies, the shape of the resulting neutron detection time profile after the pulse can be used to calculate the degree of subcritical multiplication [81], which is an important parameter for criticality safety and emergency response applications.

1.5.5. Delayed Neutron Emission

A subset of fission fragments called *delayed neutron precursors* emit neutrons in their radioactive decay, with half-lives ranging from seconds to minutes [82]. These β-delayed neutrons are important for reactor control but also offer unique signatures of nuclear material isotopes under active interrogation. Each fissionable isotope has a different precursor yield distribution, such that their overall β-delayed neutron build-up and decay time profiles are unique. These build-up and decay time profiles have been demonstrated for the measurement of uranium enrichment [83], [84]. β-delayed neutron time profile analysis is a calibration-free technique and resilient to shielding [85], making it an attractive alternative to γ-based methods particularly when shielding conditions and material composition are unknown.

1.6. ^{4}He for Fast Neutron Detection

In recent years, fast neutron detectors based on elastic scattering on ^{4}He have developed. From Eq. (1.1), neutrons can transfer up to 64% of their kinetic energy to a ^{4}He nucleus in a single collision, which is lower than but still comparable to energy transfer on ^{1}H or ^{2}H. Unlike ^{3}He, ^{4}He represents the vast majority of naturally-occurring helium and is relatively abundant and inexpensive. The first investigations of ^{4}He as a fast neutron detection medium were made in proportional counters [86], [87]. However, ion transport in proportional counters limits the possible operating pressure of these systems, and ^{4}He-based proportional counters consequently are limited to relatively poor efficiency.

At high pressures, helium also scintillates in response to charged particle interactions [88], [89]. The scintillation properties of helium remain useful up to very high pressures, such that these detectors can have much larger neutron detection efficiencies

than their proportional detector counterparts. High-pressure ^{4}He-based scintillation detectors are commercially available from Arktis Radiation Detectors Ltd. The original Arktis ^{4}He detector was pressurized to 150 bar in a cylindrical tube, with the scintillation light read out by two photomultiplier tubes (PMT), one on each end [90], [91]. The scintillation response of this detector has been previously characterized to some extent [92], and several of its applications to nuclear security and safeguards have been demonstrated [90], [93]. The current iteration of their ^{4}He detector is pressurized to 190 bar, with the scintillation light read out by an array of silicon photomultipliers (SiPM) along the axis of the tube [94].

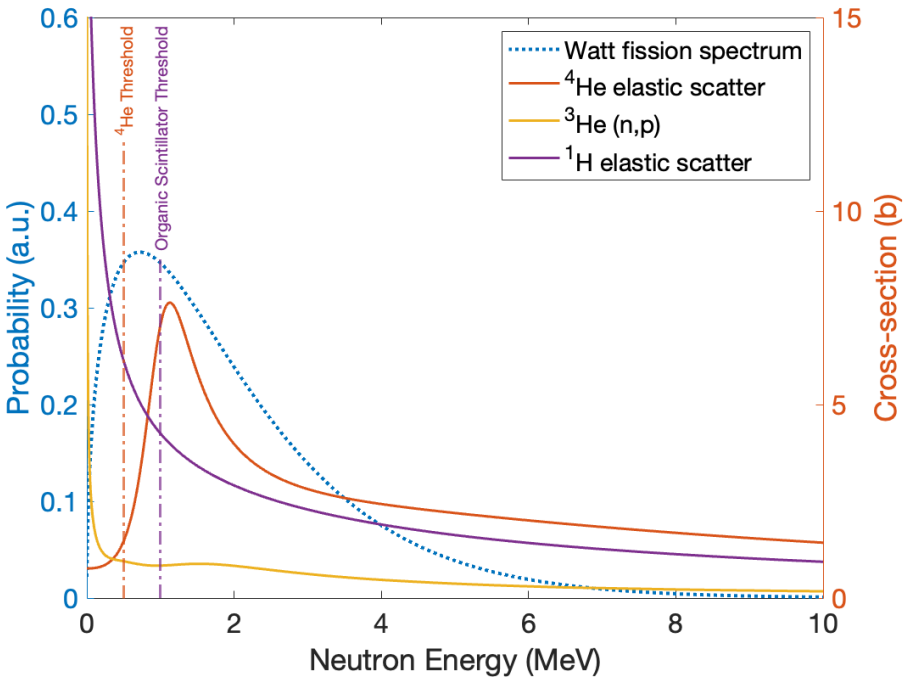

Figure 1.4: Comparison of ^{4}He and ^{1}H elastic scattering and ^{3}He(n,p) cross-sections with the Watt fission spectrum [19].

It is useful to compare the properties of ^{4}He scintillation detectors to those of organic scintillators. While the atom density of ^{4}He in these detectors is lower than that of

^{1}H in organic scintillators, the ^{4}He elastic scattering cross-section is significantly larger than that of ^{1}H above about 800 keV. Furthermore, organic scintillators are typically only capable of efficient PSD for recoil protons above 1 MeV, whereas ^{4}He scintillators can efficiently discriminate γ rays with a 300 keV recoil energy threshold, making them sensitive to a much larger portion of the fission neutron spectrum, as shown in Figure 1.4. Since ^{4}He detectors are gaseous, γ rays can be discriminated based on energy deposition rather than pulse shape: γ rays have a negligible probability of interaction with ^{4}He, and electrons generated from γ-ray interactions, many of which occur in the detector wall, typically have a range much larger than the detector dimensions, and consequently only deposit a fraction of their energy in the gas. γ-ray discrimination based on pulse height can be performed with very simple traditional electronics, so these detectors can be operated with a smaller computational footprint than organic scintillator systems for neutron detection. Due to their intrinsic decreased sensitivity to γ rays, ^{4}He-based scintillation detectors may be most advantageous over organic scintillators in applications that involve extreme γ-ray environments. Specifically, ^{4}He scintillators have been investigated for measurement of spent nuclear fuel [95] and in photon active interrogation [96].

Chapter 2

Digital Pulse Analysis for Fast Neutron Recoil Spectroscopy with a ^{4}He Scintillation Detector

This chapter is adapted from the 2023 publication in *Nuclear Instruments and Methods in Physics Research A* with the same name, by O. Searfus, K. Ogren, and I. Jovanovic [97].

2.1. Introduction

The detection of neutrons is essential for many nuclear nonproliferation and safeguards applications, as most sources of neutrons, spontaneous or induced, are associated with nuclear materials or the nuclear fuel cycle [98], [99]. Measurement of the neutron energy spectrum can facilitate discrimination of fission from non-fission sources of neutrons [46], [63], [92]. Pulse shape discrimination-capable organic scintillators are the most widely-used class of detectors for fast-neutron spectroscopy. However, they are subject to multiple drawbacks and constraints, including high sensitivity to gamma rays, nonlinearity of detector response with respect to nuclear recoil energy, and contamination of the proton recoil spectrum by gamma rays at lower energies and gamma-ray pile-up at higher energies [65]. ^{4}He-based scintillation detectors offer an alternative means of fast

neutron detection and spectroscopy, with a different set of response characteristics that may be favorable over the organic scintillator technology in certain settings.

In ^{4}He-based fast neutron detection, neutrons undergo elastic scattering on the ^{4}He nucleus, and the stopping of recoiling alpha particle produces the ionization signal. Due to the scattering kinematics, a neutron can deposit up to 64% of its kinetic energy in a single scatter on ^{4}He. The total scattering cross-section of ^{4}He is greater than that of ^{1}H for fast neutrons [19], as seen in Figure 2.1, but unlike ^{1}H, the elastic scattering cross-section of ^{4}He is highly anisotropic [86]. Furthermore, depending on their pressure and dimensions, these detectors may exhibit the "wall effect", where the recoil alpha particle can reach the detector wall before stopping, as the range of alpha particles is typically significant compared to the dimensions of a ^{4}He-based detector [100]. While these two effects complicate the detector response to fast neutrons, they are counterbalanced by the benefit provided by the low gamma-ray response. ^{4}He is a low-Z element that has low probability of gamma-ray interaction. Consequently, gamma-rays tend to interact with the wall of the detector, and in some cases the resultant high-energy electron escapes into the gas. Even in this scenario, the stopping power of high-energy electrons in ^{4}He gas is low enough such that the electron can only deposit a small fraction of its energy before being reabsorbed in the wall. As a result, gamma rays can usually be rejected with a simple energy threshold [91].

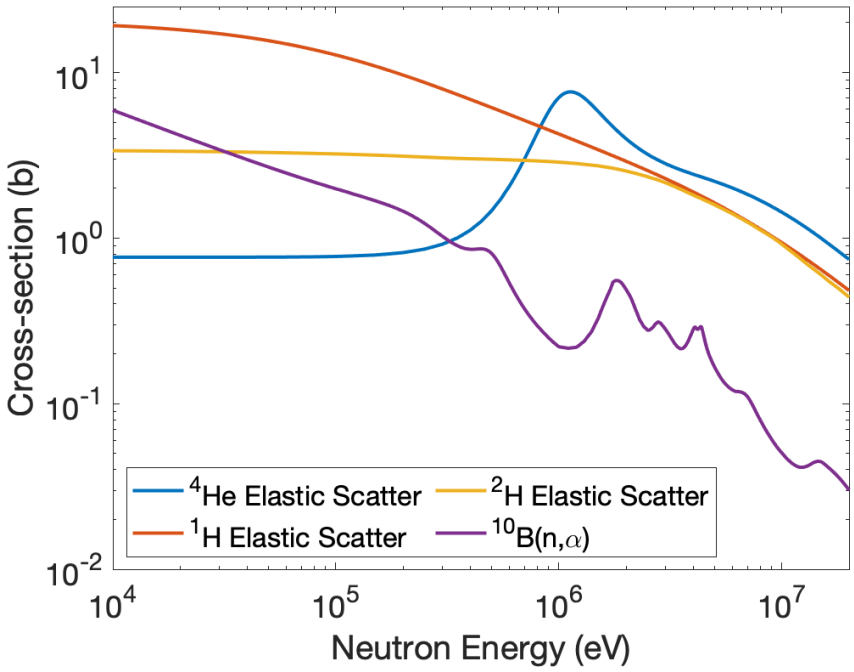

Figure 2.1: Neutron cross-sections for various fast neutron detection media over the typical energy range of neutrons emitted in fission [19]

At high pressure, ^{4}He scintillates in response to radiation-induced ionization [88]. The scintillation process occurs over a relatively short time scale, on the order of µs [91], which is considerably shorter than the charge collection in proportional counters and ionization chambers (on the order of $10 - 100$ µs [98]). Furthermore, higher pressure corresponds to higher ^{4}He density and therefore greater efficiency for neutrons than lower-pressure proportional counters. The gas pressure and active volume dimensions can still be chosen to strike a favorable balance between the gamma-ray response and neutron efficiency. The scintillation light can be measured using photomultiplier tubes (PMT) or silicon photomultipliers (SiPM).

The linearity of the scintillation signal produced in high-pressure ^{4}He at low recoil energies, from 83 to 626 keV, has been demonstrated [101]. A scintillation light out-

put function was proposed [92] for the spectral range of 0.25–4.5 MeV in the form of a power function, with the most pronounced deviation from linearity at low energies, below 1 MeV. The disagreement between these characterizations may be due to the differences in the method by which the quasi-monoenergetic experimental data points were obtained: Ref. [101] utilizes a monoenergetic (2.45-MeV) neutron source in conjunction with organic scintillation backing detectors to restrict the neutron scattering angle and obtain spectral peaks, while Ref. [92] analyzes the edges of recoil continua corresponding to quasi-monoenergetic neutron energies, gated by time-of-flight (TOF). Since the ^{4}He elastic scattering cross-section is anisotropic and its angular distribution varies with energy [86], the shape of the recoil continuum edge manifests differently for different incident neutron energies, and a consistent adjudication of the edge location is challenging. Furthermore, the quasi-monoenergetic neutron spectra obtained in Ref. [92] span 0.5 MeV each. Consequently, the restricted neutron scattering angle approach is likely to be more physically accurate, as it relies on a more plausibly monoenergetic source, yielding spectral peaks. While both of these approaches help characterize the scintillation characteristics of ^{4}He , neither proposes a method of recoil energy calibration that is expedient in the laboratory or field setting, and both are limited in their dynamic range.

Helium-4 fast neutron detectors are commercially available from Arktis Radiation Detectors Ltd. The detector described in this work is the S670 model, which contains only natural helium pressurized to approximately 180 bars, with the scintillation light read out with an array of SiPMs [94]. The detector is optically partitioned into three segments, with the SiPMs in each segment biased at 30.5 V. The signals produced by the SiPMs in each segment are internally amplified differently such that each segment has a different intrinsic gain (low-, medium-, and high-gain). Inside each segment are eight

SiPMs, which are paired and read out as four independent channels. Since these four channels are immersed in the same optical volume, it is likely that multiple channels will observe the same scintillation event, as shown in Figure 2.2. This can lead to double counting of neutron events and poor time and energy resolution if the channels within a segment are analyzed independently. The standard commercial version of the S670 detector only provides a single time-over-threshold output for each segment, which in prior work was shown not to be well-suited for neutron spectroscopy applications [96]. The detector discussed in this work has been modified to permit direct access to each SiPM channel, so that all waveforms can be digitized and analyzed. In this work, we develop a method to merge data from all available SiPM channels within a single segment to improve the detector time and energy resolution, compared to when each SiPM channel is analyzed individually. Furthermore, we report for the first time the response of high-pressure ^{4}He detectors to 14.1-MeV neutrons, propose a simple method for calibration of ^{4}He-based detectors without the need for backing detectors or TOF analysis, and demonstrate the linearity of ^{4}He scintillation over a broader dynamic range than has been previously reported, from 1.57 to 9.02 MeV recoil energy.

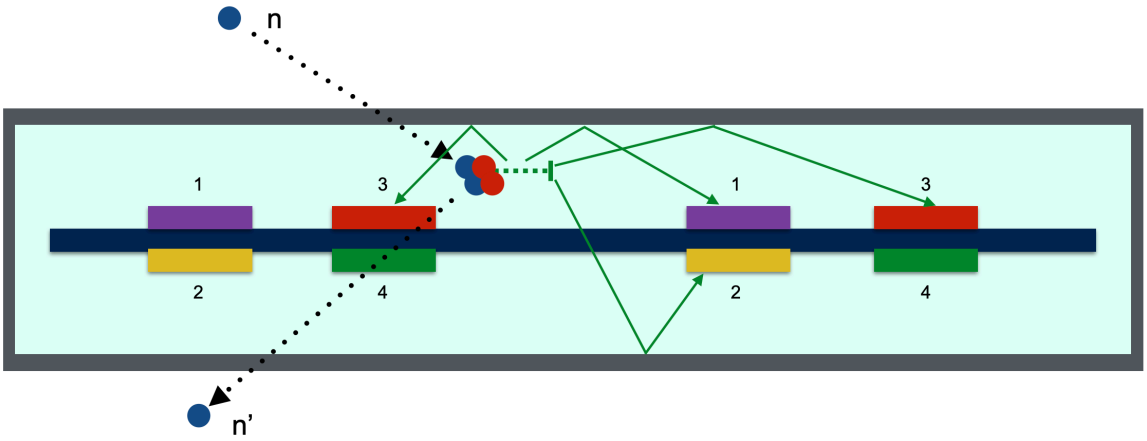

Figure 2.2: An illustration of the ^{4}He detector operating principle, showing a single segment of the detector. The dashed green line represents the ionization track of the recoiling ^{4}He nucleus, and the solid green arrows represent possible individual scintillation photon paths. The detector includes three such identical segments. Each color corresponds to a SiPM pair output channel.

2.2. Methods

The Arktis S670 detector requires one 30.5-V DC input to supply bias to the SiPMs and a 5-V DC input to power the internal readout electronics. The SiPMs in each of the three segments are read out as four channels, for a total of twelve channels. The waveforms from all twelve channels are digitized using a 14-bit, 250-MHz CAEN V1725 VME digitizer and recorded using CAEN's CoMPASS software [102]. The digitizer leading-edge trigger level for each segment was selected to be just above the level corresponding to thermal dark pulses in the SiPMs. This level was 80, 150, and 400 bits above baseline for the low-, medium-, and high-gain segments, respectively.

To characterize the detector response to fast neutrons, three neutron sources were measured. Monoenergetic D-D and D-T neutron generators provide neutrons with en-

ergies of 2.45 and 14.1 MeV, respectively, allowing for an endpoint-based energy calibration and qualitative observation of the detector energy resolution. A ^{252}Cf spontaneous fission source was also used to provide a Watt spectrum of neutrons for characterization over a wide, continuous energy range. The D-D neutron generator used is a Thermo Scientific MP320, which yields $\sim 1 \times 10^6$ n/s nearly isotropically and is shown in Figure 2.3. The D-T neutron generator used is a Thermo Scientific P211, which yields $\sim 1 \times 10^8$ n/s, also nearly isotropically. The ^{252}Cf source emitted $\sim 1.29 \times 10^5$ n/s as of the time of measurement. Furthermore, a 5 µCi ^{137}Cs source was used to measure the response of the detector to gamma rays. The detector and neutron sources were elevated more than 1 meter from the laboratory floor to minimize the contributions of scattered neutrons to the measurement.

Figure 2.3: An example experimental setup, showing the ^{4}He detector and its associated electronics (right) and the MP320 D-D neutron generator (left). The generator is elevated from the laboratory floor using a steel lab cart and several layers of low-density polyurethane foam and polystyrene foam such that the center of the generator target is at the same elevation as the center of the detector.

To measure the time resolution of the detector, a standard 2" EJ-309 liquid organic scintillator cell was used to measure the gamma-ray TOF from ^{252}Cf fission events in close proximity to the ^{4}He detector, as shown in Figure 2.4. The ^{252}Cf source was approximately 1 cm from the face of the ^{4}He detector and 25 cm from the face of the EJ-309 detector. In this measurement, the neutrons from fission interact immediately

in the ^{4}He detector, and gamma rays from fission interact in the organic scintillator with a constant TOF. The width of the corresponding gamma-ray peak in the time difference spectrum is the time resolution. The intrinsic time resolution of a typical EJ-309 detector is on the order of 1–2 ns and is not expected to contribute to the overall time resolution of this measurement.

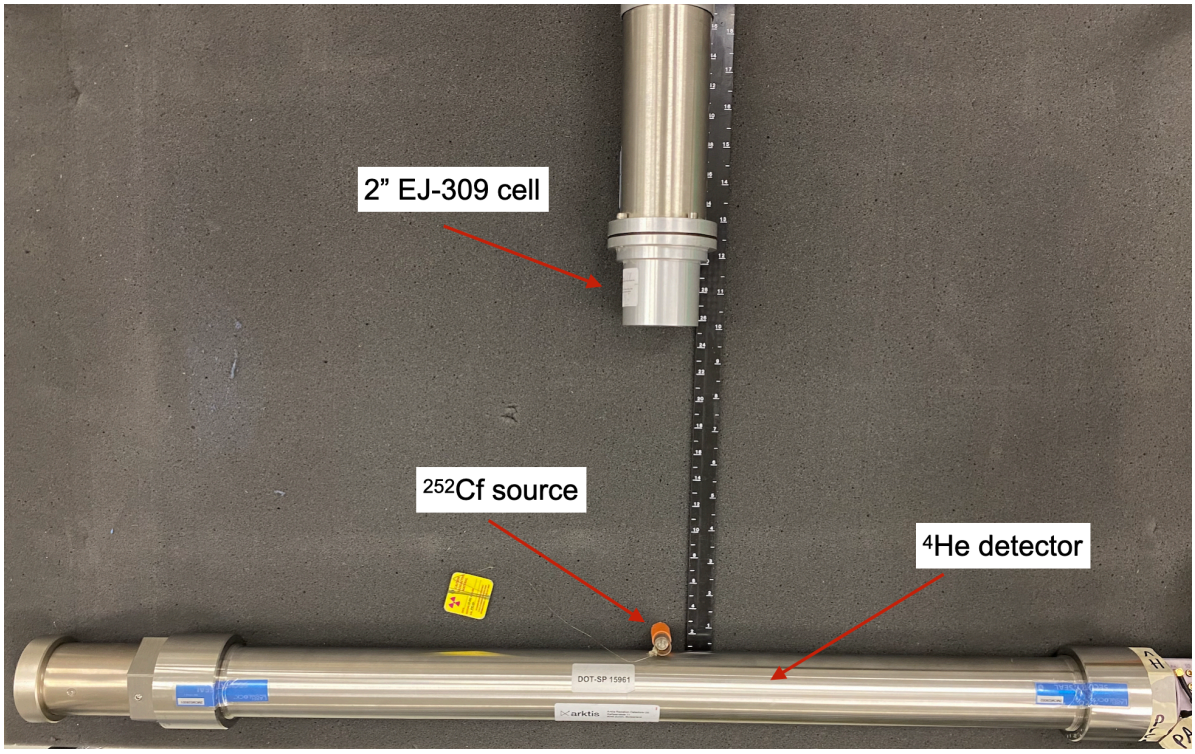

Figure 2.4: Experimental setup for measurement of the detector time resolution.

2.3. Results

The analysis presented here focuses on the results measured in the medium-gain segment of the detector, but equivalent analyses may be performed on the low- and high-gain segments. The medium-gain segment was chosen for analysis in this work for its compatibility with the dynamic range of the waveform digitizer, which spans 2 V. The spectrum

measured with this segment in response to 14.1-MeV neutrons occupies approximately 70% of the digitizer dynamic range, which is the best fit among the detector segments.

From Figure 2.2, it is likely that a single energy deposition event in a given segment of the detector will be observed in multiple channels of that segment. Consequently, coincident channel triggers within the same segment must be treated carefully so as to prevent multiple-counting of neutrons and to improve the energy resolution. Figure 2.5 shows the spectrum measured in each channel of the detector segment in response to D-T neutrons and an average output waveform.

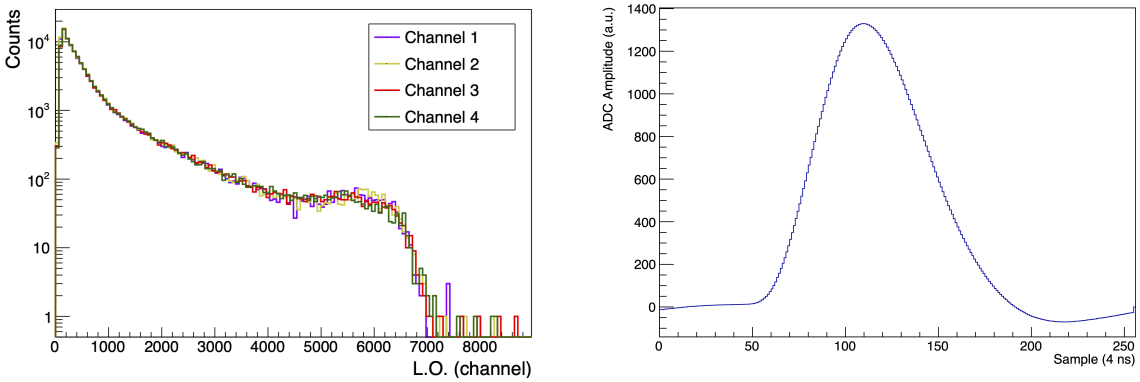

(a) **(b)**

Figure 2.5: (a) Pulse height spectrum measured by each of four channels in the medium-gain segment of the detector in response to 14.1-MeV neutrons. The colors correspond to the SiPM configuration shown in Figure 2.2. (b) The average amplified SiPM waveform from the medium-gain segment of the detector. Only a narrow band of the spectrum was used in constructing the average waveform.

To aggregate the pulse from all four channels into a single data list, the waveforms from each channel were sorted in time to produce a pulse train, as illustrated in Figure 2.6. Following the first pulse in the train, a window is opened for a set time period, and all proceeding pulses in the train that occur before the window closes are considered to

correspond to the same energy deposition event.

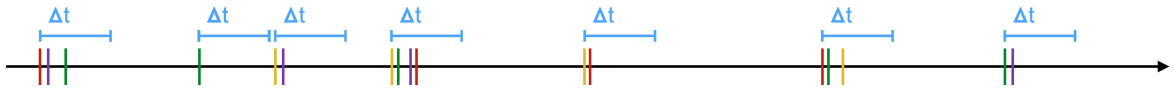

Figure 2.6: A conceptual pulse train illustrating the logic for combining multiple pulses corresponding to the same energy deposition event. The colors correspond to those from the illustration in Figure 2.2.

In order to select an appropriate time window size, the histogram of inter-pulse times is analyzed, as shown in Figure 2.7. The time difference encompassing 99% of inter-pulse times is selected, and since in the extreme case of all four channels triggering there are three inter-pulse times within the same event window, this time difference is multiplied by three. In this case, the 99% acceptance window is 75 ns, and the corresponding pulse-train time window for data condensation is 225 ns. The nature of this relatively poor inter-channel time resolution is not immediately clear, but is likely due to the long rise time of the amplified SiPM waveform, as shown in Figure 2.5.

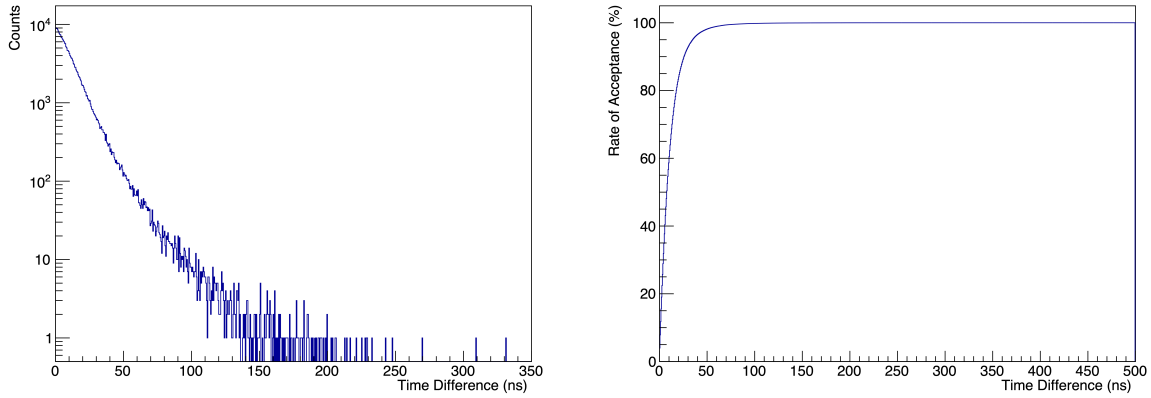

(a) **(b)**

Figure 2.7: (a) Distribution of inter-pulse times in the medium-gain detector segment; (b) Dependence of the acceptance rate of pulses on the acceptance window width.

For pulses corresponding to a single event, the "total" pulse height for the event is taken to be the sum of the pulse heights within the time window. This relationship stems from the fact that the different SiPM channels in the segment measure different scintillation photons, and the SiPMs in a single segment are gain-matched (as shown in Figure 2.5), such that the total pulse height is directly proportional to the amount of scintillation light measured. The time stamp corresponding to an event is taken as the arithmetic mean of time stamps within the time window. This relationship holds if all SiPM channels exhibit the same delay with respect to the digitizer. This condition is ensured by measuring the distribution of time differences between the first channel and the remaining channels within a coincidence window of 225 ns. The measured inter-channel time difference distributions for channels two through four with respect to channel one are shown in Figure 2.8. Each measured distribution's mean can then be subtracted from its corresponding channel's time stamp such that all channels synchronize with

channel one.

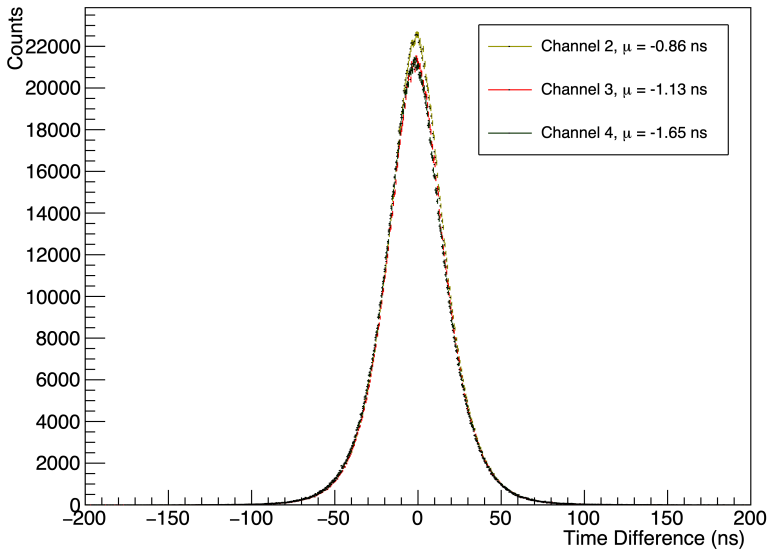

Figure 2.8: The distribution of time differences measured between the first channel and remaining channels of the same segment. The mean of the distribution is denoted by μ.

Once this logic is applied and the segment data is aggregated into a single list, the measured pulse height distributions can be calibrated using the end-points of the D-D and D-T neutron spectra. The end-points correspond to maximum kinetic energy transferred from the neutron to the ^{4}He nucleus, which is 64% of the initial neutron kinetic energy. This equates to a maximum energy deposition of 9.02 MeV for 14.1-MeV neutrons and 1.57 MeV for 2.45-MeV neutrons. The end-points of the energy deposition spectra are determined by adjudicating the local minimum in the first derivative of the pulse-height spectrum. The spectra of these two neutron sources and their negative derivatives are shown in Figure 2.9. The peak-like features in the derivative are not Gaussian, but can be approximated and fit as such in order to estimate their centroids, corresponding to the best estimate of the local maximum. The centroids of the peak-

like features are then used to perform a two-point calibration of the detector, shown in Figure 2.10.

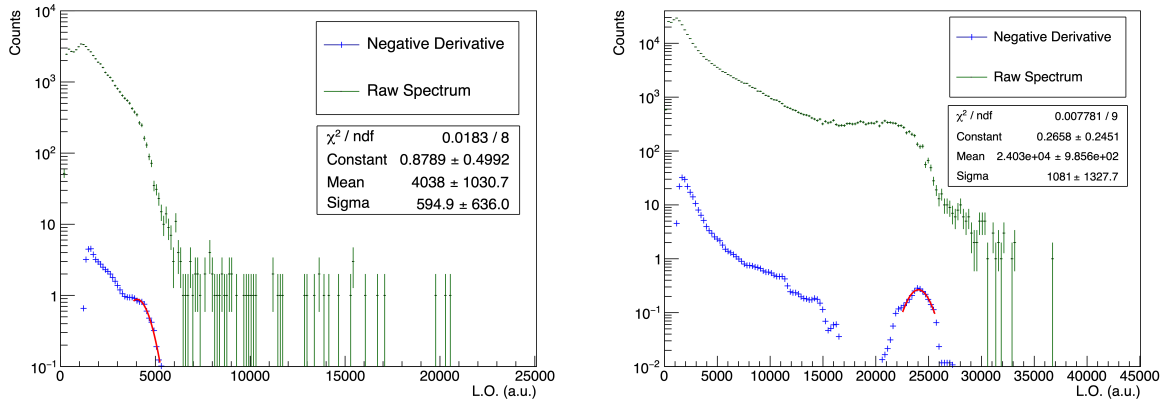

(a) **(b)**

Figure 2.9: Measured spectrum and smoothed derivative in response to (a) 2.45-MeV neutrons and (b) 14.1-MeV neutrons. Gaussian fits to peaks are shown in red.

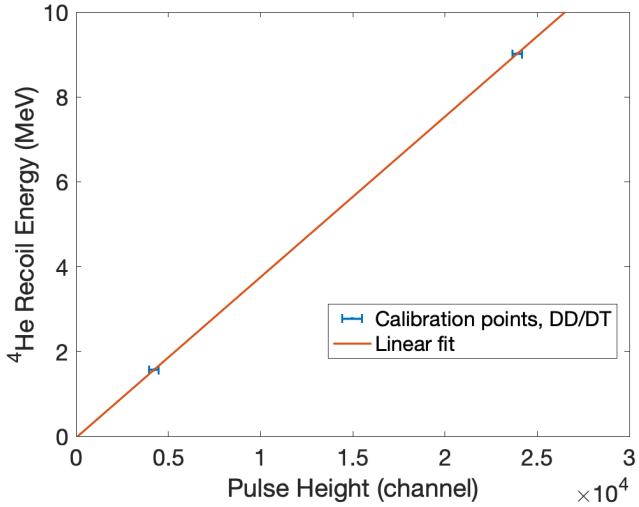

Figure 2.10: Two-point energy calibration using the 1.57- and 9.02-MeV end-points.

With the calibration function obtained, the recoil distributions measured in response

to D-D, D-T, and ^{252}Cf neutrons, as well as 662-keV gamma rays from ^{137}Cs, are shown in Figure 2.11.

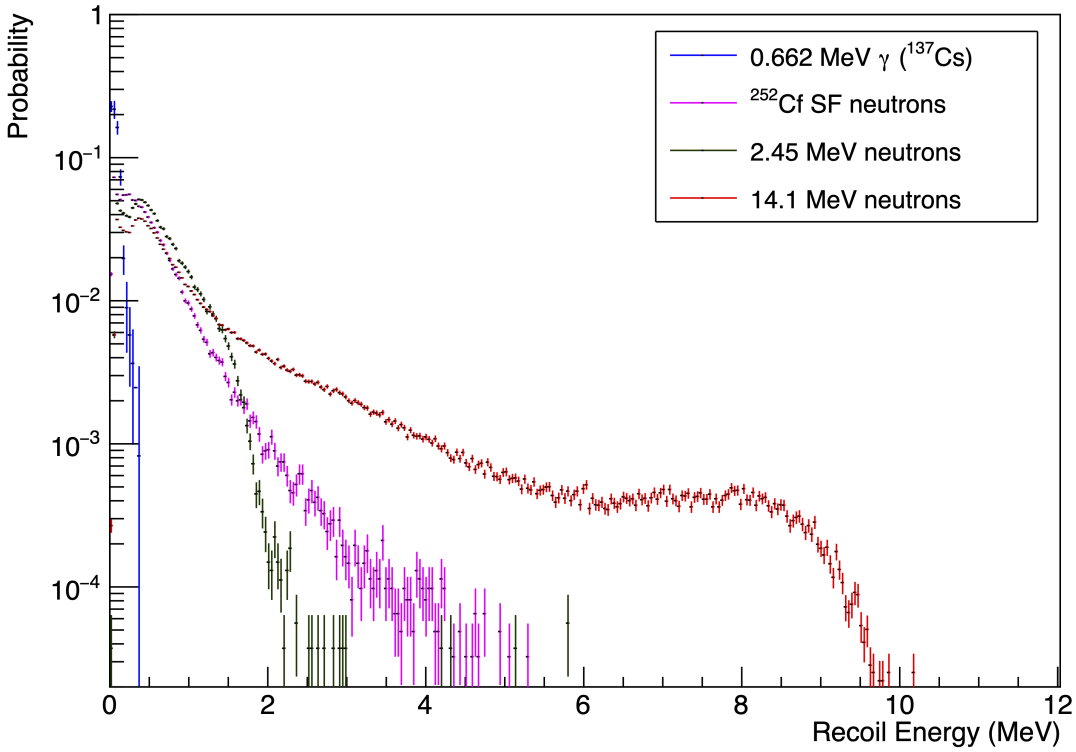

Figure 2.11: (a) Calibrated, integral normalized spectra in response to neutron sources and a ^{137}Cs gamma-ray source.

In the measurement of the detector energy resolution, PSD was used to reject neutrons interacting in the EJ-309 detector, since only gamma-rays having constant TOF were desired. A tail-to-total ratio pulse shape parameter (PSP) was used. The conservative PSD cut and energy threshold used to reject neutrons is shown in Figure 2.12. The TOF distribution for the ^{4}He detector is shown in Figure 2.13, both before and after applying the channel combination logic. The 1-σ time resolution σ_t is reduced from 9.2 to 7.1 ns, an improvement of 22%. The FWHM time resolution of this system is 16.7 ns.

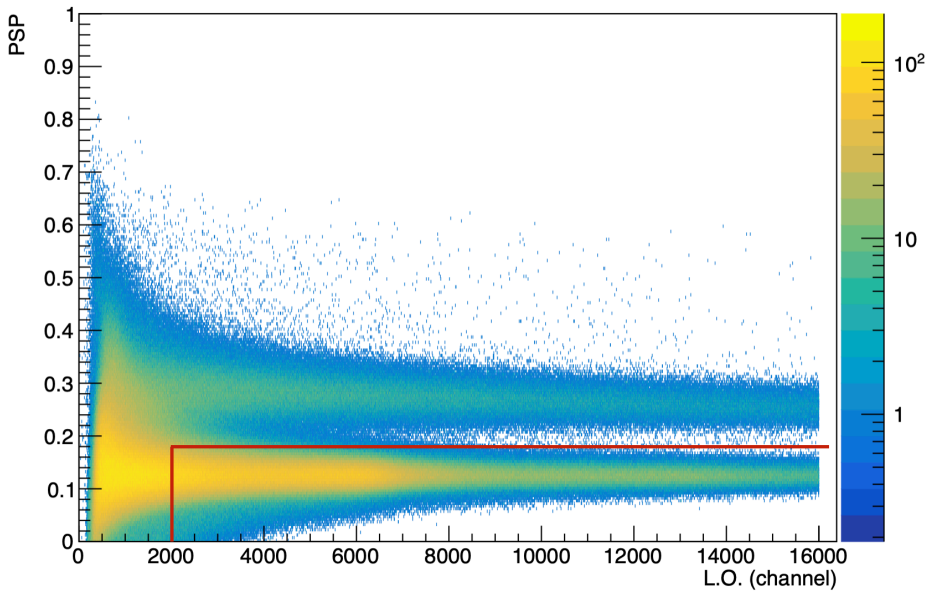

Figure 2.12: PSP and energy cuts, shown in red, used to reject neutrons from EJ-309 data to measure the ^{4}He detector time resolution.

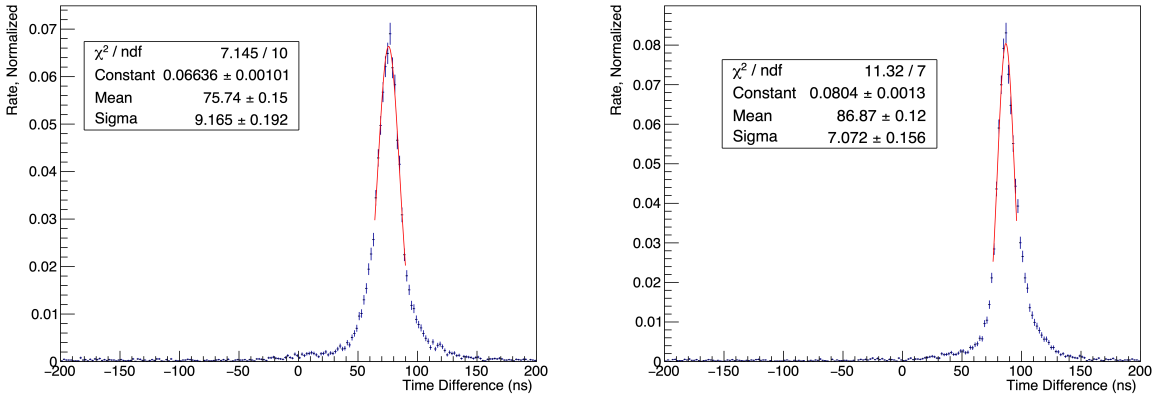

(a) **(b)**

Figure 2.13: Measured time resolution of the ^{4}He detector (a) analyzed as individual, independent channels and (b) after applying the combination logic. Gaussian fits are shown in red.

2.4. Conclusions

The neutron spectroscopy capability of the ^{4}He detector system and analysis method in this work was demonstrated. The two-point calibration obtained from the end-points of D-D and D-T neutron generators has its intercept near zero, suggesting that ^{4}He shows a high degree of linearity up to 14.1-MeV neutron energy, and a two-point calibration is sufficient for nuclear recoil spectroscopy. The demonstrated simple energy calibration technique is significant in that it can be performed on-the-fly without the need for additional detectors to measure the neutron recoil angle or TOF. Calibration of the recoil energy spectrum will help allow for comparisons with Monte Carlo simulations; however, an accurate energy resolution function is required to implement the simulation.

The response of the detector to gamma rays was shown to be weak, confirming the intrinsic gamma rejection capabilities of ^{4}He-based neutron detectors without requiring PSD. Additionally, the tail of the ^{252}Cf spontaneous fission spectrum, as measured by the ^{4}He detector, extends significantly beyond the end-point of the D-D spectrum, indicating that this detector is suitable for discrimination of prompt fission neutrons from active interrogation neutrons in a scenario where D-D neutrons are used to induce fission.

The time resolution of the detector was measured and was shown to improve significantly after the application of the channel-combination logic laid out in this work.

Currently, simulation of ^{4}He-based detectors cannot be reliably performed, as there is no empirical model of their energy resolution in the literature which can be applied over the spectral range discussed in this work. In the future, this should be resolved with a measurement of monoenergetic neutron sources in which the neutron scattering angle in the detector is restricted with the use of backing detectors, similar to the procedure in Ref. [101], to yield Gaussian peaks in the detector response over a broad dynamic range,

which could be analyzed to obtain such an empirical model of the energy resolution.

Chapter 3

Response of a High-Pressure ^{4}He Scintillation Detector to Nuclear Recoils up to 9 MeV

This chapter is adapted from the manuscript under review of the same name by O. Searfus, P. Marleau, and I. Jovanovic [103].

3.1. Introduction

Helium-4-based scintillation detectors have been developed for use as fast neutron detectors [86], most recently as high-pressure scintillation detectors [91], [92], [97], [101], [104]. Fast neutrons interact with the ^{4}He nucleus via elastic scattering, effectively transforming it into an α particle which produces a scintillation signal as it slows down in the gas [88].

These detectors are often preferable over organic scintillators for fast neutron detection in nuclear security, nonproliferation, and safeguards applications that involve extreme radiation environments [95], [96], [105], [106], since they are intrinsically less sensitive to γ rays. High-energy electrons produced by γ-ray interactions, either in the gas itself or in the detector supporting structure, typically have a range much larger than the detector dimensions. As a result, γ rays are physically limited to low energy deposition and can

be effectively discriminated with a pulse-height threshold [105] rather than pulse-shape analysis, as in many organic scintillators.

The response of ^{4}He-based detectors to neutron-induced ^{4}He recoils has been previously characterized only to a limited extent. Ref. [92] proposed a light output function for a ^{4}He detector at 150 bar, read out by photomultiplier tubes, based on a neutron time-of-flight (TOF) measurement with recoil energies between 200 keV and 5 MeV. The reported detector response was discretized into 500-keV bins, which may lead to large systematic bias in the light output function [107], and no energy resolution information was reported. Furthermore, the findings in Ref. [92] have limited applicability to the sole commercially available ^{4}He detector, which operates at 190 bar and is read out by silicon photomultipliers (SiPMs). Ref. [101] measured nuclear recoils for this same detector between 83 and 626 keV, constraining monoenergetic (2.8 MeV) neutrons in their scattering angle by several organic scintillator backing detectors, operated in coincidence with the ^{4}He detector. This technique produces peaks in the ^{4}He recoil spectrum, and thus both the scintillation linearity and energy resolution were reported in Ref. [101]. However, since the maximum recoil energy measured was only 626 keV, the reported trends have limited value for many practical applications in nuclear security and nonproliferation, where a significant fraction of the fission neutron spectrum can produce more energetic ^{4}He recoils.

3.2. Methods

3.2.1. Experimental design

To characterize the response of a high-pressure ^{4}He scintillation detector to fast neutrons, an experiment was performed with two compact neutron generators and an array of seven organic scintillator backing detectors. An Arktis S670 fast neutron detector [94] was operated in coincidence with the organic scintillator array to constrain the neutron scattering angle, which in turn constrains the ^{4}He recoil energy for monoenergetic incident neutrons. The experiment performed is similar in concept to the previously discussed work for the same detector [101] but accesses a much greater range of nuclear recoil energies both by increasing the range of recoil angles and by using two incident neutron energies, 2.45 and 14.1 MeV. This constrained scattering technique has also shown success in characterizing a plastic scintillator-based fast neutron detector [107].

The energy transferred from a fast neutron to a ^{4}He nucleus in elastic collisions is

$$E_\alpha = E_i(1-k), \tag{3.1}$$

where E_α is the ^{4}He recoil energy, E_i is the incident neutron energy, and k is the kinematic factor, given by

$$k = \left(\frac{m_n \cos\theta + \sqrt{m_\alpha^2 - m_n^2 \sin^2\theta}}{m_n + m_\alpha} \right)^2 . \tag{3.2}$$

Here m_n is the neutron mass, m_α is the ^{4}He mass, and θ is the neutron scattering angle in the laboratory frame [108]. The recoil energy obtained from Eq. (3.1) for 2.45 MeV and 14.1 MeV neutrons is shown in Figure 3.1.

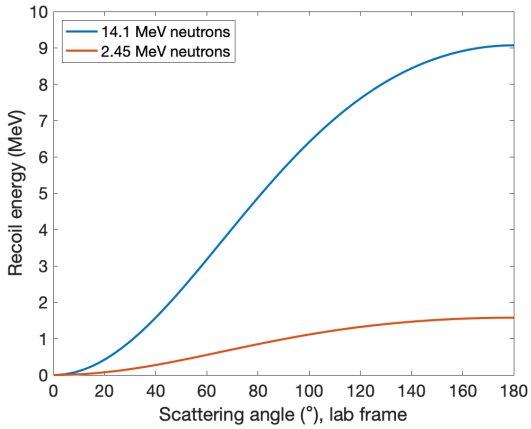

Figure 3.1: Energy transferred to a ^{4}He nucleus by 14.1 and 2.45 MeV neutrons with respect to the scattering angle θ in the laboratory frame.

In the experiment, a ^{4}He detector and an array of seven 2 × 2" EJ-309 [109] liquid organic scintillators were mounted to a 1×2 m^2 optical breadboard. Two Thermo Scientific MP320 neutron generators were used to provide neutrons for the experiment: one deuterium-tritium (D-T) to provide 14.1 MeV neutrons, and one deuterium-deuterium (D-D) to provide 2.45 MeV neutrons. The D-T generator produced $\sim 10^7$ neutrons per second, while the D-D generator produced $\sim 10^6$ neutrons per second. The ^{4}He detector was oriented vertically and served as the center of a 1 m semicircle, with one of the two neutron generators and all seven organic scintillators mounted along its perimeter, as shown in Figure 3.2. The ^{4}He detector is optically segmented into three regions, with each region having its own readout. Only the central segment, with a 20 cm height and 4.95 cm diameter (internal), was read out in this experiment. The three organic scintillation detectors closest to the generator were shielded with a combination of lead and high-density polyethylene (HDPE) along their line of sight to the generator to reduce the accidental coincidence rate while leaving the desired neutron flight path unobstructed.

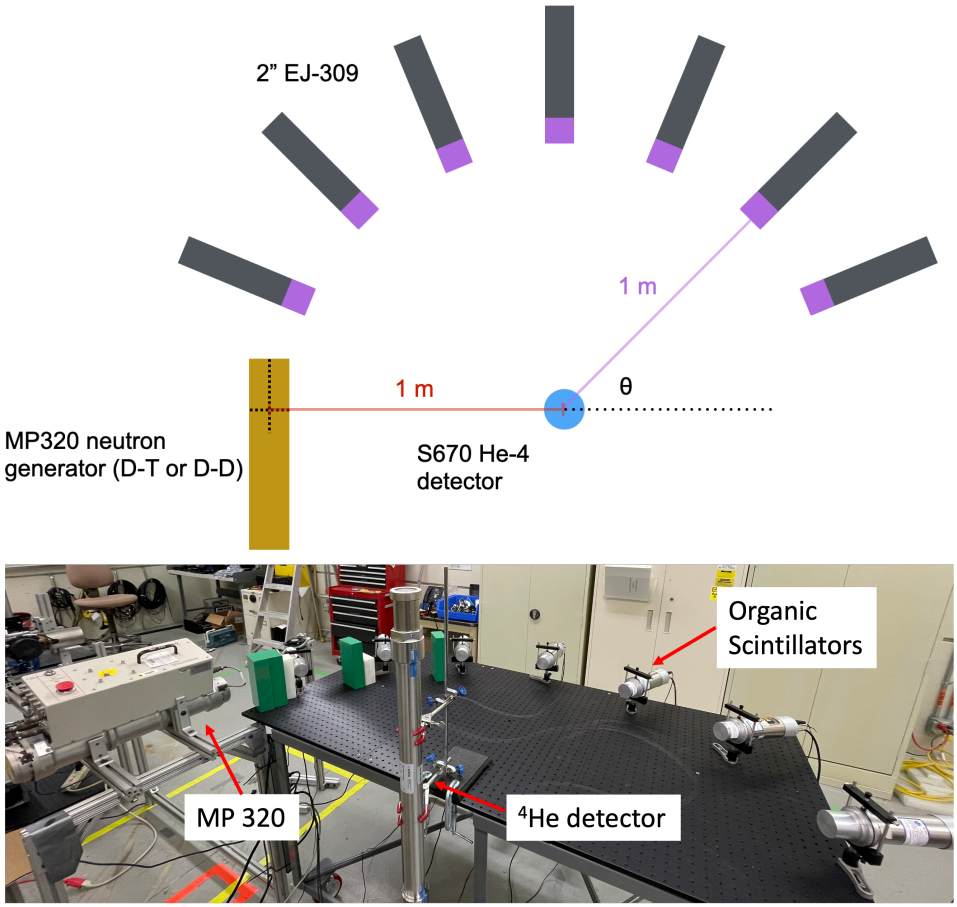

Figure 3.2: Experimental design for measuring the response of the ^{4}He detector to monoenergetic recoils (above). Measurement setup in the laboratory (below).

Waveforms from the ^{4}He detector as well as the organic scintillators were digitized using a 250 MS/s, 14-bit CAEN V1725 digitizer and read out using CAEN CoMPASS software [102]. The four SiPM output channels from the ^{4}He detector central segment were condensed into a single data list and calibrated using the D-D and D-T spectral endpoints according to the procedure in Ref. [97]. Pulse-shape discrimination (PSD) was performed on the organic scintillation detectors using optimized time gate parameters to reject γ-ray pulses. Example PSD plots are shown in Figure 3.3.

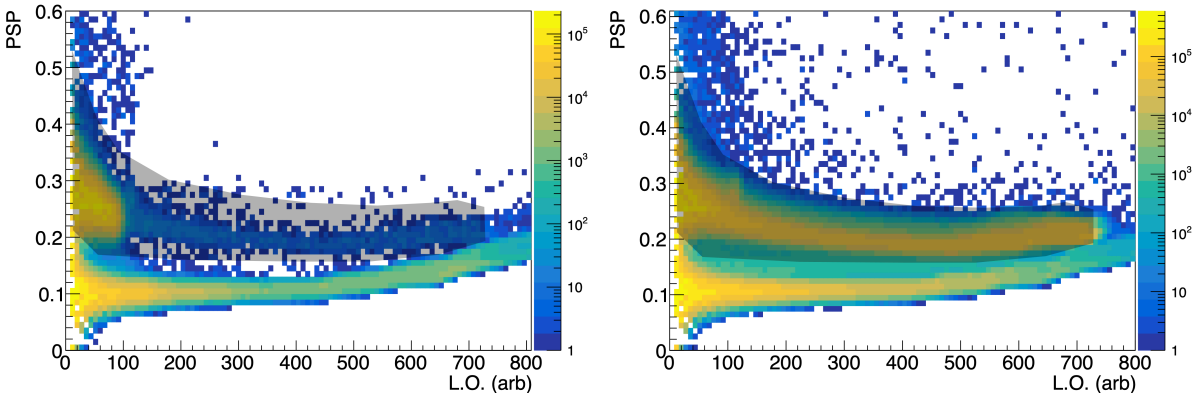

(a) **(b)**

Figure 3.3: Example PSD histograms for organic scintillators in response to (a) D-D and (b) D-T neutrons. The shaded areas represent the neutron acceptance cut, which was chosen to minimize γ-ray sensitivity.

3.2.2. Simulation of neutron transport

The assembled experimental configuration was simulated using MCNPX-PoliMi [110], [111] to determine the intrinsic spread in energy deposition in the ^{4}He detector for each organic scintillator backing detector arising from finite dimensions of the ^{4}He detector and the organic scintillator cells, as well as predict the probability of detection for the desired sequence of scattering events. The neutron generators were approximated as point sources emitting in a narrow cone of 0.0377 sr in the direction of the ^{4}He detector. Coincident events were accepted above the light-output threshold of 120 keVee in the backing organic scintillation detectors. The results of this simulation for each neutron generator-scattering angle combination are shown in Figure 3.4. A summary of the simulation results is shown in Table 3.1. In the case of 2.45 MeV neutrons undergoing 157.5° and 135° scattering on ^{4}He, the scattered neutron energy available for second scattering and detection in the organic scintillator is only 0.91 and 1.01 MeV, respec-

tively. In EJ-309, this corresponds to a maximum light output of 120 and 143 keVee, respectively [109]. Since we use a conservative light output threshold of 120 keVee for reliable PSD, none of the 157.5° scattering events and very few 135° scattering events will lead to detectable neutron pulses in the organic scintillator. Consequently, these two angles were not used for the 2.45-MeV neutron measurement.

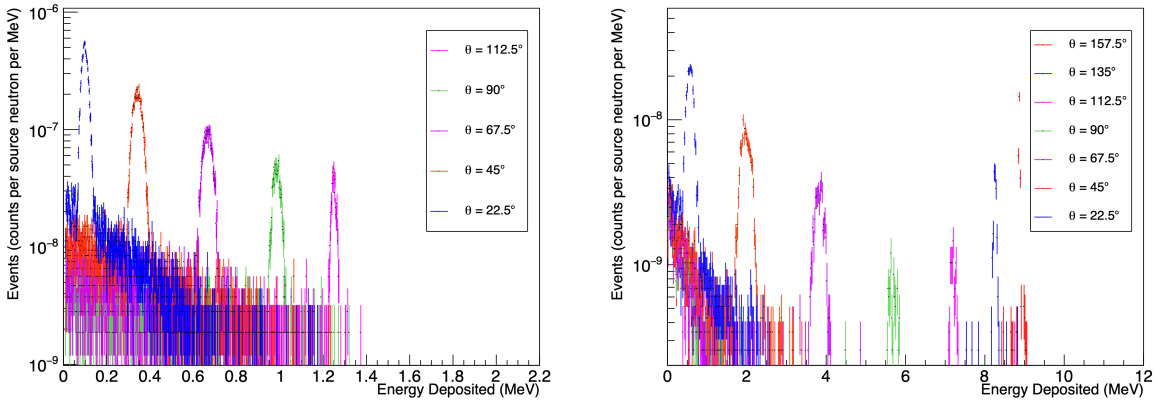

(a) **(b)**

Figure 3.4: Simulated energy deposition in the ^{4}He detector for coincidence with deposition in an organic scintillation detector for (a) D-D and (b) D-T neutron sources. Error bars represent one standard deviation.

Table 3.1: Summary of ^{4}He energy depositions and uncertainties due to detector dimensions. $\overline{E}$ is calculated from Eqs. (3.1) and (3.2), and $\sigma_{\overline{E}}$ is determined from Gaussian fits to peaks in Figure 3.4. $P(D)$ denotes the estimated probability that a neutron emitted by the neutron generator scatters in the ^{4}He detector followed by depositing at least 120 keVee by scattering in the organic scintillation detector, and is calculated by integrating the corresponding peaks in Figure 3.4.

	D-D			D-T		
θ (°)	$\overline{E}$ (MeV)	$\sigma_{\overline{E}}$ (MeV)	$P(D)$	$\overline{E}$ (MeV)	$\sigma_{\overline{E}}$ (MeV)	$P(D)$
22.5	0.0925	0.0026	1.92×10^{-8}	0.5321	0.1069	5.25×10^{-9}
45.0	0.3390	0.0061	1.16×10^{-8}	1.9512	0.1271	2.82×10^{-9}
67.5	0.6642	0.0115	5.43×10^{-9}	3.8229	0.1271	1.03×10^{-9}
90.0	0.9866	0.0185	2.21×10^{-9}	5.6780	0.1097	2.00×10^{-10}
112.5	1.2507	0.0235	1.09×10^{-9}	7.1982	0.0717	2.22×10^{-10}
135.0	1.4355	–	–	8.2615	0.0391	4.60×10^{-10}
157.5	1.5416	–	–	8.8720	0.0167	6.92×10^{-10}

3.2.3. Simulation of α-particle transport

There is a probability that a ^{4}He recoil nucleus, (*i.e.*, an α particle) produced in the collision with a fast neutron strikes the wall or other internal structure of the detector, resulting in only partial energy deposition in the scintillation medium. To account for this so-called *wall effect*, α-particle projected ranges (R_α) from the NIST ASTAR database [112], shown in Figure 3.5, are used in a procedure similar to that laid out in Ref. [86], adapted for high-pressure helium.

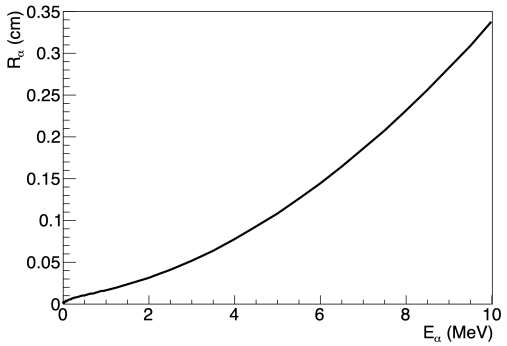

Figure 3.5: α-particle range from NIST ASTAR for a 190 atm ^{4}He gas.

The range of the α particle for each neutron scattering event was compared to the distance from the scattering position to the closest detector structure in the α particle direction of travel, r_w. For ranges shorter than this distance, the event was considered to have full energy deposition, E_0. For $R_\alpha(E_0) > r_w$, the partial energy deposition is

$$\Delta E_p = E_0 - E_\alpha \Big|_{R_\alpha(E_\alpha)=R_\alpha(E_0)-r_w} . \tag{3.3}$$

The scintillation light produced in this detector is read out using an array of SiPMs mounted to a printed circuit board (PCB) which runs along the axis of the detector. The exact dimensions of this PCB are not known, so for the purposes of accounting for the wall effect, it is approximated as a plane bisecting the detector volume. An illustration of the internal detector geometry and the manifestation of the wall effect is shown in Figure 3.6.

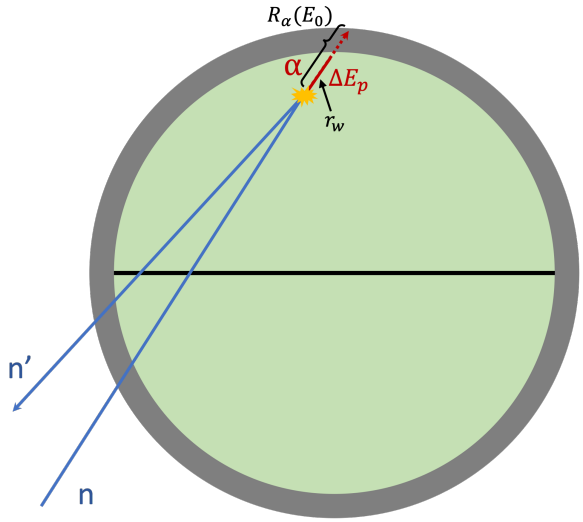

Figure 3.6: Example of an event topology resulting in the wall effect, depositing an energy ΔE_p in the gas.

3.3. Results

3.3.1. Background reduction

Several steps were taken to reduce backgrounds in the coincident data representing the ^{4}He detector response. The first of these steps was to establish a fiducial cut on the neutron TOF between the ^{4}He detector and organic scintillator in each of the generator-organic scintillator combinations. To do this, 2-D histograms of the TOF vs. ^{4}He energy deposition were created. In these histograms, there are clear clusters corresponding to the desired neutron flight path, as well as clusters arising from alternative flight paths. The fiducial cuts used represent the centroid of a region of interest (ROI) containing the signal cluster $\pm 2\sigma_t$, where σ_t is the detector time resolution of 7.1 ns [97]. Accidental coincidences manifest as a uniform background at all TOF values. An example histogram and fiducial TOF cut are shown in Figure 3.7.

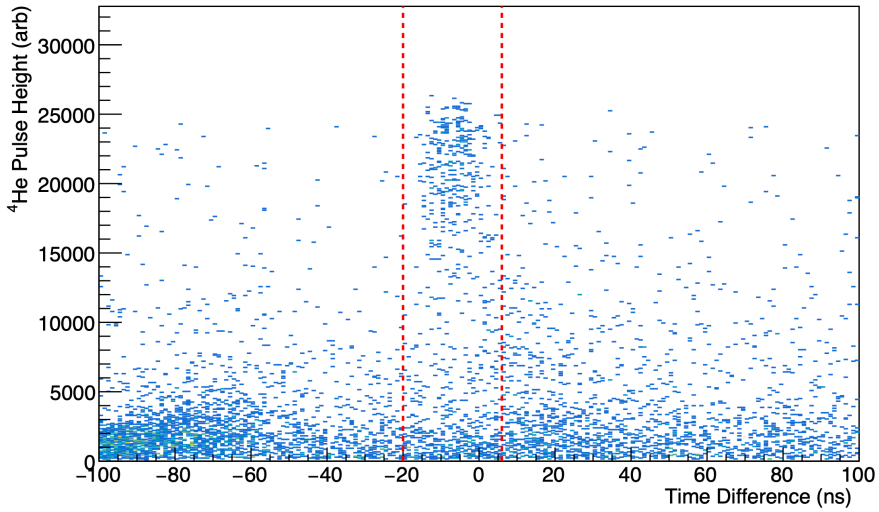

Figure 3.7: Example TOF-energy deposition histogram for D-T neutrons and 157.5° scattering. The corresponding fiducial TOF cut is shown in red. Note that TOF data has not been adjusted to account for electronic delays between the ^{4}He detector and organic scintillators.

Since each scattering angle is associated with certain energy deposition in the ^{4}He detector, the neutrons exiting the ^{4}He detector toward a given organic scintillation detector are limited in energy (*e.g.*, a 14.1 MeV neutron which deposits 8.9 MeV on a ^{4}He nucleus is only able to deposit a further 5.2 MeV in the organic scintillator). This effect can be exploited to exclude background events in which light output is recorded in an organic scintillator above the maximum value allowed by scattering kinematics. An example of this type of data cut is shown in Figure 3.8.

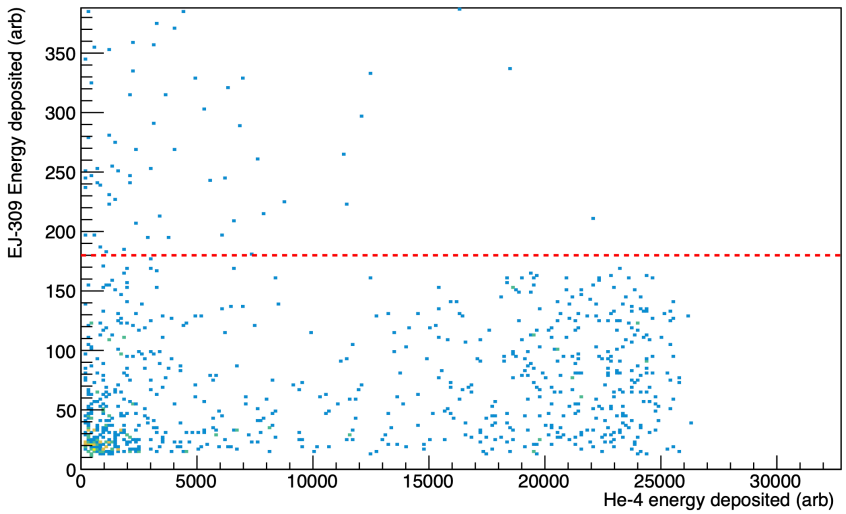

Figure 3.8: Example ^{4}He-organic energy deposition histogram for D-T neutrons and 157.5° scattering, with the maximum allowable organic scintillator energy deposition shown in red. Data above this line were rejected from the analysis.

3.3.2. Spectral response analysis

Due to the relatively low probability of neutron scattering in the ^{4}He detector followed by an organic scintillation detector and limited neutron generator run time, the coincident energy deposition spectra reflect low statistics and relatively large bin-to-bin fluctuations. To improve the determination of the mean and width of each fitted peak, the ROOT smoothing algorithm was applied to the binned data [113], [114], an example of which is shown in Figure 3.9. Then, the smoothed histograms were fit to a Gaussian atop a linear background in an ROI about the peak location. Two example fitted coincident spectra are shown in Figure 3.10.

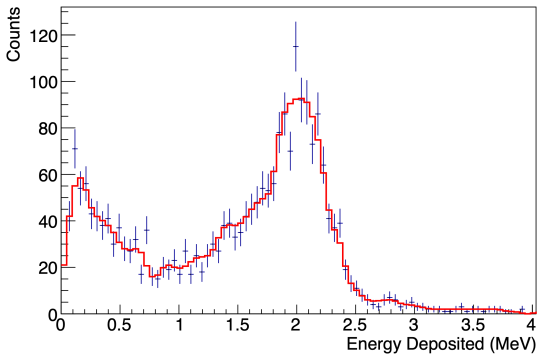

Figure 3.9: Example of histogram smoothing of data representing 45° scattering of D-T neutrons.

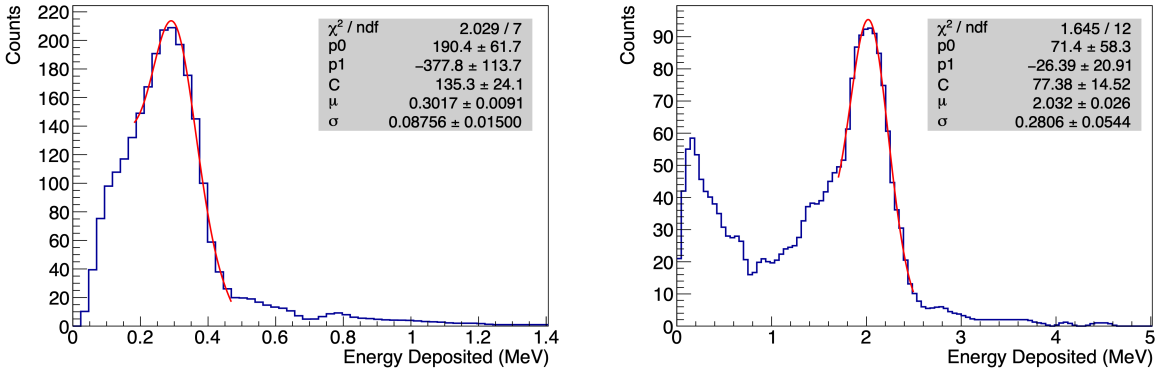

(a) **(b)**

Figure 3.10: Fitted spectral response to 45° scattering of (a) D-D and (b) D-T neutrons

3.3.3. Scintillation Linearity

The constrained energy deposition determined from Eq. 3.1 compared to the measured, calibrated energy deposition determined from the mean of each Gaussian fit is shown in Figure 3.11. When fit to a first-degree polynomial, the y-intercept is within 2σ of 0, and the slope is within 1σ of 1. Therefore, the measured scintillation response reported in this work is in good agreement with the end point-based calibration procedure in

Ref. [97] and the assumption of scintillation linearity in high-pressure ^{4}He.

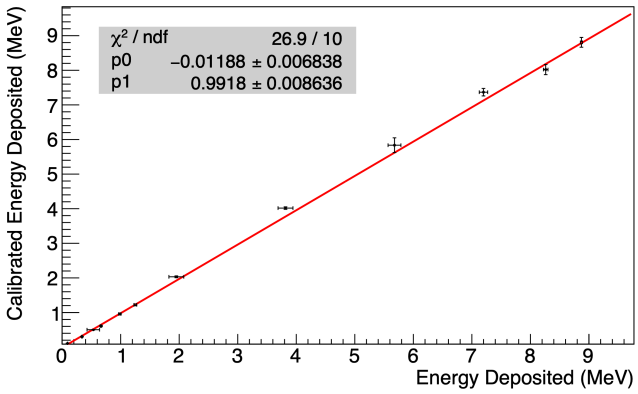

Figure 3.11: Comparison of predicted and measured energy deposition. Error bars reflect one standard deviation; horizontal error bars are $\sigma_{\overline{E}}$ from Table 3.1.

3.3.4. Energy Resolution

The measured full width at half-maximum (FWHM) R_m of each peak is determined from the measured σ_m for each Gaussian fit:

$$R_m = 2.355\sigma_m. \tag{3.4}$$

To estimate the uncertainty in this width $\sigma_{R,m}$, a Monte Carlo routine was developed using the fit parameters to simulate many spectra with the same statistics, detailed in A. To determine the width of each peak due to energy resolution alone, $\Delta E/E$, the intrinsic width due to variable scattering angle R_θ is subtracted in quadrature, as these effects are independent:

$$\frac{\Delta E}{E} = \sqrt{R_m^2 - R_\theta^2} \tag{3.5}$$

where $R_\theta = 2.355\sigma_{\overline{E}}$. The energy resolution data were then fit to a function of the form [115]

$$\frac{\Delta E}{E} = \sqrt{\alpha^2 + \frac{\beta^2}{E} + \left(\frac{\gamma}{E}\right)^2}, \tag{3.6}$$

the result of which is shown in Figure 3.12.

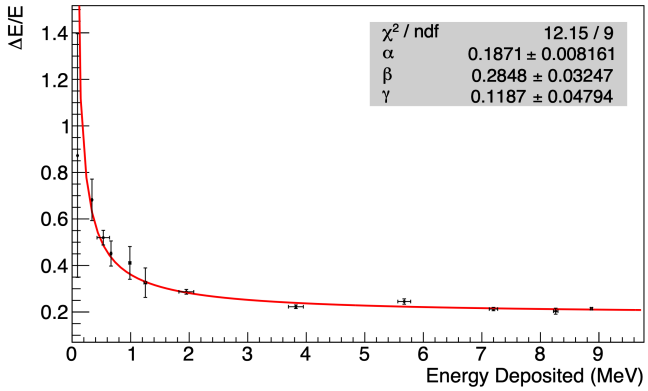

Figure 3.12: Energy resolution of the ^{4}He detector obtained in this measurement. Error bars represent one standard deviation.

The simulated response of the detector was then broadened using a Gaussian kernel with a width determined by this model of the energy resolution. The result of this broadened simulation is compared to the measured detector response in Figure 3.13.

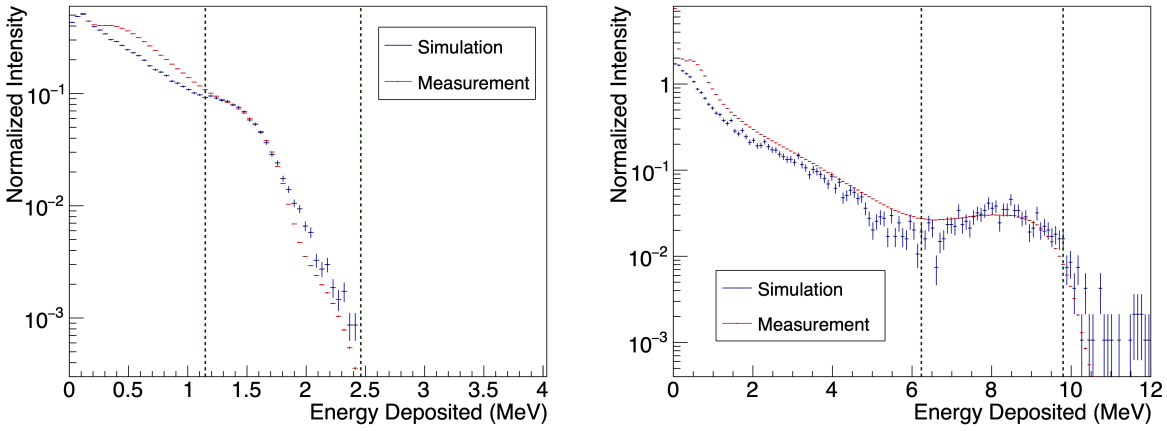

(a) **(b)**

Figure 3.13: Comparison of measured (a) D-D and (b) D-T spectra with broadened simulation. The dashed lines represent the interval for normalization. Note that these detector responses are uncorrelated, *i.e.*, not coincident with the organic scintillators.

3.4. Conclusions

In this work, we report the detailed response of a ^{4}He-based neutron scintillation detector to nuclear recoils ranging in energy from 92.5 keV to 8.87 MeV, broadening the limits of understanding of this detector medium to include all fast neutron energies of interest for nuclear safeguards and security. We provide evidence of scintillation linearity up to 9 MeV and validate the previously reported energy calibration procedure by the use of a coincident scatter detector method. This method also allowed for the measurement of energy resolution above 626 keV for the first time, which will in turn allow for complete reconstruction of the detector response to high-energy neutrons in simulation. This new capability to accurately simulate the response of this detector is essential for timely further development of its neutron spectroscopy applications in fundamental research as

well as nuclear nonproliferation. In future work, a comprehensive model of the detector response to gamma rays of various energies should be developed to determine the limits of operation in extreme environments, such as for spent nuclear fuel characterization.

Chapter 4

Characterization of the Neutron Pulse Time Profile from a Deuterium-Tritium Neutron Generator

4.1. Introduction

Electronic neutron generators have diverse applications in basic scientific research and industry, as well as nuclear security and safeguards. These devices are effectively miniaturized linear accelerators (linacs), driving a high-energy projectile ion onto a target, resulting in nuclear fusion and releasing a neutron. The most common neutron generators are based on the deuterium-deuterium (D-D) or deuterium-tritium (D-T) reactions.

4.1.1. Neutron generator design

While nearly all neutron generators are linacs, their major qualitative differences arise from the design of their ion sources. Penning ion sources [116], in which an excited atomic or molecular species collides with a target atom or molecule with ionization energy smaller than the incident species excitation energy, were the first to be developed for this application. These ion sources have small power and space requirements; however,

in neutron generator applications, there is a high probability of molecular ion formation (*i.e.*, H_2^+), which reduces the neutron production per ion generated [117]. In recent years, ion sources based on radiofrequency (RF) or microwave heating and ionization of gases have been developed, yielding improved atomic ion generation efficiency [118].

4.1.2. Applications of neutron generators

Neutron generators hold several advantages over common radioisotope-based neutron sources (*i.e.*, (α,n) and spontaneous fission) in that they do not emit neutrons when they are not in use, and they provide quasi-monoenergetic fast neutrons rather than broad spectral continua.

Monoenergetic neutrons provided by neutron generators are useful for the calibration and characterization of neutron detectors [119] and for nuclear data measurements [120]. The high neutron energy of the D-T reaction, 14.1 MeV, "unlocks" many exotic neutron-induced reactions which are inaccessible with many other fast neutron sources. For example, D-T neutron generators have been used to produce short-lived isotopic sources of high-energy γ rays and delayed neutrons for calibration of large-volume antineutrino detectors by the activation of oxygen isotopes [121].

Neutron activation analysis (NAA) is a well-established technique first demonstrated by Fermi [122] in which neutrons are used to activate some sample, whose resulting characteristic radioactive decay is indicative of the sample isotopic composition [123]. NAA is frequently used to nondestructively analyze a broad range of materials, including soil [124], artefacts [125], and minerals [126].

Prompt gamma neutron activation analysis (PGNAA) is a type of NAA in which the prompt radiative capture or inelastic scatter γ rays are measured to indicate the

composition of a sample. PGNAA is theoretically applicable to more isotopes than NAA, since nearly all isotopes emit a γ ray in the neutron capture process, whereas not all isotopes are transmuted to a radioactive isotope after neutron capture. This technique has been applied extensively for the determination of metal contents in alloys [127] and the stoichiometry of contraband materials [128].

Many neutron generators are designed to be operated in a pulsed manner, rather than continuously. These pulsed neutron generators can support additional applications that exploit their pulsed characteristics. One such application is neutron resonance transmission analysis, in which a short pulse of neutrons interacts in a neutron moderator, emitting a white epithermal neutron source. The epithermal neutrons travel along a known flight path to a neutron detector, such that the neutron's time of flight (TOF), from the neutron generator pulse to being detected, is indicative of its energy. Many nuclides have large resonances in their neutron interaction cross-sections in the 1–100 eV range, so any dips in the neutron TOF spectrum indicate that a particular nuclide is present along the flight path [77], [78]. Differential die-away (DDA) analysis is another technique relying on pulsed neutron generators for the detection of fissile isotopes. While the fast neutron background from a neutron generator decays very quickly after the pulse, the thermal neutrons in the environment will linger for much longer, up to several ms. In the presence of fissile materials, these thermal neutrons may induce fission, producing a fast neutron signal [80].

4.2. Methods

In this work, an experiment was performed to estimate the temporal distribution of pulses from a Thermo Scientific P211 D-T neutron generator. This generator is based

on the Zetatron neutron tube, developed by Sandia National Laboratories, which was designed to emit short, intense bursts of neutrons. To do this, both the Penning ion source and acceleration potential are pulsed, such that there are no neutrons emitted between pulses [129], [130]. According to the manufacturer specifications, the generator emits nominally 10^8 neutrons per second, in pulses of $\sim$10 µs at 100 Hz, corresponding to a 0.1% duty factor [131]. Many neutron generator applications, like DDA and NRTA, benefit from short and intense neutron pulses ($\leq$ 10 µs), making this generator model particularly attractive. In these applications, the exact shape of the primary neutron pulse is important for the analysis.

The interaction of the primary 14.1 MeV neutrons in the environment can generate additional radiation incident on a detector used to measure the generator time profile, as shown in Figure 4.1. The temporal signatures of these radiations, including scattered neutrons, X-rays, and activation γ rays, are distinct from that of the primary 14.1 MeV neutrons and must be considered in the detector choice and data analysis.

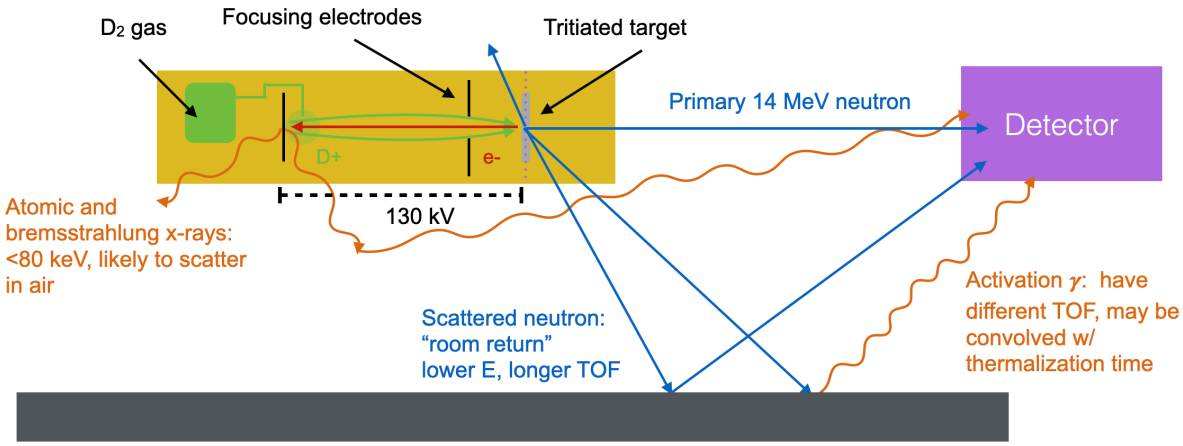

Figure 4.1: Illustration of the manifestation of primary and secondary radiations associated with neutron generators.

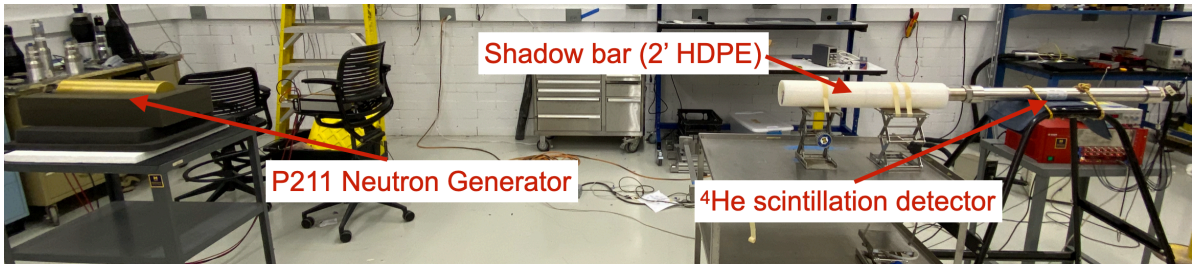

Figure 4.2: Laboratory configuration for shadow bar measurement.

4.2.1. Detectors and Electronics

A high-pressure ^{4}He scintillation detector from Arktis Radiation Detectors Ltd. [94] was used to measure the fast neutron time profile from the generator. Since this detector is intrinsically insensitive to γ rays, the measured time profile should remain unaffected by X-rays and activation γ rays, however, the scattered "room return" neutrons remain a concern. Since the ^{4}He detector is sensitive to the incident neutron energy and the scattered neutrons have lower energy than the primary neutrons, it is possible to discriminate primary neutrons from scattered neutrons based on their energy with this detector. To determine the spectral response of the detector to scattered neutrons in the laboratory and compare to the response for primary neutrons, the neutrons from the D-T generator were measured with and without a 2-foot shadow bar (SB) constructed from high-density polyethylene (HDPE), as shown in Figure 4.2. The shadow bar serves to prevent neutrons from traveling directly to the detector from the generator, while minimally interfering with the flight paths associated with neutrons scattering toward the detector from elsewhere in the laboratory. In this way, the contribution to the detector response from scattered neutrons can be characterized.

To measure the pulse time profile, it is necessary to establish a consistent temporal reference point before each pulse. The P211 pulse-forming network provides such a

reference logic signal $\sim 10\,\mu s$ before neutrons are emitted in each pulse, which was read into the same waveform digitizer used to measure the pulses from the ^{4}He detector.

4.3. Results

The response of the ^{4}He detector to the D-T generator with and without the shadow bar is shown in Figure 4.4. While it is clear that scattered neutrons are a large fraction of the low-energy events in the detector, they contribute less than 10% of the signal above 4 MeV energy deposition. Since the ^{4}He elastic scattering cross-section is significantly larger for $\sim$ 0.5–3 MeV neutrons than for 14.1 MeV neutrons, it follows that the detector is more efficient for room return neutrons than the primary neutrons.

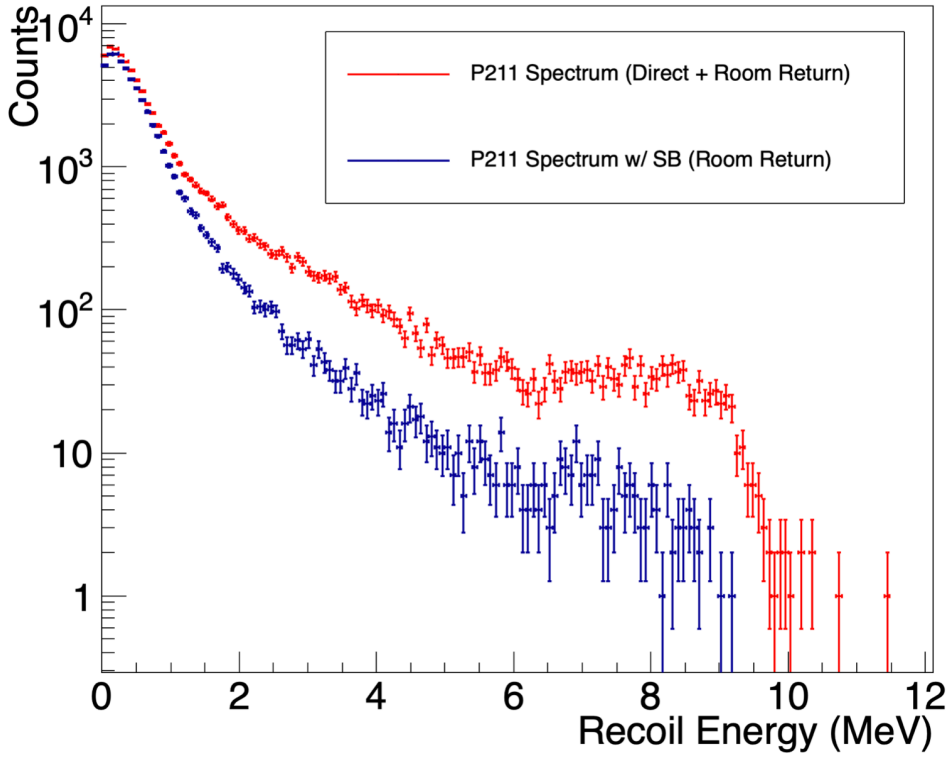

Figure 4.3: Energy deposition spectra of the D-T neutron source, with and without the shadow bar.

The neutron generator pulse time profile for all events, for events with less than 1.5 MeV energy deposition, and greater than 4 MeV energy deposition, are compared in Figure 4.4. The time profile appears to be a superposition of a narrow initial peak and a broader secondary peak. For the low-energies, the time profile dips to about 35% of the peak value between these features, whereas the high-energy time profile dips to 20% of the peak value. This illustrates the time profile distortion due to room return, since scattered neutrons arrive at the detector significantly later than neutrons traveling directly to the detector, and effectively smear the true time profile to longer delays. Further evidence for this is shown in the secondary feature of the time profile, which is significantly more intense for low-energy events than high-energy events.

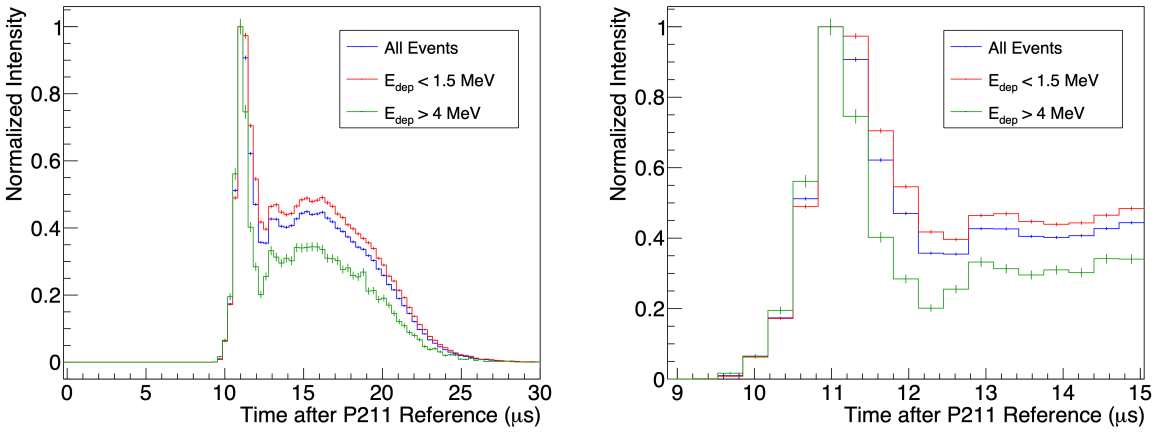

Figure 4.4: (a) Comparison of measured time profile from the D-T generator for different neutron energy deposition requirements, and (b) detail of peak feature. The time profiles are normalized to their peak values.

4.4. Conclusions

A method for the determination of the pulse time profile for a D-T neutron generator was developed, using spectral discrimination of the scattered neutron background with a ^{4}He scintillation detector. This method could be easily applied for continuous monitoring of the pulse quality in applications of neutron generators that rely on primary pulse characteristics, such as NRTA and DDA. Particularly in the case of DDA, precise knowledge of when the fast neutron background associated with the generator diminishes can have a significant impact on the system sensitivity, as the fission neutron signal is most intense immediately following the pulse.

Chapter 5

Passive and Active Neutron Signatures of ^{233}U for Nondestructive Assay

This chapter is adapted from the 2023 publication in *Physical Review Applied* of the same name by O. Searfus, P. Marleau, E. Uribe, H. Reedy, and I. Jovanovic [106].

5.1. Introduction and Background

Nuclear energy has long been considered a scalable, reliable candidate source of low-carbon electricity to replace fossil fuel-based power sources. In comparison to some other low-carbon sources like solar and wind, nuclear reactors can typically operate consistently independent of weather, time of day, or season. However, nuclear power is inextricably linked to the potential for nuclear proliferation, the risks of which must be mitigated. Proliferation risks are primarily mitigated by the International Atomic Energy Agency (IAEA) using nuclear safeguards as perscribed by the Treaty on the Non-proliferation of Nuclear Weapons (NPT). Non-destructive assay (NDA) methods are well-established and routinely practiced for plutonium, natural uranium (0.7% ^{235}U), and enriched uranium (>0.7% ^{235}U) in traditional light water reactor (LWR) and heavy water (CANDU) fuel cycles [67], [132]. However, some proposed advanced reactors and

fuel cycles pose novel challenges to the current safeguards regime. In particular, there is a lack of NDA technology to adequately safeguard ^{233}U produced in thorium fuel cycles [133], [134], compounded by the requirement that ^{233}U be accounted separately from ^{235}U when the two isotopes are colocated, since States with safeguards agreements in force with the IAEA must report quantities of ^{235}U and ^{233}U separately. [135].

5.1.1. Unique characteristics of ^{233}U in the thorium fuel cycle

Uranium-233 produced in nuclear reactors by the absorption of a neutron in ^{232}Th and the subsequent beta-decays of ^{233}Th and ^{233}Pa is always accompanied by trace quantities of ^{232}U, ranging from approximately 10 to 5000 ppm. This is due to several (n,2n) reactions and subsequent β-decays in ^{232}Th, ^{233}Pa, and ^{233}U which occur in the presence of fast neutrons [136]. The presence of ^{232}U is important, as its decay chain is associated with high specific activity and a high branching ratio for high-energy γ ray emission, principally at 2.6 MeV (^{208}Tl, 35.9% branching ratio) [137]. Since ^{232}U is typically not separated from ^{233}U in thorium-based fuel cycles, this intense γ-ray environment is inextricably linked to any macroscopic quantity of ^{233}U. The activity of the 2.6-MeV γ ray, which is emitted by ^{208}Tl in 99.75% of its decays, with respect to ^{232}U concentration and time since purification is approximated by

$$A_{208}(t, C_{232}) = B_{208} C_{232} \lambda_{232} N_{233} e^{-\lambda_{232} t} [1 - e^{\lambda_{228} t}], \tag{5.1}$$

where C_{232} is the initial ^{232}U concentration, B_{208} is the branching ratio for production of ^{208}Tl, λ_{232} is the ^{232}U decay constant, N_{233} is the ^{233}U population, and λ_{228} is the ^{228}Th decay constant. This approximation is possible since the ^{232}U half-life (69 y) is much longer than the ^{228}Th half life (1.9 y), and all other isotopes in the ^{232}U decay series

have much shorter half lives, on the order of seconds to days [138]. The results of this calculation are shown for a significant quantity (SQ) of ^{233}U (8 kg) [135] in Figure 5.1.

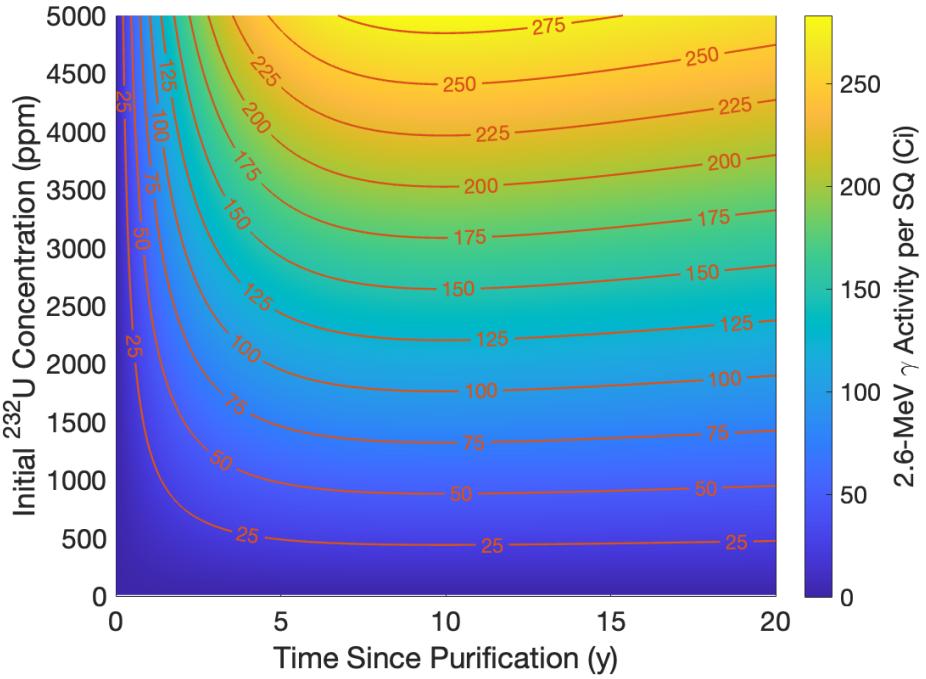

Figure 5.1: Calculated activity of 2.6-MeV γ ray per one significant quantity of ^{233}U (8 kg).

5.1.2. Challenges in measurement of ^{233}U-bearing items for safeguards

Many NDA measurements of fissionable materials conducted for the purpose of nuclear safeguards involve measurement of γ-ray spectra. These measurements may quantify the total mass of some isotope, or measure the relative concentration of isotopes in thick samples. Gamma spectroscopy, however, is not feasible for NDA of ^{233}U items due to the intense contribution of γ rays from the ^{232}U decay chain: the intensity of the 2.6

MeV γ ray line does not strictly correlate with the mass of ^{233}U, and γ rays directly associated with the decay of ^{233}U are low energy and low intensity and consequently not measurable above the Compton continua associated with the ^{232}U lines [134]. As an alternative, neutron-based NDA methods may be useful for safeguarding ^{233}U-bearing materials. Neutron signatures are relatively difficult to shield and generally provide more information about the bulk material as opposed to only the outer "skin" of the material, as may be the case due to self-shielding for γ-ray-based measurements. Some neutron emissions from ^{233}U-bearing materials may arise from (α,n) reactions in the material's chemical matrix, while others relate to the fissionable content of the material, either in aggregate or isotope-specific.

5.1.3. Neutron signatures of ^{233}U-bearing items

Spontaneous neutron emission

Uranium-233-bearing objects of safeguards relevance may be in a material matrix with low-Z elements, such as oxygen (in U_3O_8 or UO_2), lithium, beryllium, or fluorine. Alpha radiation emanating from ^{233}U can be absorbed by low-Z elements, which may then emit a neutron. These (α,n) neutrons typically have spectra that take the shape of continua up to the sum of incident α-particle energy and the Q-value of the (α,n) reaction, reduced by the excitation and recoil energy of the reaction product nucleus. The reaction pathways and average neutron energies of select (α,n) sources are shown in Table 5.1. Some (α,n) spectra contain peaks and other structure, arising from their energy-dependent cross-sections, shown in Figure 5.2. A major caveat to the (α,n)-based approach to ^{233}U NDA is that the content of ^{232}U also contributes to the (α,n) signature of ^{233}U compounds: the half-life of ^{233}U (160 ky) is 2319 times longer than that of ^{232}U (69 y), so the ^{232}U

α-activity is significant even at ppm-scale concentrations. As a result, the α-activity of ^{232}U dominates in ^{233}U samples where the ^{232}U concentration is above approximately 433 ppm. Consequently, in poor-grade (high ^{232}U content) samples, measurements based on (α,n) reactions attribute most of the neutron signal to the non-fissile ^{232}U.

Table 5.1: Potential (α,n) reactions in ^{233}U-bearing compounds. Note that Ref. [139] gives (α,n) spectra for α-radiation from ^{234}U, which is similar to that of ^{233}U.

Element	(α,n) reaction(s)	Q (MeV)	$\overline{E}_n$ for ^{234}U α [139]
O	$^{17}O + \alpha \rightarrow n + {}^{20}Ne$	0.587	2.24
	$^{18}O + \alpha \rightarrow n + {}^{21}Ne$	−0.697	
Be	$^{9}Be + \alpha \rightarrow n + {}^{12}C$	5.702	4.76
Li	$^{7}Li + \alpha \rightarrow n + {}^{10}B$	−2.790	0.33
F	$^{19}F + \alpha \rightarrow n + {}^{22}Na$	−1.952	1.24

The (α,n) neutrons may induce fission in ^{233}U or other fissionable species present, and thereby produce additional neutrons, with a probability determined by the multiplication of the matrix, k_{eff}. Induced fission neutrons have a distinct multiplicity and spectrum from (α,n) neutrons, so the ratio of spontaneous (α,n) to induced fission neutrons can theoretically be measured. Since this ratio is related to multiplication, it may help indicate the fissionable matrix composition.

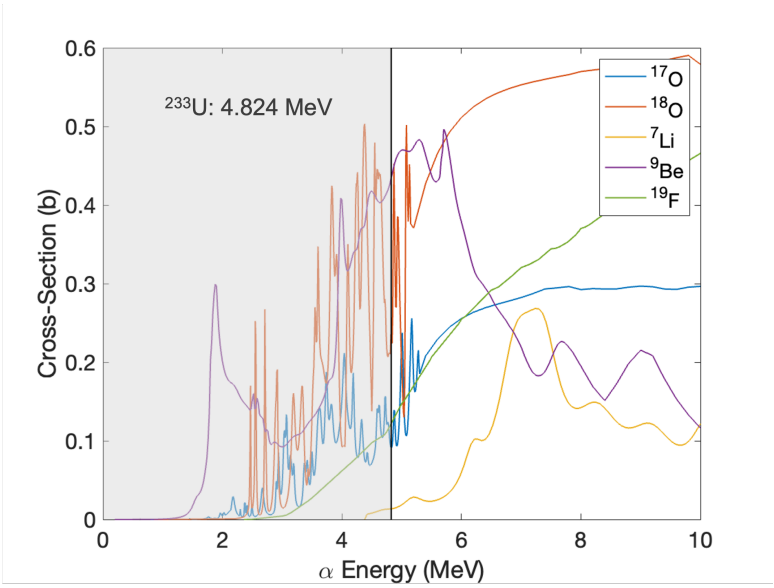

Figure 5.2: (α,n) cross-sections for various low-Z isotopes of interest in the thorium fuel cycle [140]. The shaded area represents possible α energies for ^{233}U, as α-particles lose energy via electronic interaction before interacting with any target nucleus.

Differential die-away

Pulsed differential die-away (DDA) is a technique that measures the presence of fission neutrons emitted by a target after a pulsed active interrogation source is turned off [141]. Neutrons thermalizing in the environment typically have a long life-time compared to the duration of an active interrogation pulse, and the resultant thermal neutron population that persists beyond the fast neutron pulse has a high probability of inducing fission in fissile materials [81]. Measurement of DDA is best done with a detector which is sensitive to fast neutrons only, as the signal-to-noise ratio (SNR) when fissile material is present is orders of magnitude higher for fast neutrons than for thermal neutrons after the pulse [79]. This technique has been previously demonstrated using cadmium-shielded ^{3}He detectors [141] and with organic scintillation detectors [80], [81], the latter

showing a more rapid die-away of the interrogation active background. In the case of ^{233}U and its associated γ-ray environment, however, organic scintillators may not be well-suited, since the probability of pulse pile-up leading to particle misclassification may lead to an unacceptable increase of the observed neutron background, or require extensive digital post-processing [65].

Delayed neutron emission

When nuclei undergo fission, the resultant neutron-rich fission fragments have some probability of emitting neutrons during their radioactive decay [142]–[144]. This process is referred to as β-delayed neutron emission, since these neutrons are emitted in coincidence with β-radiation [145]. There are many delayed neutron precursors, which are typically condensed into six groups determined by their half-lives, ranging from 0.1 to 60 seconds [82]. Each fissionable isotope has a unique yield for each delayed neutron group, resulting in a unique delayed neutron time profile $R(t)$ that can be modeled as

$$R(t) = B + C\sum_{i=1}^{6} Y_i[1 - e^{-t_b/\tau_i}]e^{-t/\tau_i}, \tag{5.2}$$

where B is a constant background, C is a scaling factor, i is the group, Y_i is the group yield, t_b is the buildup or irradiation time, and τ_i is the group mean lifetime, which is equivalent to $t_{1/2,i}/\ln(2)$ where $t_{1/2,i}$ is the group half-life. The delayed neutron group yields for ^{233}U are shown in Table 5.2 and compared against those of ^{235}U. When fission is induced during active neutron interrogation, this time profile can be measured to indicate the isotopic composition of fissionable material [83], [84], and has been shown to be resilient to common neutron shielding [85]. The delayed neutron time profiles for fast neutron-induced fission of ^{233}U and ^{235}U are shown in Figure 5.3

Table 5.2: Normalized delayed neutron group yields and half-lives for fast neutron-induced fission in ^{233}U and ^{235}U. [146]

Isotope	Group	1	2	3	4	5	6
^{233}U	Half-life (s)	55.6	19.3	5.04	2.18	0.57	0.221
	Yield	0.095	0.208	0.242	0.327	0.087	0.041
^{235}U	Half-life (s)	54.6	20.2	5.36	2.38	0.77	0.24
	Yield	0.057	0.192	0.190	0.357	0.120	0.084

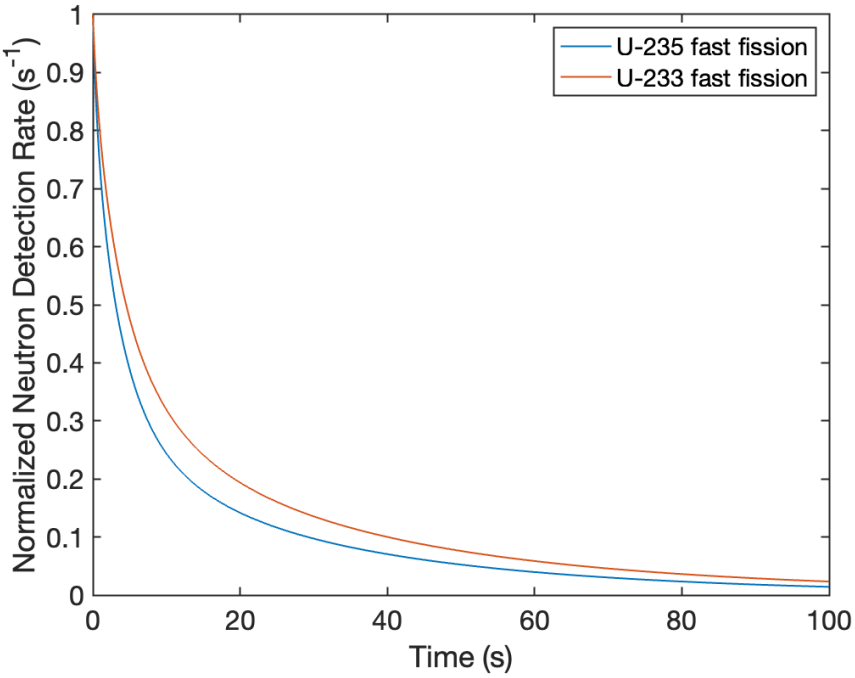

Figure 5.3: Delayed neutron time profiles for fast neutron-induced fission of ^{233}U and ^{235}U, from Eq. (5.2) and Table 5.2, assuming 60 s of irradiation. The neutron reaction rates are normalized to their values at $t = 0$.

5.2. Methods

In this work, measurement of the neutron signatures of ^{233}U took place at the National Criticality Experiments Research Center (NCERC), an experimental venue at the Nevada National Security Site (NSSS) which holds a variety of test objects containing nuclear materials.

5.2.1. Target and interrogation source

The material used in the experiments described in this work was a set of fuel plates fabricated for the Zero Power Reactor (ZPR) at Argonne National Laboratory. These plates comprise 33 g $^{233}U_3O_8$ powder in stainless steel packets measuring $2 \times 3 \times 1/4$ " [147]. The plates are stored in groups of twelve in steel "soup cans", three of which are stored in a triangular lattice within an AT-400R radioisotope storage container. In these measurements, the ZPR plates could not be removed from their AT-400R container, which also contains a 1.5" lead pig around the cans. Each AT-400R container holds a total of 1.188 kg $^{233}U_3O_8$, approximately 984 g of which is ^{233}U. The ^{233}U used to fabricate these ZPR plates was produced with low ^{232}U contamination, the average of which in all plates is 7 ppm. Even at this low concentration, the radiation exposure rate due to ^{232}U daughters at equilibrium in a single plate is 1000 mR/h, measured 1.5" from the center of the plate surface. Among all 36 plates, the total ^{232}U activity is approximately 157 mCi, and the corresponding ^{208}Tl activity is 56.5 mCi. At this exposure level, most γ-sensitive detectors cannot be operated due to pulse pile-up issues. In this experiment, a single AT-400R containing 36 $^{233}U_3O_8$ ZPR plates was characterized. Due to the weight of the container and its lead pig, it was placed on the concrete floor of the laboratory.

The D-T generator used as an interrogation source was a Thermo Scientific model P211. This generator has a nominal total output of 10^8 n/s, in pulses of approximately 10 µs duration, operating up to 100 Hz. This low duty cycle and high pulse intensity is advantageous for DDA analysis, as the instantaneous neutron output during pulses is high, and there is sufficient time for the neutron population to decay between pulses.

5.2.2. Neutron detectors

To detect the fast neutron signatures corresponding to passive (α,n) emissions and active interrogation DDA, an Arktis Radiation Detectors S670 [94] high-pressure ^{4}He scintillation detector was used. This detector is intrinsically sensitive to only fast neutrons if an energy deposition threshold of approximately 300 keV is used [105], measures the energy of fast neutron-induced ^{4}He recoils, and in doing so provides information on the incident neutron spectrum. This detector has a faster response time, smaller dead-time, and better time resolution than most gas-based detectors based upon collection of ionization signal, since the ^{4}He scintillation pulses have a duration of approximately 1 µs. The detector and pulse analysis system applied is described in greater detail in Ref. [97].

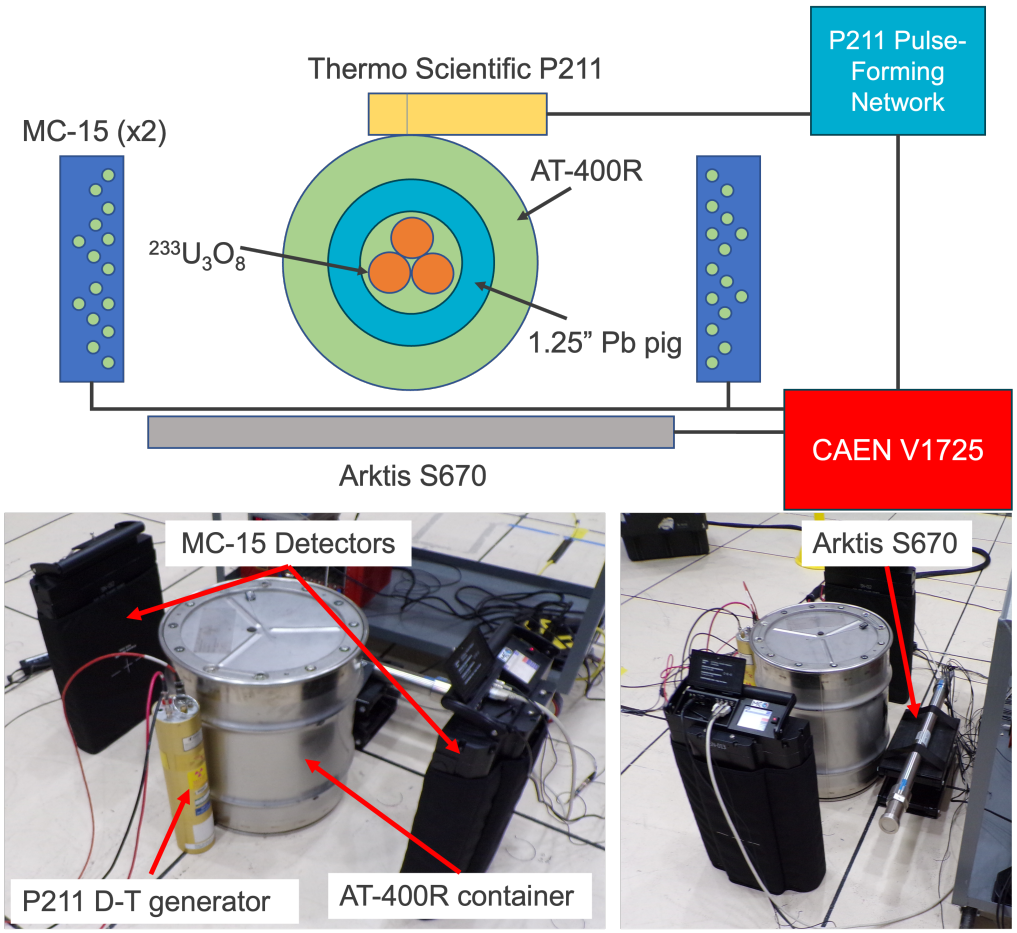

Figure 5.4: Conceptual diagram illustrating the arrangement of detectors and electronics used to measure the ^{233}U plates (above). Images of the measurement setup at NCERC (below).

Two MC-15 neutron multiplicity counters were also used to measure the delayed neutron time profile of the $^{233}U_3O_8$ plates. MC-15 detectors comprise an array of 15 ^{3}He proportional counters embedded in a slab of high-density polyethylene (HDPE) and are sensitive to a wide range of neutron energies [148]. They are self-contained, do not require any external electronics to function, and provide a logic (TTL) pulse output for each neutron detection event. These detectors are efficient in detecting neutrons in

the energy range of delayed neutrons (≈1 keV to 2 MeV [145]), but because they must thermalize neutrons before detecting them, their time resolution is poor compared to the S670 detector. Consequently, MC-15 detectors were used to measure the time profile of delayed neutrons, but not DDA. The measurement configuration, showing the target material, interrogation source, and detectors are shown in Figure 5.4.

5.2.3. Electronics and experimental operation

A CAEN V1725 14-bit, 250 MS/s digitizer and CAEN CoMPASS 2.0 software [102] were used to collect waveforms from the S670 and MC-15 detectors. The P211 D-T generator has analog control, and was configured to run at 100 Hz for 6,000 pulses. A trigger out logic signal from the P211 pulse-forming network, approximately 10 µs prior to neutron production, was also digitized. To measure the DDA time profile, the time period between events in the S670 detector and the most recent logic signal from the pulse-forming network were considered (i.e., between pulses), whereas for the delayed neutron time profile, the time period between events in the MC-15 detectors and the 6,000$^{\text{th}}$ logic signal were considered (i.e., after the D-T generator was turned off). While the P211 settings ideally correspond to a total irradiation period of 60 s, it was observed that the actual pulse frequency of the generator was approximately 107 Hz, corresponding to an actual irradiation period of 56 s.

The passive fast neutron emission signature of the $^{233}U_3O_8$ plates was measured using the S670 detector for a total period of 1200 s, and also provided the passive background for measurement of the DDA signature. To measure DDA and delayed neutron emission, 40 irradiation cycles were carried out. The irradiation cycle period was 300 s, of which 56 s corresponds to pulsed irradiation to build up the delayed neutron precursor

population and measure the DDA signature, and the remainder corresponds to D-T generator off time, which allows for measurement of the delayed neutron time profile. An additional 10 irradiation cycles were performed with the AT-400R container removed, to serve as an active background for the DDA measurement. The analysis shown in this work represents the data from all irradiation cycles in aggregate.

5.2.4. Monte Carlo Simulation

The DDA and DN signatures of the $^{233}U_3O_8$ plates were simulated using MCNPX-PoliMi [110], [111]. The geometry of the AT-400R container, shielding, and its contained ZPR plates is based on Refs. [149], [150] and is shown in Figure 5.5. The P211 D-T generator was approximated as a monoenergetic 14.1-MeV isotropic point source. In post processing, the temporal behavior of the neutron source was approximated by adding time randomly sampled from a 10 µs-wide uniform distribution to each history in the PoliMi collisional output file. To simulate the delayed neutron time profile, neutron emissions from the ^{233}U plates that occur more than 10 ms after the D-T generator pulse were recorded, since delayed neutron emissions occur on such a long time scale that their time signature is immune to radiation transport-induced time distortion effects. To approximate the effect of the D-T generator irradiation period, time randomly sampled from a 56 s-wide uniform distribution was added to the delayed neutron histories.

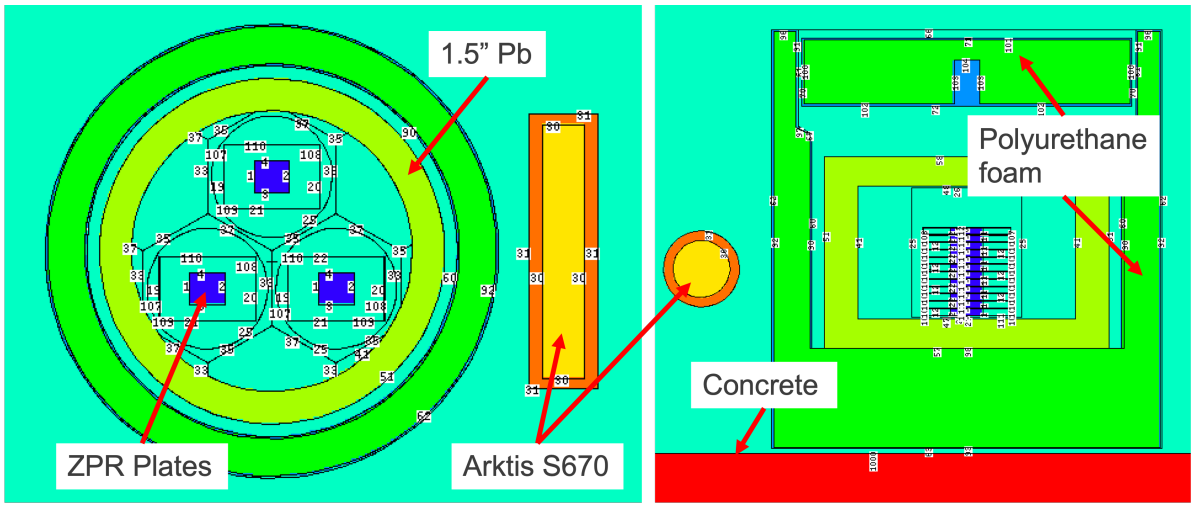

Figure 5.5: MCNP geometry for simulation of DDA and DN signatures.

5.3. Results

5.3.1. Passive signatures

The passive spectrum of $^{233}U_3O_8$ is shown in Figure 5.6 and compared against a ^{252}Cf spontaneous fission neutron source, as measured with the S670 ^4He detector. The neutron source emanating from the $^{233}U_3O_8$ plates exhibits a characteristically lower-energy end-point when compared to the ^{252}Cf fission source, as is expected from $^{17,18}O(\alpha,n)$ reactions. The intensity of this ^{233}U O(α,n) spectrum is proportional to ^{233}U mass at low concentrations of ^{232}U and at low multiplication, and is consequently a potential candidate for NDA of ^{233}U under these circumstances.

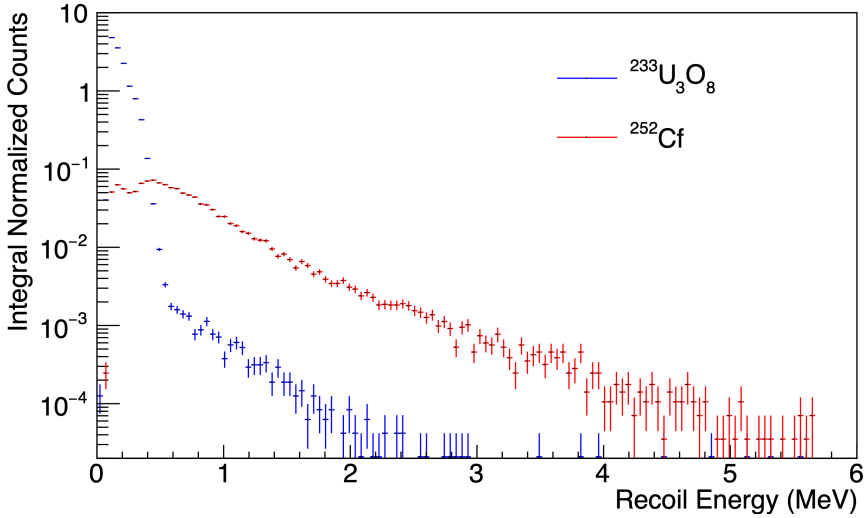

Figure 5.6: Passive fast neutron spectral signature of $^{233}U_3O_8$ measured with the S670 ^{4}He detector, compared to the measured spectrum of ^{252}Cf. The spectra are normalized to their integral above 300 keV energy deposition, above which there are no contributions from γ-radiation.

5.3.2. Differential die-away

The DDA microscopic time profile of the ZPR plates measured with the S670 ^{4}He detector is shown in Figure 5.7 and compared against the sum of active and passive backgrounds. Only pulses corresponding to at least 300-keV recoil energy deposition were accepted in generating DDA time profiles, for both measurement and simulation. The fission neutron signal remained visible above background for about 1200 µs after the generator pulse, in agreement with simulation. The measured DDA time profile shows a clear exponential decay significantly above the background, implying that DDA measured with this detector may be a strong candidate for confirmation of the presence of ^{233}U. At low multiplication, the fast neutron DDA signal intensity is proportional to fissile mass, so this technique may be used for quantification of total fissile content in the

presence of ^{233}U, in the case that the measurement and neutron moderation geometries are tightly constrained.

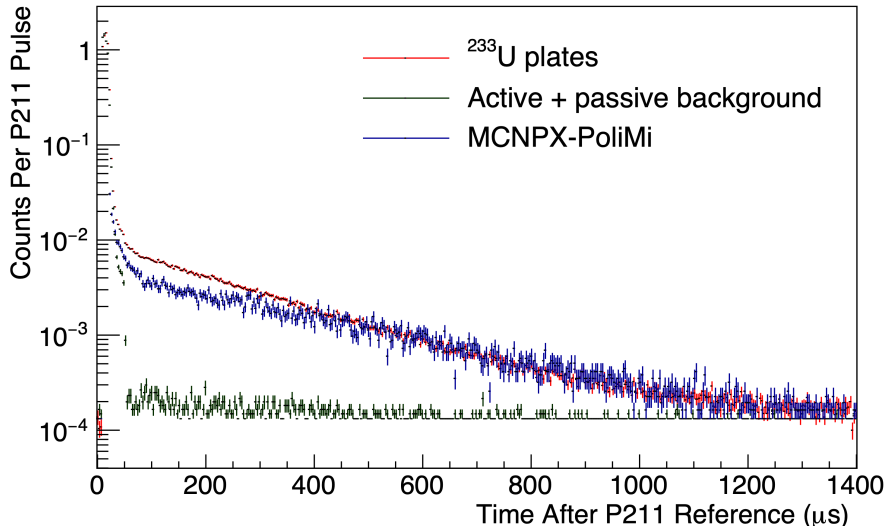

Figure 5.7: DDA measurement of ZPR plates with the S670 ^{4}He detector, compared against background and simulation.

5.3.3. Delayed neutrons

The delayed neutron time profile of ^{233}U measured with the MC-15 detectors is shown in Figure 5.8, and compared to the simulated time profile. The time profiles are fit to Eq. (5.2), with tabular delayed neutron yields and half-lives for ^{233}U for 14.1 MeV neutrons given in Table 5.2. The only fitting parameters used are the scaling factor C and the flat constant background B. To demonstrate the uniqueness of these fits to delayed neutrons from ^{233}U specifically, the fit results when the time profiles are forced to fit delayed neutron yield parameters for other fissionable isotopes are shown in Table 5.3. Both the measured and simulated time profiles are best fit by the delayed neutron parameters for ^{233}U, however, the distinction is clearer in the simulated time

profile, likely due to its superior statistics and lack of passive background.

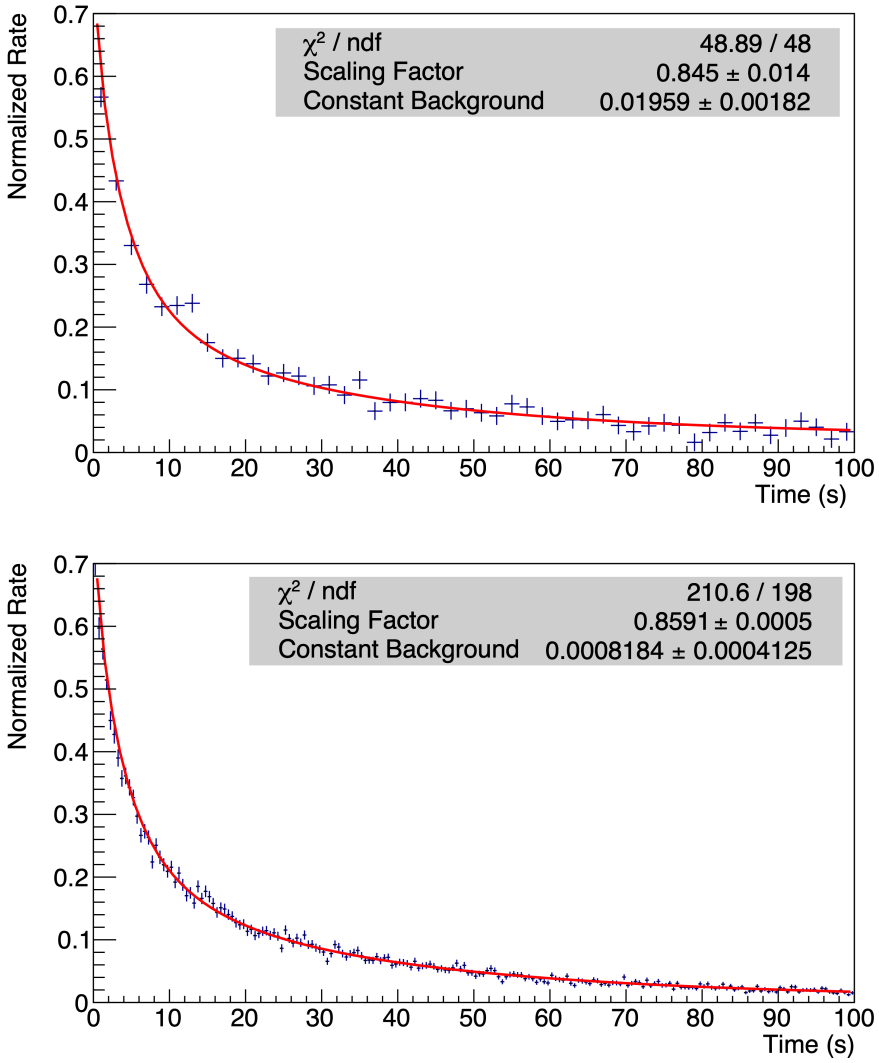

Figure 5.8: Delayed neutron decay measurement of ZPR plates as measured with MC-15 detectors (above) and simulated with MCNPX-PoliMi (below). Time profiles are normalized to the sum of the first four seconds. The measured time profile has 2 s-wide bins, while the simulated time profile has 0.5 s-wide bins. Fits to Eq. (5.2) and Table 5.2 are shown in red.

Table 5.3: Results of fitting delayed neutron data in this work to various fissionable isotope delayed neutron parameters. Parameters for ^{233}U and ^{235}U from Ref. [146], for ^{238}U from Ref. [151], for ^{239}Pu from Ref. [152], and for ^{232}Th from Ref. [153].

Isotope	Dataset	C	B	χ^2/ndf
^{233}U	measured	0.8450 ± 0.0140	0.0196 ± 0.0018	48.9 / 48
^{235}U		0.9146 ± 0.0172	0.0249 ± 0.0021	58.6 / 48
^{238}U		1.454 ± 0.080	0.0008 ± 0.2615	547 / 48
^{239}Pu		0.9288 ± 0.0046	0.025 ± 0.002	65.3 / 48
^{232}Th		1.012 ± 0.005	0.0306 ± 0.0018	96.0 / 48
^{233}U	MCNPX-PoliMi	0.8591 ± 0.0005	0.00082 ± 0.00041	211 / 198
^{235}U		0.9202 ± 0.0007	0.0064 ± 0.0004	294 / 198
^{238}U		1.152 ± 0.007	0.0138 ± 0.0003	936 / 198
^{239}Pu		0.9369 ± 0.0064	0.0062 ± 0.0003	369 / 198
^{232}Th		1.031 ± 0.009	0.0109 ± 0.0006	777 / 198

5.4. Conclusions and future work

In this work, three novel signatures of ^{233}U were investigated for their feasibility in future NDA methods for international safeguards of thorium fuel cycles: passive fast neutron spectroscopy, differential die-away analysis, and delayed neutron time profile analysis. An experiment was performed to measure these signatures at NCERC, using nearly a kilogram of ^{233}U in the form of $^{233}U_3O_8$, representing the largest-scale NDA measurement of ^{233}U to date.

The fast neutron spectral signature of $^{233}U_3O_8$ is shown to be readily measurable

with the γ-insensitive S670 ^{4}He detector, and clearly differentiable from a generic spontaneous fission neutron source. Consequently, this technique could be well-suited to discriminating between oxides of ^{233}U and plutonium, for example.

Measurement of the fast neutron DDA time profile of ^{233}U was also demonstrated with the S670 detector and a pulsed D-T neutron generator for the first time, indicating a potentially unique capability of the ^{4}He scintillation detector.

The delayed neutron time profile of ^{233}U, induced using the same D-T neutron generator, was measured using an array of moderated ^{3}He proportional counters. The measured time profile showed a good fit to the time profile generated from nuclear data, and matched the simulated time profile. Delayed neutron time profiles are isotope specific, so their measurement may allow for discrimination between and separate quantification of ^{233}U and ^{235}U, which is one of the primary challenges in NDA for safeguarding thorium fuel cycles. In future work, delayed neutron-based techniques should be further investigated with mixed-isotope (^{233}U and ^{235}U) items, so that separate isotope quantification can be demonstrated.

Chapter 6

Detection of Uranium Photofission Neutrons with a ^{4}He Scintillation Detector

This chapter is adapted from the manuscript under review of the same name by O. Searfus, C. Meert, S. Clarke, S. Pozzi, and I. Jovanovic [154].

6.1. Introduction

Photon active interrogation (PAI) is a powerful, highly penetrating technique that uses energetic X rays to induce photofission in special nuclear material (SNM) and produce characteristic fission signatures, including high-energy neutrons [79], [155], [156]. While fast neutrons are routinely observed in detectors that employ elastic scattering, the intense photon environment associated with PAI poses a challenge to most conventional fast neutron detectors. The sensitivity of PAI techniques can be improved if the fast neutron spectrum is measured such that photofission neutrons can be separated from the low-energy fast neutron background produced by photonuclear reactions in the interrogating source and the environment. The most common detectors that offer neutron spectroscopic capability, pulse-shape discrimination (PSD)-capable organic scintillators, are also highly sensitive to photons and are typically overwhelmed by the direct or scat-

tered photons from the interrogation source.

6.1.1. Applications of photon active interrogation

The detection of uranium is a problem of particular interest for nuclear nonproliferation [157], safeguards [67], [158], security [159], and arms control [160]. Compared to plutonium, which spontaneously emits significant neutron and gamma radiation, the passive emissions of uranium are of low intensity and are easily shielded, with the primary radiation signature of ^{235}U being the 186-keV photon [68]. Active interrogation can be used to induce more intense and penetrating signatures of uranium [79], [80], enabling its detection even when shielding inhibits the passive emissions. Photofission has an energy threshold of approximately 5 MeV for uranium isotopes, such that photon sources with a component of the spectrum above this energy can induce fission. The principal signatures of induced fission are from fission neutrons, whose energy is distributed according to the Watt spectrum, typically between 100 keV and 10 MeV, and whose multiplicity distribution is unique to the fissioning isotope.

6.1.2. Photon sources for active interrogation

Photon interrogation sources must be sufficiently energetic to induce photonuclear reactions and penetrate potential shielding, and sufficiently intense to produce statistically significant neutron emissions in a timely manner. Bremsstrahlung sources are typically used for active interrogation applications because linear accelerators (linacs) can accelerate electrons to energies of 6 MeV or greater within a convenient form factor. Similar bremsstrahlung sources are widely available because they are also used in medical applications such as radiation oncology [161]. The bremsstrahlung spectrum emitted from

multi-MeV linacs peaks at 511 keV due to pair production and positron annihilation prevalent in the bremsstrahlung converter and has a long tail extending to the endpoint energy, *i.e.*, the incident electron energy. Because relatively few photons are near the endpoint, interrogation sources should have energies significantly higher than the threshold(s) of interest. For example, although a 6-MeV bremsstrahlung source can induce photofission in uranium, a 9-MeV source yields a greater number of photons with energies $\gtrsim$5 MeV, which produces a stronger photofission signature. Inverse Compton scattering sources are under development and may be capable of yielding high-energy, quasi-monoenergetic photon sources to avoid this issue [162]; however, existing systems are not technologically mature or widely available.

6.1.3. Effects of photon background

Because photon interrogation sources are typically intense, pulsed sources, the photon background is orders of magnitude greater than the natural background. They are difficult to shield due to the penetrative nature of high-energy photons, so the background they produce is similar in energy to the linac photon energy spectrum. Furthermore, the vast majority of the bremsstrahlung energy spectrum is below the photofission threshold, such that most interrogation photons contribute to the background without contributing to the desired signal.

When using traditional fast neutron detectors, such as organic scintillators, the active photon background is typically so intense that any fast neutron signal is obscured by the γ ray flash, which induces significant pulse pile-up. Several approaches, typically applied in combination, have been investigated to mitigate the photon background in organic scintillators in these scenarios. The first approach is to utilize thick heterogeneous

shields consisting of a thick layer of lead, which absorbs the incident photons, followed by thin tin and copper layers, which absorb the secondary lead X-rays that escape the primary shielding [64], [66]. The primary disadvantage of this approach is the scattering of incident neutrons away from the detector by the shield. The second approach is to finely segment the detector volume, such that each detector element has a relatively small detection efficiency for photons, which reduces the probability of pile-up [163], at the cost of increased data acquisition channels for an equivalent volume monolithic detector. The third approach is to utilize computational algorithms to remove or recover piled-up pulses in the post-processing data analysis, often using artificial neural networks [66], [164]. This approach can be effective; however, it introduces a significant increase in the computational overhead which may inhibit its use in certain applications.

6.1.4. Neutron backgrounds

Because the primary observable signature of SNM in PAI are fission neutrons, characterization of the neutron background – both passive and active – is crucial in determining the sensitivity of a PAI-detector system. In the case of ^{235}U and ^{238}U, the passive neutron emission rate is very low: their spontaneous fission (SF) half-lives are 1.05×10^{19} and 8.27×10^{13} years, respectively. On the other hand, active neutron backgrounds associated with PAI photon sources are relatively intense. Typically, these photon sources use high-Z collimators and beam-stops for operator safety, almost always constructed from lead. Two of the most abundant lead isotopes, ^{206}Pb and ^{207}Pb, have (γ,n) reaction energy thresholds and microscopic cross-sections similar to those for photofission in uranium isotopes. As a result, there is always some (γ,n) neutron active background (ABG) associated with linac photon sources. In contrast to fission, (γ,n) processes in

lead are endothermic, such that the resultant neutron energy is simply the difference between the source photon energy and the neutron separation energy [165]. This effect manifests as a definite end-point in the (γ,n) neutron spectrum, compared to the high-energy tail of the fission neutron spectrum. As a result, (γ,n) neutrons can generally be discriminated from photofission neutrons based on their energy. The cross-sections for photofission in uranium isotopes and (γ,n) in select lead and iron isotopes are shown in Figure 6.1, and a conceptual illustration of the PAI signal and background neutrons is shown in Figure 6.2.

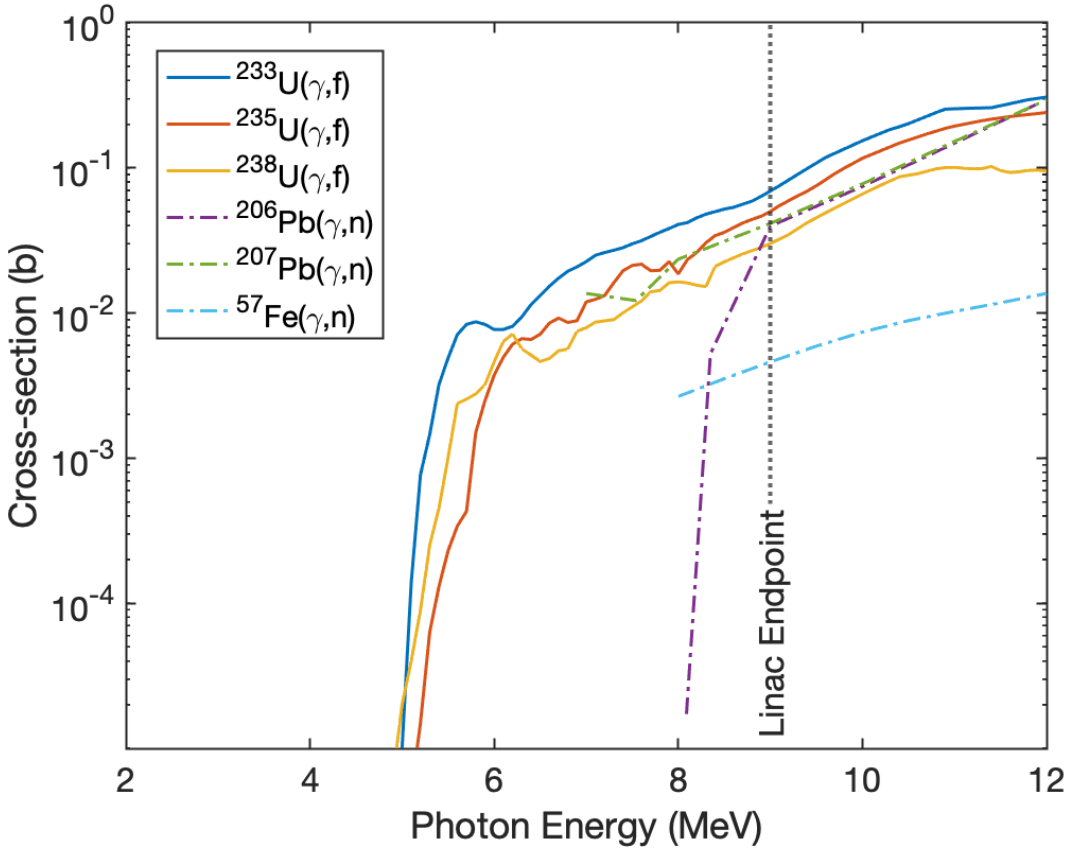

Figure 6.1: Photonuclear cross-sections of select uranium, lead, and iron isotopes [19]. The endpoint of the linac spectrum used is also shown.

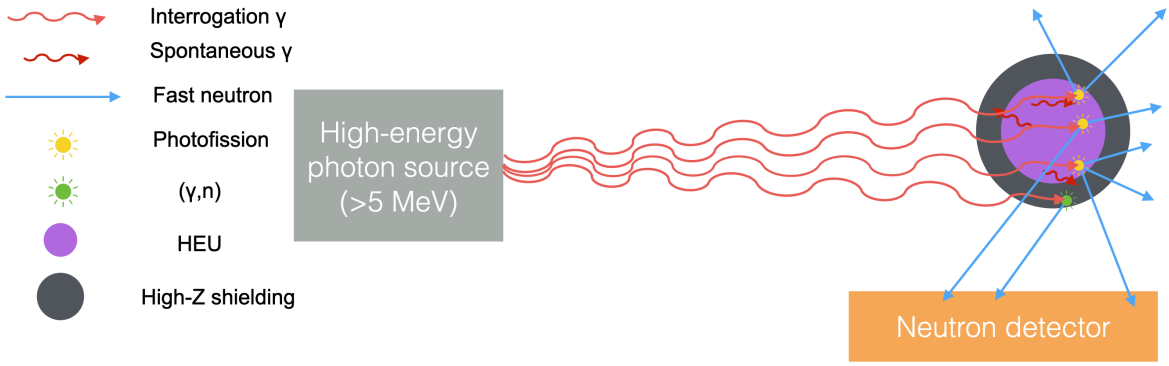

Figure 6.2: Concept of photon active interrogation for detection of highly-enriched uranium (HEU).

6.1.5. Helium-4 scintillation detectors

Gaseous ^{4}He-based detectors have been previously demonstrated for fast neutron detection, either as proportional counters [86] or, more recently, as high-pressure scintillators [91], [92], [97], [101]. Similarly to organic scintillators, the fast neutron signal appears as a nuclear recoil upon elastic scattering. Unlike organic scintillators, ^{4}He-based scintillators are in the low-density gas phase and are thus relatively insensitive to γ rays: in such a low-density, low-Z gas, γ rays have a low interaction probability, and in the case that a γ ray interacts in the detector wall and injects an electron into the gas active volume, the range of electron is typically much longer than the detector dimensions, limiting the energy deposition. In contrast, ^{4}He recoils resulting from fast neutron elastic scattering have ranges that are short in comparison to the detector dimensions. A comparison of ^{4}He recoil and electron ranges in 190-bar helium gas is shown in Table 6.1. ^{4}He-based detectors have been investigated for use in extreme γ ray environments, such as measurement of ^{233}U [106] and spent nuclear fuel [95].

Table 6.1: Select ranges of ^{4}He recoils and electrons in 190-bar helium gas. The ^{4}He and electron ranges are taken from NIST ASTAR and ESTAR [112].

Range	^{4}He recoil	e^-
0.1 MeV	40 µm	47 mm
0.5 MeV	102 µm	58.7 mm
1 MeV	163 µm	145.7 mm
2 MeV	314 µm	324.7 mm
5 MeV	1.07 mm	832.4 mm
10 MeV	3.3 mm	1.6 m

6.2. Methods

High-pressure ^{4}He scintillators are commercially available from Arktis Radiation Detectors Ltd. For this experiment, the model S670 detector was used [94], which operates at ≈190 bar and has an active length of 60 cm, which is subdivided into three optically segmented regions. The scintillation signal in each segment is read out with an array of eight silicon photomultipliers (SiPM) along the axis of the detector, which are summed in pairs, resulting in four output channels for each segment. In this measurement, the output channels from the central segment were condensed into a single data list and calibrated using the D-D and D-T spectral endpoints according to the procedure in Ref. [97].

6.2.1. γ-ray rejection

A method based on Ref. [166] was followed to measure the γ-ray rejection capability of the ^{4}He detector and compare it to a 5.08 cm diameter, 5.08 cm height EJ-309 liquid organic scintillation detector [109]. The detectors were exposed to a ^{252}Cf spontaneous fission neutron source emitting $\sim 4.4 \times 10^{6}$ n/s at a distance of 150 cm, as shown in Figure 6.3. This measurement was then repeated with the addition of a combination of ^{137}Cs, ^{60}Co, and ^{22}Na γ-ray sources, which yielded an exposure rate of ∼20 mR/h on contact with the detector, as measured with a Fluke 451B survey meter.

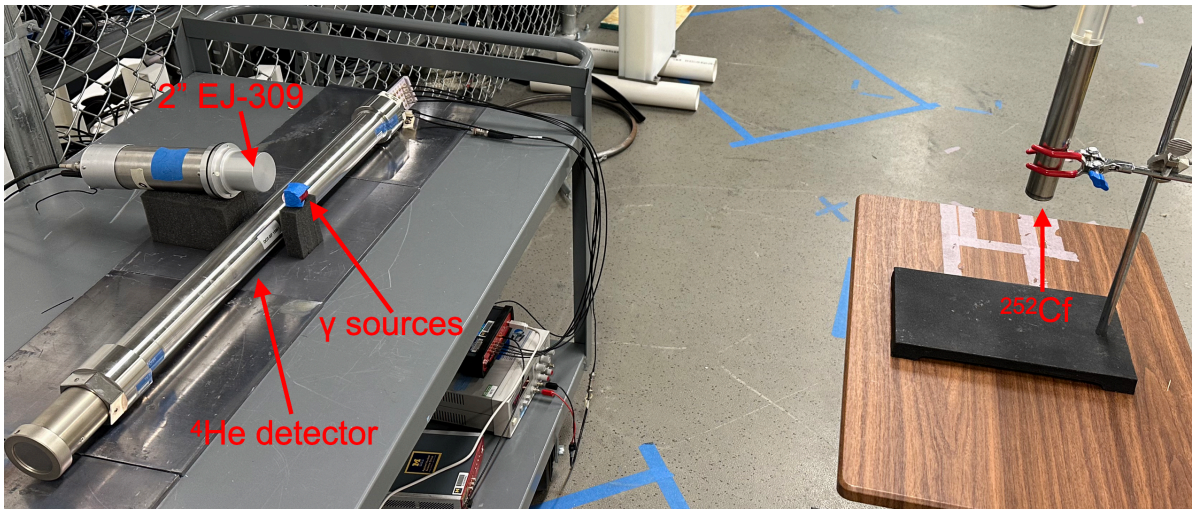

Figure 6.3: Detector configuration for measurement of γ-ray rejection.

This procedure defines the *gamma absolute rejection ratio for neutrons (GARRn)* as $\epsilon_{n\gamma}/\epsilon_{n}$, where $\epsilon_{n\gamma}$ is the neutron detection efficiency for the ^{252}Cf source measured with the additional γ-ray sources, and ϵ_{n} is the neutron detection efficiency for the ^{252}Cf source alone. Ref. [166] requires $0.9 < GARRn < 1.1$ for neutron counters in γ-ray environments. If the geometry and laboratory conditions are maintained between these two measurements, GARRn simplifies to $r_{\gamma n}/r_{n}$, where r is the count rate. Gamma-ray

rejection is dependent on the threshold, *i.e.,* the minimum energy deposition in the detector. Consequently, GARRn is described as a function of this energy threshold,

$$GARRn(E_{min}) = \frac{\int_{E_{min}}^{\infty} r_{n\gamma}(E)dE}{\int_{E_{min}}^{\infty} r_n(E)dE}, \tag{6.1}$$

where E is deposited energy and E_{min} is the energy threshold. The energy deposition threshold at which the requirement of $0.9 < GARRn < 1.1$ is met is selected for operation.

6.2.2. Photon source

The photon interrogation source used in the experiments was a Varex M9 linear accelerator (linac) [167]. The linac produces electrons with an energy of 9 MeV, but the resulting bremsstrahlung spectrum is relatively soft, with only $\sim 4\%$ of emitted photons above the threshold for photofission in ^{238}U or (γ,n) reactions in lead. The beam is collimated with lead and tungsten, which results in nuisance neutron emissions, or *active background neutrons* (ABG).

We simulated the experimental laboratory space using the MCNPX Monte Carlo code [110]. The laboratory model was initially developed to quantify dose rates as part of facility licensing [168]. The linac is simulated as a directional photon source: first, a direction relative to the electron beam is sampled, and then the corresponding photon energy is sampled. Because photonuclear thresholds for lead are ≈7 MeV and the photofission threshold for ^{238}U is ≈5 MeV [169], many of the bremsstrahlung photons produced by the linac are incapable of producing neutrons. Using source biasing, to increase the simulated production of high-energy photons, and photonuclear biasing, which forces the photonuclear reactions to occur when possible, neutron production can

be simulated with less computational expense than an unbiased Monte Carlo simulation.

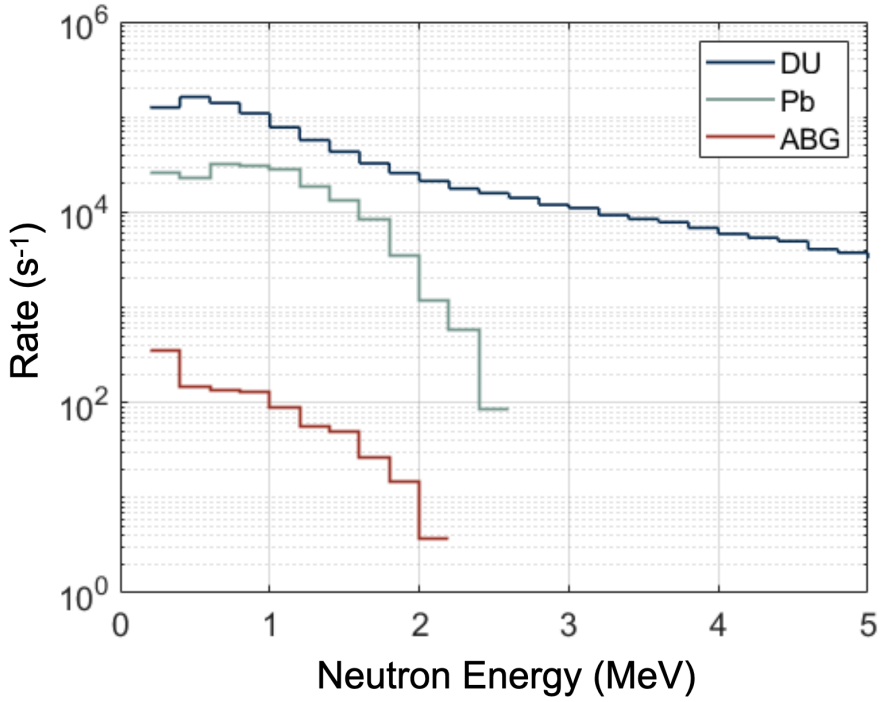

Figure 6.4: Simulated neutron spectra emitted from the irradiation target.

6.2.3. Photofission neutron measurement

Several targets were irradiated to assess the discrimination of photofission neutrons from other photonuclear reactions and expected backgrounds with the ^{4}He detector. The centroids of the targets were aligned with the center of the beamline 6.1 m from the collimator face, as shown in Figure 6.5. The ^{4}He detector was then placed 1.66 m from the target, with the axis of the detector parallel to the beamline. While the ^{4}He detector is much less sensitive to γ rays than organic scintillators, the high intensity of the linac photon source still produces a substantial signal rate in the detector without mitigation. Consequently, a modest shield was constructed to contain the ^{4}He detector, comprised of 5.08 cm lead on the sides of the detector, and 1 cm lead above and below

the detector.

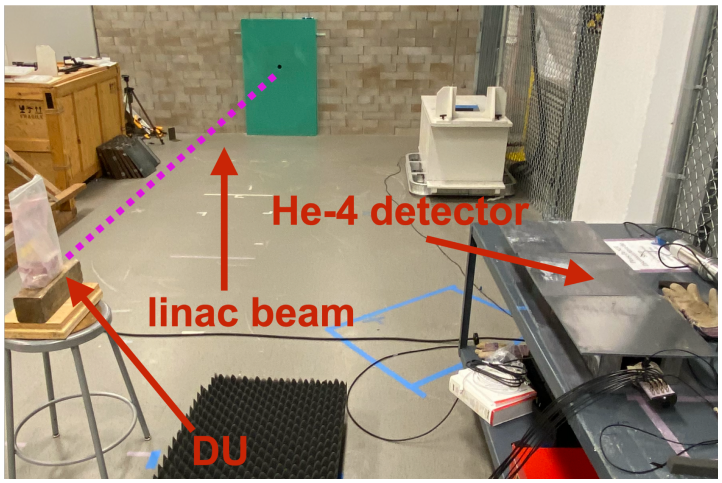

Figure 6.5: Active interrogation measurement configuration.

A 2.8 kg cube of depleted uranium (DU) was irradiated to produce photofission neutrons and serve as a surrogate for several fissile nuclides of interest, such as ^{235}U, ^{233}U, and ^{239}Pu. A 2 kg block of natural Pb was irradiated to produce (γ,n) neutrons, whose spectrum represents the most likely source of active background in linac-based PAI systems. A 2 kg block of natural iron was also irradiated to serve primarily as a scatterer/absorber of γrays, as only ^{57}Fe (2.12% abundance) is capable of (γ,n) reactions with a 9-MeV bremsstrahlung source. However, the iron increases the γ-ray flux at the detector location by scattering photons out of the beamline. Furthermore, it is desirable to understand the response of a PAI system to iron, as it is commonly encountered in the form of steel containers for nuclear materials and benign cargo.

6.3. Results

6.3.1. Photon rejection

The organic scintillator PSD performance in response to ^{252}Cf neutrons, with and without the additional γ-ray sources, is shown in Figure 6.6. The effect of significant pulse pile-up is clear when the additional γ-ray sources are present, particularly at low energies, where there is not a clear band corresponding to neutrons. Some neutron events are distinguishable at high energy; however, these appear with reduced intensity compared to the ^{252}Cf source alone. This result is likely due to the increased probability that real neutron pulses of all energies are contaminated with γ ray pulse pile-up, removing them from the neutron band.

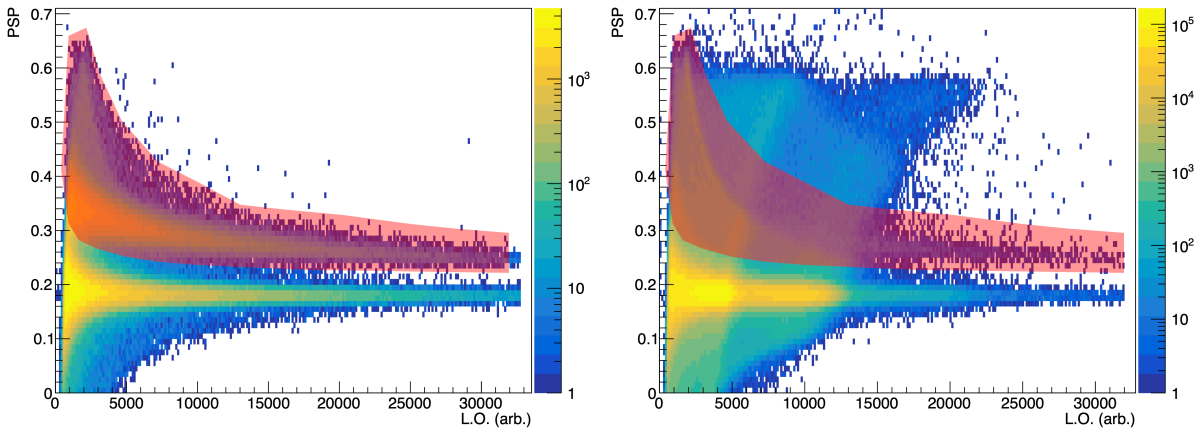

Figure 6.6: Histograms of pulse shape parameter (PSP) and light output (L.O.) for (left) the ^{252}Cf source alone and (right) with additional γ-ray source measured with the organic scintillation detector. PSP was calculated using the tail-to-total ratio method, with a 16-ns short gate and 120-ns long gate. The shaded area represents the neutron acceptance cut.

The ^{4}He recoil spectra and the organic scintillator light output spectra in response to

the ^{252}Cf source with and without γ-ray sources are shown in Figure 6.7. The two spectra from the ^{4}He detector clearly converge above approximately 300 keV recoil energy, whereas the two spectra from the organic scintillator do not converge in any energy range. This is further reflected in the calculated GARRn over a range of energy deposition thresholds shown in Figure 6.8, with the ^{4}He detector achieving a stable GARRn value of 1 at a deposited energy threshold $\gtrsim$300 keV, whereas the GARRn for the organic scintillator does not stabilize with any energy deposition threshold, transitioning from an overestimate of the neutron spectral intensity below about 1.2 MeVee to a degradation of the neutron detection efficiency above this energy. From this result, it is clear that the ^{4}He detector is well-suited for normal operation in substantial γ-ray environments in which organic scintillators require significant additional measures to mitigate pulse pile-up.

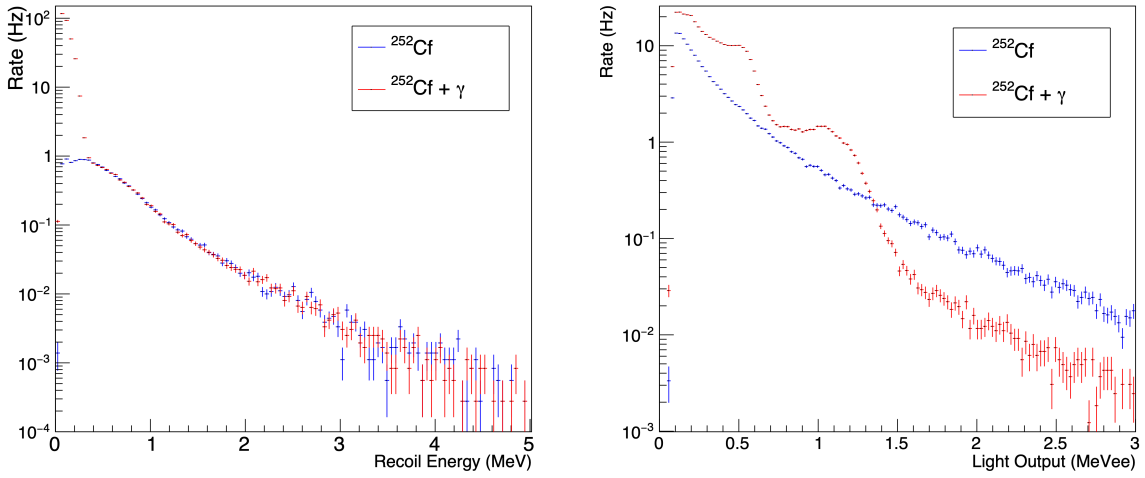

Figure 6.7: Comparison of ^{252}Cf spontaneous fission neutron spectrum with and without additional ∼20 mR/hr γ-ray source for (left) the ^{4}He detector and (right) organic scintillation detector. Only events within the neutron acceptance cut are shown for the organic scintillator.

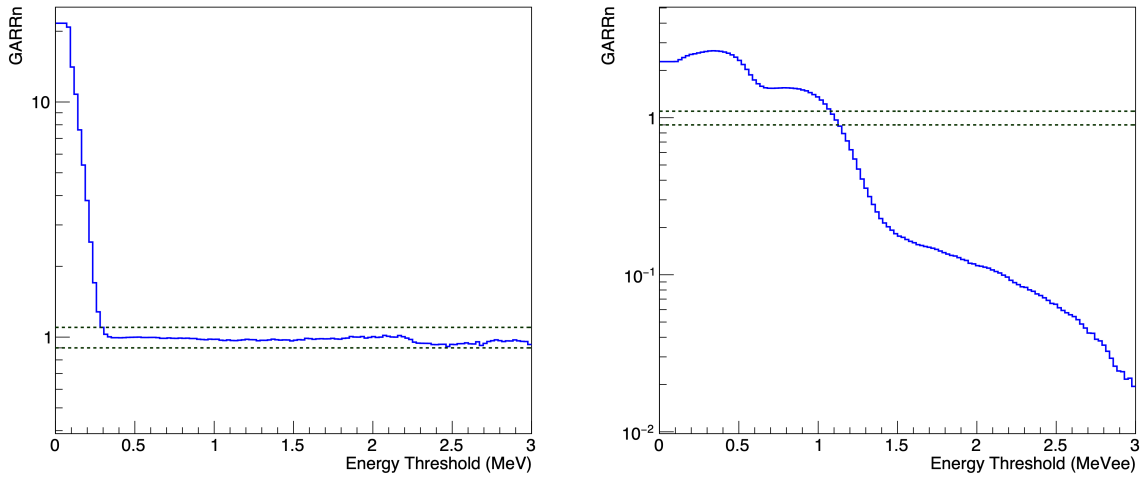

Figure 6.8: GARRn as a function of energy threshold in (left) the ^{4}He detector and (right) the organic scintillation detector. The dashed lines represent the $0.9 < GARRn < 1.1$ requirement.

Since increasing the energy deposition threshold corresponds to a decrease in the neutron detection efficiency, it is desirable to select the minimum threshold that satisfies the requirement of $0.9 < GARRn < 1.1$. For the ^{4}He detector, as evidenced in Figure 6.8, this minimum threshold is 300 keV.

6.3.2. Discrimination of photofission neutrons from photons and (γ,n) neutrons

The energy spectra measured in the ^{4}He detector of the DU, Pb, and Fe sources, interrogated by the linac, along with the ABG and passive background (PBG), are shown in Figure 6.9. The DU spectrum, and to a lesser extent the Pb spectrum, are evident above the active background at energies $\gtrsim$300 keV. The DU spectrum also has an endpoint at higher energy than Pb, which is consistent with the expected difference between

^{238}U(γ,f) and Pb(γ,n) neutron source spectra. The Fe signal is marginally above the background, indicating that the presence of common structural materials containing steel does not produce a significant nuisance neutron rate.

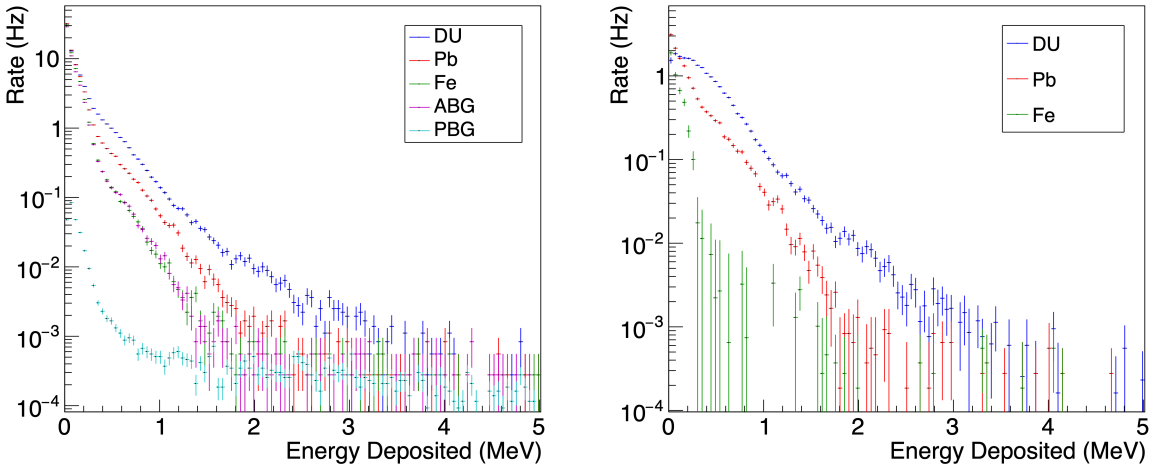

Figure 6.9: Spectra of (left) active interrogation targets and backgrounds, and (right) background-subtracted energy deposition spectra for DU, Pb, and Fe targets.

To quantify the difference in the measured spectral shape between DU and Pb, a double spectral integration technique was developed. The quantity R is defined as the ratio of the integrals of two different regions of the spectrum, bisected at the bifurcation energy E^*:

$$R(E^*) = \frac{\int_{E^*}^{\infty} S(E)dE}{\int_{E_{min}}^{E^*} S(E)dE}, \tag{6.2}$$

where $S(E)$ represents the measured spectrum, and E_{min} is the energy deposition threshold determined by the GARRn measurement, in this case 300 keV. To determine the optimum value of E^* for the purpose of discriminating between ^{238}U(γ,f) and Pb(γ,n)

neutron sources, a figure of merit (FOM) can be defined as

$$FOM_R(E^*) = \frac{R_{DU}(E^*) - R_{Pb}(E^*)}{|\sigma_{R,DU}(E^*) + \sigma_{R,Pb}(E^*)|}, \tag{6.3}$$

where σ_R is the standard deviation of the calculated value of R. The calculation of R for DU, Pb, and Fe, and its FOM for discriminating DU from Pb, is shown in Figure 6.10. This FOM has a maximum of approximately 9, which is stable in the range $1.2 < E^* < 1.7$ MeV. This wide stability is significant, as it indicates that an operational system based on PAI with a ^{4}He detector would be insensitive to possible fluctuations in the detector gain, such that it would not require frequent re-calibration.

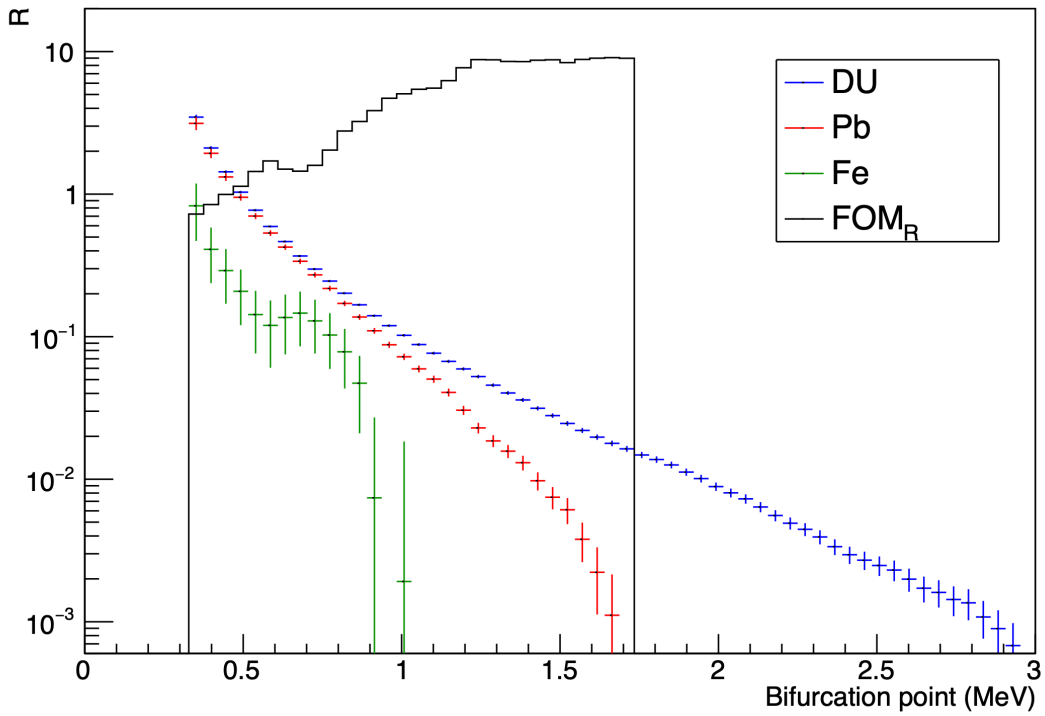

Figure 6.10: Discrimination between DU photofission spectrum and Pb (γ,n) spectrum by the double integration technique.

Using a bifurcation energy $E^* = 1.45$ MeV, which is the center of the FOM stable region, R for DU and Pb was calculated over a range of irradiation times, shown in Figure 6.11. The R values for the two targets separate within seconds, indicating that this technique has a potential for use in applications that demand high throughput, such as border crossings or safeguards inspections.

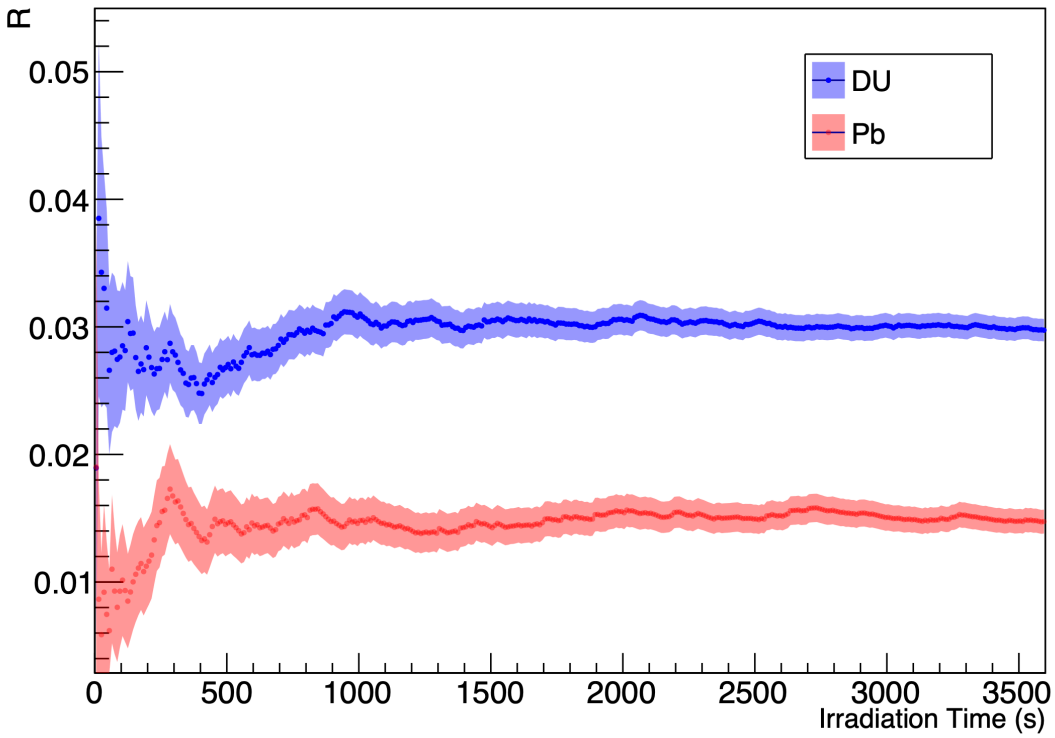

Figure 6.11: Spectral ratio R with respect to irradiation time for DU and Pb. The shaded areas represent 1-σ statistical errors.

6.4. Conclusions

In this work, we demonstrated the feasibility of a photon active interrogation system for detecting uranium photofission neutrons using a high-pressure ^{4}He scintillation detector

and a 9 MV linac. In contrast to similar techniques utilizing organic scintillation detectors, the spectral discrimination of ^{238}U(γ,f) and Pb(γ,n) neutrons was demonstrated without the need for pulse shape discrimination or algorithms for pile-up correction. The discrimination of γ rays from fast neutrons in ^{4}He detectors was shown to be effective with a simple pulse-height threshold, in comparison to the double pulse integration required in organic scintillators. Furthermore, this γ-ray discrimination capability was unaffected by the introduction of a $\sim$ 20 mR/hr γ-ray environment, which significantly degraded the performance of a common organic scintillation detector.

We evaluated a method to quantify the measured spectral signatures of DU and Pb using a spectral ratio, which was optimized for the discrimination between these two targets. The performance of this method was consistent over a broad range of bifurcation energies, indicating that discrimination capability between (γ,f) and (γ,n) spectra is unaffected by potential fluctuations in the detector gain. While the strong statistical separation between the spectral ratios for DU and lead was achieved in a matter of minutes, the irradiation time required to achieve this separation could be further reduced by either increasing the number of detectors used, which would increase the system's absolute efficiency, or by modifying the detector design to have a higher helium fill pressure, which would increase the detector's intrinsic efficiency.

In future work, the resilience of this technique should be evaluated with the introduction of various shielding materials (*e.g.*, lead, high-density polyethylene, and concrete) about the target, to examine its application range.

Chapter 7

Conclusions and Future Work

The substantial benefits of civil nuclear energy and the catastrophic risks of nuclear weapons proliferation have hung in the balance for most of the past century, with little hope for nuclear disarmament in this century. With the looming threat of climate change, it is more important than ever to accelerate the development of new nuclear reactors and fuel cycles to replace fossil fuels, while at the same time investing in new technology to maintain international nuclear safeguards and security. To this end, ^{4}He-based fast neutron scintillation detectors are an emerging technology with the potential to extend essential nondestructive assay measurements to challenging environments, where conventional techniques fail. This collection of work represents several advancements in the fundamental understanding of high-pressure ^{4}He scintillation detectors as well as the exploration of their applications in nuclear security and nonproliferation. The results in this dissertation show that ^{4}He-based fast neutron detectors have the potential to address several important nuclear safeguards needs. However, there are many other applications to be explored, and additional work remains to optimize their performance for operational deployment.

7.1. Summary of major results

The only commercially available ^{4}He-based detector, the Arktis S670, has a unique construction, with each scintillation volume read out by four channels, and each channel corresponding to a pair of SiPMs. All SiPM channels can observe any scintillation event, so a procedure was developed to collate the channel data into a single list for each scintillation volume. While significant timing jitter was observed between channels, this procedure improved the detector time resolution by 22% when compared to the analysis of individual channels. Furthermore, a two-point calibration based on the spectral endpoints in the detector response to monoenergetic neutrons was demonstrated, yielding a zero y-intercept when fit to a linear function, suggesting that helium behaves as a linear scintillation medium at high pressure.

The energy resolution of ^{4}He scintillation detectors had not yet been well-characterized over a broad range of energy depositions, which limited the ability to deconvolve source spectra. An experiment was performed to characterize the response of the Arktis S670 ^{4}He detector to nuclear recoils corresponding to fast neutrons of interest for nuclear safeguards and security. The ^{4}He detector was positioned in the center of a semicircular array of organic scintillation detectors operated in coincidence, which provided geometrically constrained nuclear recoils in conjunction with monoenergetic neutrons. The detector response provides evidence for scintillation linearity and the existence of wall effect, especially for high-energy recoils. The measured response was used to develop an energy resolution function applicable to this energy range and enables high-fidelity detector simulation for future applications.

Precise knowledge of the temporal output profile of a pulsed neutron generator has the potential to increase the sensitivity of neutron active interrogation techniques, allowing

for the simultaneous measurement of the characteristic decay time profile and gamma-ray energy spectrum of an induced isotopic species during the neutron pulse. In most neutron generators, it is not sufficient to assume that the output pulse is a simple square wave in time. The true temporal profile is often difficult to measure, as both scattered primary radiation from the generator and secondary radiation induced by the generator can significantly distort the direct, primary signal. The direct, primary temporal profile of a pulsed deuterium-tritium neutron generator was isolated from scattered and induced contaminants with a ^{4}He scintillation detector. This detector allows for fast timing and is sensitive to the neutron spectrum, so that the time profiles of high-energy depositions (corresponding to primary neutrons incident directly from the generator) and low-energy depositions (corresponding to scattered and secondary radiation in addition to primary direct radiation) can be separated. This spectro-temporal analysis has the potential to improve the sensitivity of many prompt neutron active interrogation techniques.

The thorium fuel cycle is emerging as an attractive alternative to conventional nuclear fuel cycles, as it does not require the enrichment of uranium for long-term sustainability. The operating principle of this fuel cycle is the irradiation of ^{232}Th to produce ^{233}U, which is fissile and sustains the fission chain reaction. The production of ^{233}U poses unique challenges for nuclear safeguards, as it is associated with an extreme γ ray environment from ^{232}U contamination which limits the feasibility of γ-ray-based assay, as well as more conservative accountability requirements than for ^{235}U set by the International Atomic Energy Agency. Consequently, instrumentation used for safeguarding ^{235}U in traditional fuel cycles may be inapplicable. It is essential that the nondestructive signatures of ^{233}U be characterized so that nuclear safeguards can be applied to thorium fuel cycle facilities as they come online. A set of $^{233}U_3O_8$ plates, containing 984 g ^{233}U, was measured at the National Criticality Experiments Research Center. A

high-pressure ^{4}He gaseous scintillation detector was used to perform the first passive fast neutron spectral signature measurement of $^{233}U_3O_8$. It was subsequently used in conjunction with a pulsed deuterium-tritium neutron generator to demonstrate the first differential die-away signature of $^{233}U_3O_8$. Furthermore, an array of ^{3}He detectors was used to measure the delayed neutron time profile of ^{233}U induced by a neutron generator, which is unique to this nuclide. These measurements provide a benchmark for future nondestructive assay instrumentation development and demonstrate a set of key neutron signatures to be leveraged for nuclear safeguards in the thorium fuel cycle.

The use of photon active interrogation for the detection of special nuclear material has held significant theoretical promise, as the interrogating source particles, photons, are fundamentally different from one of the main signatures of special nuclear material – neutrons produced in nuclear fission. However, neutrons produced by photonuclear reactions in the accelerator target, collimator, and environment can obscure the fission neutron signal. These (γ,n) neutrons could be discriminated from fission neutrons by their energy spectrum, but common detectors sensitive to the neutron spectrum, like organic scintillators, are typically hampered by the intense photon background characteristic of photon-based active interrogation. In contrast, high-pressure ^{4}He-based scintillation detectors are well-suited to photon active interrogation, as they are similarly sensitive to fast neutrons and can measure their spectrum, but show little response to gamma rays. A photon active interrogation system utilizing a ^{4}He scintillation detector and a 9 MeV linac-bremsstrahlung X-ray source was experimentally evaluated. The detector was shown to be capable of operating in intense gamma-ray environments and detecting photofission neutrons from ^{238}U when interrogated by this X-ray source. The photofission neutrons show clear spectral separation from (γ,n) neutrons produced in lead, a common shielding material.

7.2. Recommendations for future work

7.2.1. ^{4}He spectral unfolding

This work contains several demonstrations of recoil spectrum-based discrimination with a ^{4}He detector. Unfolding these recoil spectra to determine the incident neutron spectra could allow for improved discrimination between different neutron sources. Spectral unfolding requires a detector response matrix, comprised of the spectral response to a range of monoenergetic neutrons. The quality of the reconstructed neutron spectrum depends on the density of monoenergetic neutron spectra in the response matrix, (*i.e.*, number of monoenergetic neutron responses per unit energy). Prior efforts have been made to perform spectral unfolding with ^{4}He-based detectors [92]; however, the neutron time-of-flight method was used to obtain quasi-monoenergetic neutrons, which yields large uncertainty in the neutron energy due to the poor time resolution of this detector. Consequently, large (500 keV) bins were used, and the resulting unfolded neutron spectra were similarly very coarsely binned. To improve upon this, accelerator-based monoenergetic neutron sources, such as the ^{7}Li(p,n) reaction, could be used to achieve smaller widths of the incident neutron spectra, independent of the detector time resolution.

7.2.2. Delayed neutron & differential die-away analysis

Delayed neutron temporal signatures have been demonstrated for the discrimination of fissionable materials under active interrogation and determination of the isotopic ratio for mixed-isotope materials, while differential die-away has been shown to measure the prompt fission neutron population after a neutron generator pulse. With further development, differential die-away may be capable of fissile mass-quantitative assay in

certain scenarios. Using a pulsed neutron generator, it is possible to measure both of these signatures quasi-simultaneously, (*i.e.*, in different time windows of the same measurement), such that the delayed neutron signatures indicate the fissionable isotopic content of an item, while the differential die-away signature indicates the total fissile mass. The combination of these data would allow for a mass-quantitative neutron-based assay of each constituent fissile nuclide. This method would be of particular importance for safeguarding steps in nuclear fuel cycles where the γ-ray background is prohibitive for traditional γ-based assay, such as spent nuclear fuel and reprocessed ^{233}U fuel.

7.2.3. ^{4}He multiplicity counters

Neutron multiplicity is one of the most powerful and well-studied neutron signatures of fission, and is used frequently in international nuclear safeguards and emergency response missions to verify the presence of special nuclear materials. Traditional neutron multiplicity counters rely on an array of ^{3}He proportional counters in conjunction with a moderator to slow the fast fission neutrons to thermal energies, typically high-density polyethylene (HDPE). Much of the temporal information from the moment of fission is lost in the neutron moderation and diffusion process, such that coincidence windows in these multiplicity counters must be large, typically 50 µs or more, which can result in large accidental coincidence backgrounds. Fast neutron multiplicity counters avoid this drawback, as the neutrons can be detected directly after being emitted, with coincidence windows on the order of 100 ns. However, previous fast neutron multiplicity counter designs based on organic scintillation detectors have suffered from gamma-ray pulse pile-up and large computational overhead associated with pulse-shape discrimination.

The time resolution of ^{4}He detectors is only slightly larger than typical organic scin-

tillators and much smaller than any thermal neutron detector. Fast fission neutron correlations are usually on the order of 100 ns, so the ^{4}He resolution of 16.7 ns would not impact acceptance windows. Furthermore, ^{4}He detectors are available with and without a ^{6}Li coating, which provides sensitivity to thermal neutrons in addition to fast neutrons in the same detector. Fast and thermal neutrons can be discriminated to some extent by pulse height, so, if desired, a ^{4}He multiplicity counter with this layer could provide both fast and thermal multiplicity distributions depending on the moderation of the object being measured.

Appendix A

Monte Carlo uncertainty estimator

To estimate the uncertainty in the measured width of each measured detector response, we use a Monte Carlo routine to observe the variance for many trial distributions with the same statistics as the measured distributions. The fits to each peak corresponding to each scattering angle-neutron generator combination consist of a Gaussian superimposed on a linear background. For 10^4 trials in each angle-generator combination, the mean μ and standard deviation σ resulting from each fit were used to build a Gaussian probability density function (PDF). The integral of the peak above the background in each measured spectrum was used to determine the number of random samples N to take from this PDF per trial. In each trial, the standard deviation of the dataset consisting of N samples was used to fill a histogram. After all 10^4 trials, the standard deviation of this histogram was used as an estimate of the uncertainty in the measured Gaussian standard deviation, σ_σ. These histograms for each of the angle-generator combinations are shown in Figure A.1.

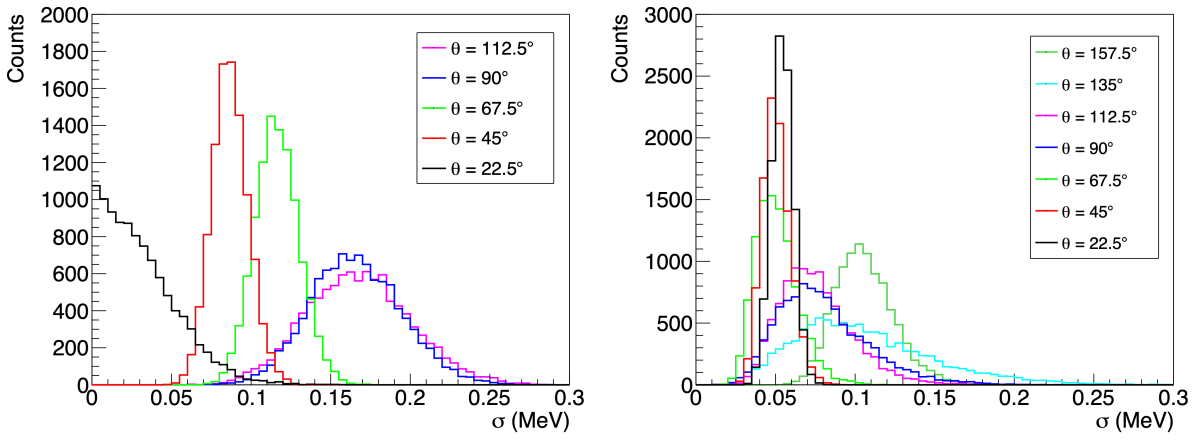

(a) **(b)**

Figure A.1: Histograms of trial spectra widths used to estimate fit parameter uncertainties for (a) D-D and (b) D-T neutrons.

Bibliography

[1] J. Chadwick, "The existence of a neutron," *Proceedings of the Royal Society of London. Series A, Containing Papers of a Mathematical and Physical Character*, vol. 136, no. 830, pp. 692–708, Jun. 1932, Publisher: Royal Society. DOI: 10.1098/rspa.1932.0112. [Online]. Available: https://royalsocietypublishing.org/doi/10.1098/rspa.1932.0112 (visited on 01/25/2024).

[2] O. Hahn and F. Strassmann, "Über den Nachweis und das Verhalten der bei der Bestrahlung des Urans mittels Neutronen entstehenden Erdalkalimetalle," de, *Naturwissenschaften*, vol. 27, no. 1, pp. 11–15, Jan. 1939, ISSN: 1432-1904. DOI: 10.1007/BF01488241. [Online]. Available: https://doi.org/10.1007/BF01488241 (visited on 01/25/2024).

[3] O. R. Frisch, "Physical Evidence for the Division of Heavy Nuclei under Neutron Bombardment," *Nature*, vol. 143, no. 3616, pp. 276–276, Feb. 1939, Number: 3616 Publisher: Nature Publishing Group, ISSN: 1476-4687. DOI: 10.1038/143276a0. [Online]. Available: https://www.nature.com/articles/143276a0 (visited on 01/25/2024).

[4] L. Meitner and O. Frisch, "Disintegration of uranium by neutrons: A new type of nuclear reaction [1]," *Nature*, vol. 143, no. 3615, pp. 239–240, 1939, ISSN: 0028-0836. DOI: 10.1038/143239a0.

[5] "Key World Energy Statistics 2021," International Energy Agency, Paris, FR, Tech. Rep. [Online]. Available: https://www.iea.org/reports/key-world-energy-statistics-2021/supply (visited on 01/29/2024).

[6] *Energy, Electricity and Nuclear Power Estimates for the Period up to 2050* (Reference Data Series 1). Vienna: INTERNATIONAL ATOMIC ENERGY AGENCY, 2018, ISBN: 978-92-0-104918-6. [Online]. Available: https://www.iaea.org/publications/13412/energy-electricity-and-nuclear-power-estimates-for-the-period-up-to-2050.

[7] H. Paillere and J. Donovan, *Nuclear Power 10 Years After Fukushima: The Long Road Back*, Text, Publisher: IAEA, Mar. 2021. [Online]. Available: https://www.iaea.org/newscenter/news/nuclear-power-10-years-after-fukushima-the-long-road-back (visited on 01/29/2024).

[8] G. Vaidyanathan and R. D. Kale, "India's nuclear power program: A critical review," *Sādhanā*, vol. 47, no. 3, p. 181, Aug. 2022, ISSN: 0973-7677. DOI: 10.1007/s12046-022-01953-9. [Online]. Available: https://doi.org/10.1007/s12046-022-01953-9 (visited on 01/29/2024).

[9] "India Nuclear Power Sector," U.S. International Trade Administration, Tech. Rep., Apr. 2023. [Online]. Available: https://www.trade.gov/market-intelligence/india-nuclear-power-sector (visited on 01/29/2024).

[10] J. Tollefson, "Is nuclear war more likely after Russia's suspension of the New START treaty?" *Nature*, vol. 615, no. 7952, pp. 386–386, Mar. 2023, ISSN: 0028-0836, 1476-4687. DOI: 10.1038/d41586-023-00679-w. [Online]. Available: https://www.nature.com/articles/d41586-023-00679-w (visited on 01/29/2024).

[11] *Treaty on the Non-Proliferation of Nuclear Weapons*, Text, Publisher: IAEA, Apr. 1970. [Online]. Available: https://www.iaea.org/publications/documents/infcircs/treaty-non-proliferation-nuclear-weapons (visited on 01/29/2024).

[12] *Additional Protocol*, Publisher: IAEA, May 1997. [Online]. Available: https://www.iaea.org/topics/additional-protocol (visited on 01/29/2024).

[13] N. Schunck and D. Regnier, "Theory of nuclear fission," *Progress in Particle and Nuclear Physics*, vol. 125, p. 103 963, Jul. 2022, ISSN: 0146-6410. DOI: 10.1016/j.ppnp.2022.103963. [Online]. Available: https://www.sciencedirect.com/science/article/pii/S0146641022000242 (visited on 01/25/2024).

[14] C. Wagemans, *The Nuclear Fission Process*. CRC Press, Sep. 1991, Google-Books-ID: ERD3yypjgD4C, ISBN: 978-0-8493-5434-2.

[15] M. Okamura, S. Ikeda, T. Kanesue, K. Takahashi, A. Cannavó, G. Ceccio, and A. Cassisa, "Demonstration of an intense lithium beam for forward-directed pulsed neutron generation," *Scientific Reports*, vol. 12, no. 1, p. 14 016, Aug. 2022, Number: 1 Publisher: Nature Publishing Group, ISSN: 2045-2322. DOI: 10.1038/s41598-022-18270-0. [Online]. Available: https://www.nature.com/articles/s41598-022-18270-0 (visited on 01/25/2024).

[16] C. L. Cowan, F. Reines, F. B. Harrison, H. W. Kruse, and A. D. McGuire, "Detection of the Free Neutrino: A Confirmation," *Science*, vol. 124, no. 3212, pp. 103–104, 1956, Publisher: American Association for the Advancement of Science, ISSN: 0036-8075. [Online]. Available: https://www.jstor.org/stable/1751492 (visited on 01/29/2024).

[17] J. W. McKlveen, "A Compilation of Fast Neutron Interactions, Cross Sections, Gamma Spectra and Gamma Decay Energies," *IEEE Transactions on Nuclear Science*, vol. 28, no. 2, pp. 1632–1634, 1981, ISSN: 0018-9499. DOI: 10.1109/TNS.1981.4331484. [Online]. Available: http://ieeexplore.ieee.org/document/4331484/ (visited on 01/29/2024).

[18] N. Cindro, "A Survey of Fast-Neutron Reactions," *Reviews of Modern Physics*, vol. 38, no. 3, pp. 391–446, Jul. 1966, ISSN: 0034-6861. DOI: 10.1103/RevModPhys.38.391. [Online]. Available: https://link.aps.org/doi/10.1103/RevModPhys.38.391 (visited on 01/29/2024).

[19] D. A. Brown, M. B. Chadwick, R. Capote, A. C. Kahler, A. Trkov, M. W. Herman, A. A. Sonzogni, Y. Danon, A. D. Carlson, M. Dunn, D. L. Smith, G. M. Hale, G. Arbanas, R. Arcilla, C. R. Bates, B. Beck, B. Becker, F. Brown, R. J. Casperson, J. Conlin, D. E. Cullen, M. Descalle, R. Firestone, T. Gaines, K. H. Guber, A. I. Hawari, J. Holmes, T. D. Johnson, T. Kawano, B. C. Kiedrowski, A. J. Koning, S. Kopecky, L. Leal, J. P. Lestone, C. Lubitz, J. I. Marquez Damian, C. M. Mattoon, E. A. McCutchan, S. Mughabghab, P. Navratil, D. Neudecker, G. P. A. Nobre, G. Noguere, M. Paris, M. T. Pigni, A. J. Plompen, B. Pritychenko, V. G. Pronyaev, D. Roubtsov, D. Rochman, P. Romano, P. Schillebeeckx, S. Simakov, M. Sin, I. Sirakov, B. Sleaford, V. Sobes, E. S. Soukhovitskii, I. Stetcu, P. Talou, I. Thompson, S. van der Marck, L. Welser-Sherrill, D. Wiarda, M. White, J. L. Wormald, R. Q. Wright, M. Zerkle, G. Zerovnik, and Y. Zhu, "ENDF/B-VIII.0: The 8th Major Release of the Nuclear Reaction Data Library with CIELO-project Cross Sections, New Standards and Thermal Scattering Data," *Nuclear Data Sheets*, Special Issue on Nuclear Reaction Data, vol. 148, pp. 1–142, Feb. 2018, ISSN: 0090-3752. DOI: 10.1016/j.nds.2018.02.001. [Online]. Available: https://www.sciencedirect.com/science/article/pii/S0090375218300206.

[20] "Conceptual Research and Development Plan for Low-Enriched Uranium Naval Fuel," National Nuclear Security Administration, Washington, DC, Report to Congress, Jul. 2016.

[21] S. Richter, R. Eykens, H. Kühn, Y. Aregbe, A. Verbruggen, and S. Weyer, "New average values for the n(238U)/n(235U) isotope ratios of natural uranium standards," *International Journal of Mass Spectrometry*, vol. 295, no. 1-2, pp. 94–97, Jul. 2010, ISSN: 13873806. DOI: 10.1016/j.ijms.2010.06.004. [Online]. Available: https://linkinghub.elsevier.com/retrieve/pii/S1387380610001879 (visited on 01/30/2024).

[22] H. D. W. Smyth, *Atomic energy for military purposes : the official report on the development of the atomic bomb under the auspices of the United States government, 1940-1945*. New Jersey: Princeton University Press, 1945, 1945. (visited on 01/31/2024).

[23] *Paducah GDP Shutdown and Deactivation*. [Online]. Available: https://www.energy.gov/pppo/paducah-gdp-shutdown-and-deactivation (visited on 01/31/2024).

[24] I. Heriot, "Uranium enrichment by gas centrifuge," Commission of the European Communities, Marlow, UK, Tech. Rep. EUR 11486, 1988.

[25] I. L. Morgan, "Helium-3 thermal neutron proportional counter," US3240971A, Mar. 1966. [Online]. Available: https://patents.google.com/patent/US3240971A/en (visited on 02/01/2024).

[26] W. R. Mills Jr., R. L. Caldwell, and I. L. Morgan, "Low Voltage He3-Filled Proportional Counter for Efficient Detection of Thermal and Epithermal Neutrons," *Review of Scientific Instruments*, vol. 33, no. 8, pp. 866–868, May 1962, ISSN: 0034-6748. DOI: 10.1063/1.1717994. [Online]. Available: https://doi.org/10.1063/1.1717994 (visited on 02/02/2024).

[27] T. Qian, P. Tonner, N. Keller, and W. Buyers, "A method for comparing degradation of boron trifluoride and helium detectors in neutron and gamma fields," *IEEE Transactions on Nuclear Science*, vol. 45, no. 3, pp. 636–642, Jun. 1998, Conference Name: IEEE Transactions on Nuclear Science, ISSN: 1558-1578. DOI: 10.1109/23.682463. [Online]. Available: https://ieeexplore.ieee.org/document/682463 (visited on 02/01/2024).

[28] R. Batchelor, R. Aves, and T. H. R. Skyrme, "Helium-3 Filled Proportional Counter for Neutron Spectroscopy," *Review of Scientific Instruments*, vol. 26, no. 11, pp. 1037–1047, Nov. 1955, ISSN: 0034-6748. DOI: 10.1063/1.1715182. [Online]. Available: https://doi.org/10.1063/1.1715182 (visited on 02/02/2024).

[29] A. Oed, "Detectors for thermal neutrons," *Nuclear Instruments and Methods in Physics Research Section A: Accelerators, Spectrometers, Detectors and Associated Equipment*, Proceedings of the International Conference on Imaging Techniques in Subatomic Physics, Astrophysics, Medicine, Biology and Industry, vol. 525, no. 1, pp. 62–68, Jun. 2004, ISSN: 0168-9002. DOI: 10.1016/j.nima.2004.03.025. [Online]. Available: https://www.sciencedirect.com/science/article/pii/S0168900204003523 (visited on 02/04/2024).

[30] I. Stefanescu, Y. Abdullahi, J. Birch, I. Defendi, R. Hall-Wilton, C. Höglund, L. Hultman, D. Seiler, and K. Zeitelhack, "Development of a novel macrostructured cathode for large-area neutron detectors based on the 10B-containing solid converter," *Nuclear Instruments and Methods in Physics Research Section A: Accelerators, Spectrometers, Detectors and Associated Equipment*, vol. 727, pp. 109–125, Nov. 2013, ISSN: 0168-9002. DOI: 10.1016/j.nima.2013.06.003. [Online]. Available: https://www.sciencedirect.com/science/article/pii/S0168900213008231 (visited on 02/01/2024).

[31] H. Yang, N. Menaa, F. Bronson, M. Kastner, R. Venkataraman, and W. F. Mueller, "Evaluation of a LiI(Eu) neutron detector with coincident double photodiode readout," *Nuclear Instruments and Methods in Physics Research Section A: Accelerators, Spectrometers, Detectors and Associated Equipment*, Symposium on Radiation Measurements and Applications (SORMA) XII 2010, vol. 652, no. 1, pp. 364–369, Oct. 2011, ISSN: 0168-9002. DOI: 10.1016/j.nima.2010.08.119. [Online]. Available: https://www.sciencedirect.com/science/article/pii/S0168900210019078 (visited on 02/01/2024).

[32] S. Arai, M. Koshimizu, Y. Fujimoto, T. Yanagida, and K. Asai, "Development of liquid scintillators based on mixed-organic solvents containing 6Li for neutron detection," *Nuclear Instruments and Methods in Physics Research Section A: Accelerators, Spectrometers, Detectors and Associated Equipment*, Symposium on Radiation Measurements and Applications XVII, vol. 954, p. 161 632, Feb. 2020, ISSN: 0168-9002. DOI: 10.1016/j.nima.2018.11.091. [Online]. Available: https://www.sciencedirect.com/science/article/pii/S0168900218317182 (visited on 02/01/2024).

[33] G. Ban, K. Bodek, T. Lefort, O. Naviliat-Cuncic, E. Pierre, C. Plonka, and G. Rogel, "UCN detection with 6Li-doped glass scintillators," *Nuclear Instruments and Methods in Physics Research Section A: Accelerators, Spectrometers, Detectors and Associated Equipment*, Particle Physics with Slow Neutrons, vol. 611, no. 2, pp. 280–283, Dec. 2009, ISSN: 0168-9002. DOI: 10.1016/j.nima.2009.07.083. [Online]. Available: https://www.sciencedirect.com/science/article/pii/S0168900209015447 (visited on 02/01/2024).

[34] M. E. Moore, J. Lousteau, P. Trtik, H. Z. Bilheux, D. Pugliese, D. Milanese, A. T. Simone, G. Brambilla, and J. P. Hayward, "Fabrication and experimental evaluation of microstructured 6Li silicate fiber arrays for high spatial resolution neutron imaging," *Nuclear Instruments and Methods in Physics Research Section A: Accelerators, Spectrometers, Detectors and Associated Equipment*, Symposium on Radiation Measurements and Applications XVII, vol. 954, p. 161 695, Feb. 2020, ISSN: 0168-9002. DOI: 10.1016/j.nima.2018.12.010. [Online]. Available: https://www.sciencedirect.com/science/article/pii/S0168900218318084 (visited on 02/01/2024).

[35] D. G. Langner, J. E. Stewart, M. M. Pickrell, M. S. Krick, N. Ensslin, and W. C. Harker, "Application Guide to Neutron Multiplicity Counting," Los Alamos National Laboratory, Los Alamos, NM, Tech. Rep. LA-13422-M, Nov. 1998. DOI: 10.2172/1679. [Online]. Available: https://www.osti.gov/biblio/1679 (visited on 02/02/2024).

[36] R. L. Bramblett, R. I. Ewing, and T. W. Bonner, "A new type of neutron spectrometer," *Nuclear Instruments and Methods*, vol. 9, no. 1, pp. 1–12, Oct. 1960,

ISSN: 0029-554X. DOI: 10.1016/0029-554X(60)90043-4. [Online]. Available: https://www.sciencedirect.com/science/article/pii/0029554X60900434 (visited on 02/02/2024).

[37] A. Sayres and M. Coppola, "3He Neutron Spectrometer Using Pulse Risetime Discrimination," *Review of Scientific Instruments*, vol. 35, no. 4, pp. 431–437, 1964, ISSN: 0034-6748. DOI: 10.1063/1.1718839. [Online]. Available: https://doi.org/10.1063/1.1718839 (visited on 02/02/2024).

[38] S. D. Howe, P. W. Lisowski, G. J. Russell, N. S. P. King, and H. J. Donnert, "Determination of the absolute efficiency of an organic scintillator for neutrons with energies between 0.5 and 800 MeV," *Nuclear Instruments and Methods in Physics Research Section A: Accelerators, Spectrometers, Detectors and Associated Equipment*, vol. 227, no. 3, pp. 565–570, Dec. 1984, ISSN: 0168-9002. DOI: 10.1016/0168-9002(84)90216-X. [Online]. Available: https://www.sciencedirect.com/science/article/pii/016890028490216X (visited on 02/02/2024).

[39] T. A. King, R. Voltz, and B. H. Flowers, "The time dependence of scintillation intensity in aromatic materials," *Proceedings of the Royal Society of London. Series A. Mathematical and Physical Sciences*, vol. 289, no. 1418, pp. 424–439, Jan. 1966, Publisher: Royal Society. DOI: 10.1098/rspa.1966.0021. [Online]. Available: https://royalsocietypublishing.org/doi/abs/10.1098/rspa.1966.0021 (visited on 02/04/2024).

[40] M. I. Pinilla-Orjuela, K. E. Mesick, P. F. Bloser, and J. R. Tutt, "Performance evaluation of pulse shape discrimination capable organic scintillators for space applications," *Nuclear Instruments and Methods in Physics Research Section A: Accelerators, Spectrometers, Detectors and Associated Equipment*, vol. 1053, p. 168 309, Aug. 2023, ISSN: 0168-9002. DOI: 10.1016/j.nima.2023.168309. [Online]. Available: https://www.sciencedirect.com/science/article/pii/S0168900223002991 (visited on 02/02/2024).

[41] C. L. Morris, J. E. Bolger, G. W. Hoffmann, C. F. Moore, L. E. Smith, and H. A. Thiessen, "A digital technique for neutron-gamma pulse shape discrimination," *Nuclear Instruments and Methods*, vol. 137, no. 2, pp. 397–398, Sep. 1976, ISSN: 0029-554X. DOI: 10.1016/0029-554X(76)90353-0. [Online]. Available: https://www.sciencedirect.com/science/article/pii/0029554X76903530 (visited on 02/27/2024).

[42] J. B. Garg, "A fast neutron time-of-flight spectrometer," *Nuclear Instruments and Methods*, vol. 6, pp. 72–82, Dec. 1959, ISSN: 0029-554X. DOI: 10.1016/0029-554X(59)90101-6. [Online]. Available: https://www.sciencedirect.com/science/article/pii/0029554X59901016 (visited on 02/04/2024).

[43] R. Böttger, H. Klein, A. Chalupka, and B. Strohmaier, "Investigation of the Spectral Fluence of Neutrons from Spontaneous Fission of 252Cf by Means of Time-of-Flight Spectrometry," *Nuclear Science and Engineering*, vol. 106, no. 3, pp. 377–398, Nov. 1990, Publisher: Taylor & Francis _eprint: https://doi.org/10.13182/NSE90-A29065, ISSN: 0029-5639. DOI: 10.13182/NSE90-A29065. [Online]. Available: https://doi.org/10.13182/NSE90-A29065 (visited on 02/02/2024).

[44] N. Colonna and G. Tagliente, "Response of liquid scintillator detectors to neutrons of En<1 MeV," *Nuclear Instruments and Methods in Physics Research Section A: Accelerators, Spectrometers, Detectors and Associated Equipment*, vol. 416, no. 1, pp. 109–114, Oct. 1998, ISSN: 0168-9002. DOI: 10.1016/S0168-9002(98)00485-9. [Online]. Available: https://www.sciencedirect.com/science/article/pii/S0168900298004859 (visited on 02/02/2024).

[45] S. D. Clarke, M. C. Hamel, A. Di fulvio, and S. A. Pozzi, "Neutron and gamma-ray energy reconstruction for characterization of special nuclear material," *Nuclear Engineering and Technology*, Special Issue on International Conference on Mathematics and Computational Methods Applied to Nuclear Science and Engineering 2017 (M&C 2017), vol. 49, no. 6, pp. 1354–1357, Sep. 2017, ISSN: 1738-5733. DOI: 10.1016/j.net.2017.06.005. [Online]. Available: https://www.sciencedirect.com/science/article/pii/S1738573317302899 (visited on 02/02/2024).

[46] S. A. Pozzi, Y. Xu, T. Zak, S. D. Clarke, M. Bourne, M. Flaska, T. J. Downar, P. Peerani, and V. Protopopescu, "Fast neutron spectrum unfolding for nuclear nonproliferation and safeguards applications," *Il Nuovo Cimento C*, no. Online First, pp. 1–99 999, Mar. 2010, ISSN: 03905551, 03905551. DOI: 10.1393/ncc/i2010-10587-y. [Online]. Available: https://doi.org/10.1393/ncc/i2010-10587-y (visited on 12/05/2023).

[47] A. Poitrasson-Rivière, M. C. Hamel, J. K. Polack, M. Flaska, S. D. Clarke, and S. A. Pozzi, "Dual-particle imaging system based on simultaneous detection of photon and neutron collision events," *Nuclear Instruments and Methods in Physics Research Section A: Accelerators, Spectrometers, Detectors and Associated Equipment*, vol. 760, pp. 40–45, Oct. 2014, ISSN: 0168-9002. DOI: 10.1016/j.nima.2014.05.056. [Online]. Available: https://www.sciencedirect.com/science/article/pii/S0168900214005889 (visited on 02/02/2024).

[48] M. C. Hamel, J. K. Polack, A. Poitrasson-Rivière, M. Flaska, S. D. Clarke, S. A. Pozzi, A. Tomanin, and P. Peerani, "Stochastic image reconstruction for a dual-particle imaging system," *Nuclear Instruments and Methods in Physics Research Section A: Accelerators, Spectrometers, Detectors and Associated Equipment*, vol. 810, pp. 120–131, Feb. 2016, ISSN: 0168-9002. DOI: 10.1016/j.nima.2015.

12.002. [Online]. Available: https://www.sciencedirect.com/science/article/pii/S016890021501551X (visited on 02/02/2024).

[49] K. Weinfurther, J. Mattingly, E. Brubaker, and J. Steele, "Model-based design evaluation of a compact, high-efficiency neutron scatter camera," *Nuclear Instruments and Methods in Physics Research Section A: Accelerators, Spectrometers, Detectors and Associated Equipment*, vol. 883, pp. 115–135, Mar. 2018, ISSN: 0168-9002. DOI: 10.1016/j.nima.2017.11.025. [Online]. Available: https://www.sciencedirect.com/science/article/pii/S0168900217312238 (visited on 02/02/2024).

[50] W. Steinberger, N. Giha, M. Hua, S. Clarke, and S. Pozzi, "Anisotropic neutron response of trans-stilbene and impact on a handheld dual particle imager," *Nuclear Instruments and Methods in Physics Research Section A: Accelerators, Spectrometers, Detectors and Associated Equipment*, vol. 1003, p. 165 266, Jul. 2021, ISSN: 0168-9002. DOI: 10.1016/j.nima.2021.165266. [Online]. Available: https://www.sciencedirect.com/science/article/pii/S0168900221002503 (visited on 02/02/2024).

[51] R. Lopez, W. M. Steinberger, N. Giha, P. Marleau, S. D. Clarke, and S. A. Pozzi, "Neutron and gamma imaging using an organic glass scintillator handheld dual particle imager," *Nuclear Instruments and Methods in Physics Research Section A: Accelerators, Spectrometers, Detectors and Associated Equipment*, vol. 1042, p. 167 407, Nov. 2022, ISSN: 0168-9002. DOI: 10.1016/j.nima.2022.167407. [Online]. Available: https://www.sciencedirect.com/science/article/pii/S0168900222007033 (visited on 02/02/2024).

[52] M. Flaska and S. A. Pozzi, "Digital pulse shape analysis for the capture-gated liquid scintillator BC-523A," *Nuclear Instruments and Methods in Physics Research Section A: Accelerators, Spectrometers, Detectors and Associated Equipment*, vol. 599, no. 2, pp. 221–225, Feb. 2009, ISSN: 0168-9002. DOI: 10.1016/j.nima.2008.10.030. [Online]. Available: https://www.sciencedirect.com/science/article/pii/S0168900208015465 (visited on 02/02/2024).

[53] T. Shi, J. Nattress, M. Mayer, M. .-. Lin, and I. Jovanovic, "Neutron spectroscopy by thermalization light yield measurement in a composite heterogeneous scintillator," *Nuclear Instruments and Methods in Physics Research Section A: Accelerators, Spectrometers, Detectors and Associated Equipment*, vol. 839, pp. 86–91, Dec. 2016, ISSN: 0168-9002. DOI: 10.1016/j.nima.2016.09.041. [Online]. Available: https://www.sciencedirect.com/science/article/pii/S0168900216309809 (visited on 02/02/2024).

[54] K. Wilhelm, J. Nattress, and I. Jovanovic, "Development and operation of a 6LiF:ZnS(Ag)—scintillating plastic capture-gated detector," *Nuclear Instruments and Methods in Physics Research Section A: Accelerators, Spectrometers, Detec-*

tors and Associated Equipment, vol. 842, pp. 54–61, Jan. 2017, ISSN: 0168-9002. DOI: 10.1016/j.nima.2016.10.042. [Online]. Available: https://www.sciencedirect.com/science/article/pii/S0168900216310865 (visited on 02/02/2024).

[55] M. Sharma, J. Nattress, K. Wilhelm, and I. Jovanovic, "Triple pulse shape discrimination and capture-gated spectroscopy in a composite heterogeneous scintillator," *Nuclear Instruments and Methods in Physics Research Section A: Accelerators, Spectrometers, Detectors and Associated Equipment*, vol. 857, pp. 75–81, Jun. 2017, ISSN: 0168-9002. DOI: 10.1016/j.nima.2017.03.019. [Online]. Available: https://www.sciencedirect.com/science/article/pii/S016890021730356X (visited on 02/02/2024).

[56] J. B. Czirr and G. L. Jensen, "A neutron coincidence spectrometer," *Nuclear Instruments and Methods in Physics Research Section A: Accelerators, Spectrometers, Detectors and Associated Equipment*, vol. 284, no. 2, pp. 365–369, Dec. 1989, ISSN: 0168-9002. DOI: 10.1016/0168-9002(89)90303-3. [Online]. Available: https://www.sciencedirect.com/science/article/pii/0168900289903033 (visited on 02/04/2024).

[57] J. B. Czirr, D. B. Merrill, D. Buehler, T. K. McKnight, J. L. Carroll, T. Abbott, and E. Wilcox, "Capture-gated neutron spectrometry," *Nuclear Instruments and Methods in Physics Research Section A: Accelerators, Spectrometers, Detectors and Associated Equipment*, Int. Workshop on Neutron Field Spectrometry in Science, Technolog y and Radiation Protection, vol. 476, no. 1, pp. 309–312, Jan. 2002, ISSN: 0168-9002. DOI: 10.1016/S0168-9002(01)01445-0. [Online]. Available: https://www.sciencedirect.com/science/article/pii/S0168900201014450 (visited on 02/04/2024).

[58] W. Tornow, W. Arnold, J. Herdtweck, and G. Mertens, "Measurement of the response of the deuterated scintillators NE 232 and NE 230 to protons and deuterons," *Nuclear Instruments and Methods in Physics Research Section A: Accelerators, Spectrometers, Detectors and Associated Equipment*, vol. 244, no. 3, pp. 477–482, Apr. 1986, ISSN: 0168-9002. DOI: 10.1016/0168-9002(86)91070-3. [Online]. Available: https://www.sciencedirect.com/science/article/pii/0168900286910703 (visited on 02/27/2024).

[59] V. Bildstein, P. E. Garrett, J. Wong, D. Bandyopadhyay, J. Bangay, L. Bianco, B. Hadinia, K. G. Leach, C. Sumithrarachchi, S. F. Ashley, B. P. Crider, M. T. McEllistrem, E. E. Peters, F. M. Prados-Estévez, S. W. Yates, and J. R. Vanhoy, "Comparison of deuterated and normal liquid scintillators for fast-neutron detection," *Nuclear Instruments and Methods in Physics Research Section A: Accelerators, Spectrometers, Detectors and Associated Equipment*, vol. 729, pp. 188–197, Nov. 2013, ISSN: 0168-9002. DOI: 10.1016/j.nima.2013.06.082. [On-

line]. Available: https://www.sciencedirect.com/science/article/pii/S0168900213009285 (visited on 02/02/2024).

[60] H. Wang, D. Carter, T. N. Massey, and A. Enqvist, "Neutron light output function and resolution investigation of the deuterated organic liquid scintillator EJ-315," *Radiation Measurements*, vol. 89, pp. 99–106, Jun. 2016, ISSN: 1350-4487. DOI: 10.1016/j.radmeas.2016.03.009. [Online]. Available: https://www.sciencedirect.com/science/article/pii/S1350448716300798 (visited on 02/02/2024).

[61] F. D. Becchetti, R. O. Torres-Isea, A. Di Fulvio, S. A. Pozzi, J. Nattress, I. Jovanovic, M. Febbraro, N. Zaitseva, and L. Carman, "Deuterated stilbene (stilbene-d12): An improved detector for fast neutrons," *Nuclear Instruments and Methods in Physics Research Section A: Accelerators, Spectrometers, Detectors and Associated Equipment*, vol. 908, pp. 376–382, Nov. 2018, ISSN: 0168-9002. DOI: 10.1016/j.nima.2018.08.021. [Online]. Available: https://www.sciencedirect.com/science/article/pii/S0168900218309653 (visited on 02/02/2024).

[62] D. L. Smith, R. G. Polk, and T. G. Miller, "Measurement of the response of several organic scintillators to electrons, protons and deuterons," *Nuclear Instruments and Methods*, vol. 64, no. 2, pp. 157–166, Sep. 1968, ISSN: 0029-554X. DOI: 10.1016/0029-554X(68)90189-4. [Online]. Available: https://www.sciencedirect.com/science/article/pii/0029554X68901894 (visited on 02/04/2024).

[63] N. Gaughan, J. Zhou, F. D. Becchetti, R. O. Torres-Isea, M. Febbraro, N. Zaitseva, Y. Altmann, and A. Di Fulvio, "Characterization of stilbene-d12 for neutron spectroscopy without time of flight," *Nuclear Instruments and Methods in Physics Research Section A: Accelerators, Spectrometers, Detectors and Associated Equipment*, vol. 1018, p. 165 822, Dec. 2021, ISSN: 0168-9002. DOI: 10.1016/j.nima.2021.165822. [Online]. Available: https://www.sciencedirect.com/science/article/pii/S016890022100807X (visited on 12/05/2023).

[64] N. Kleedtke, M. Hua, and S. Pozzi, "Genetic algorithm optimization of tin–copper graded shielding for improved plutonium safeguards measurements," *Nuclear Instruments and Methods in Physics Research Section A: Accelerators, Spectrometers, Detectors and Associated Equipment*, vol. 988, p. 164 877, Feb. 2021, ISSN: 0168-9002. DOI: 10.1016/j.nima.2020.164877. [Online]. Available: https://www.sciencedirect.com/science/article/pii/S0168900220312742 (visited on 02/03/2024).

[65] X. L. Luo, V. Modamio, J. Nyberg, J. J. Valiente-Dobón, Q. Nishada, G. de Angelis, J. Agramunt, F. J. Egea, M. N. Erduran, S. Ertürk, G. de France, A. Gadea, V. González, A. Goasduff, T. Hüyük, G. Jaworski, M. Moszyński, A. Di

Nitto, M. Palacz, P. .-. Söderström, E. Sanchis, A. Triossi, and R. Wadsworth, "Pulse pile-up identification and reconstruction for liquid scintillator based neutron detectors," *Nuclear Instruments and Methods in Physics Research Section A: Accelerators, Spectrometers, Detectors and Associated Equipment*, vol. 897, pp. 59–65, Jul. 2018, ISSN: 0168-9002. DOI: 10.1016/j.nima.2018.03.078. [Online]. Available: https://www.sciencedirect.com/science/article/pii/S0168900218304455 (visited on 12/05/2023).

[66] A. Jinia, T. Maurer, C. Meert, O. Pakari, S. Clarke, H. Kim, D. Wentzloff, and S. Pozzi, "Prompt Photofission Neutron Detection in Depleted Uranium," *Physical Review Applied*, vol. 19, no. 5, p. 054 073, May 2023, Publisher: American Physical Society. DOI: 10.1103/PhysRevApplied.19.054073. [Online]. Available: https://link.aps.org/doi/10.1103/PhysRevApplied.19.054073 (visited on 02/03/2024).

[67] D. Reilly, N. Ensslin, H. J. Smith, and S. Kreiner, "Passive nondestructive assay of nuclear materials," Nuclear Regulatory Commission, Washington, DC (United States). Office of Nuclear Regulatory Research; Los Alamos National Lab., NM (United States), Tech. Rep. NUREG/CR-5550; LA-UR-90-732, Mar. 1991. [Online]. Available: https://www.osti.gov/biblio/5428834 (visited on 12/05/2023).

[68] M. E. Anderson and J. F. Lemming, "Selected measurement data for plutonium and uranium," Tech. Rep. MLM-3009, ISPO-157, 6594300, Nov. 1982, MLM–3009, ISPO–157, 6 594 300. DOI: 10.2172/6594300. [Online]. Available: http://www.osti.gov/servlets/purl/6594300/ (visited on 01/31/2024).

[69] A. Tomanin, P. Peerani, and G. Janssens-Maenhout, "On the optimisation of the use of 3He in radiation portal monitors," *Nuclear Instruments and Methods in Physics Research Section A: Accelerators, Spectrometers, Detectors and Associated Equipment*, vol. 700, pp. 81–85, Feb. 2013, ISSN: 0168-9002. DOI: 10.1016/j.nima.2012.10.002. [Online]. Available: https://www.sciencedirect.com/science/article/pii/S0168900212011254 (visited on 02/04/2024).

[70] "Regulatory Guide: In situ assay of plutonium residual holdup. Revision 1," Nuclear Regulatory Commission, Washington, DC (USA). Office of Nuclear Regulatory Research, Tech. Rep. REG/G-5.23-Rev.1, Feb. 1984. [Online]. Available: https://www.osti.gov/biblio/5356199 (visited on 02/04/2024).

[71] A. A. Robba, E. J. Dowdy, and H. F. Atwater, "Neutron multiplication measurements using moments of the neutron counting distribution," *Nuclear Instruments and Methods in Physics Research*, vol. 215, no. 3, pp. 473–479, Oct. 1983, ISSN: 0167-5087. DOI: 10.1016/0167-5087(83)90481-7. [Online]. Available: https://www.sciencedirect.com/science/article/pii/0167508783904817 (visited on 02/03/2024).

[72] F. Ferrari and P. Peerani, "Performance of an active well coincidence counter for HEU samples," *Radiation Measurements*, vol. 45, no. 9, pp. 1034–1043, Oct. 2010, ISSN: 1350-4487. DOI: 10.1016/j.radmeas.2010.08.006. [Online]. Available: https://www.sciencedirect.com/science/article/pii/S135044871000301X (visited on 02/03/2024).

[73] D. L. Chichester, S. J. Thompson, M. T. Kinlaw, J. T. Johnson, J. L. Dolan, M. Flaska, and S. A. Pozzi, "Statistical estimation of the performance of a fast-neutron multiplicity system for nuclear material accountancy," *Nuclear Instruments and Methods in Physics Research Section A: Accelerators, Spectrometers, Detectors and Associated Equipment*, Symposium on Radiation Measurements and Applications 2014 (SORMA XV), vol. 784, pp. 448–454, Jun. 2015, ISSN: 0168-9002. DOI: 10.1016/j.nima.2014.09.027. [Online]. Available: https://www.sciencedirect.com/science/article/pii/S0168900214010286 (visited on 02/03/2024).

[74] F. B. Darby, J. D. Hutchinson, M. Y. Hua, R. A. Weldon, G. E. McKenzie, J. R. Lamproe, and S. A. Pozzi, "Comparison of NMC estimates with trans-stilbene, EJ-309, and He-3 detection systems," *Transactions of the American Nuclear Society*, vol. 125, no. 1, Dec. 2021, Institution: Los Alamos National Lab. (LANL), Los Alamos, NM (United States); Univ. of Michigan, Ann Arbor, MI (United States) Publisher: American Nuclear Society, ISSN: 0003-018X. DOI: 10.13182/T125-36636. [Online]. Available: https://www.osti.gov/biblio/1899311 (visited on 02/03/2024).

[75] T. Zak, S. D. Clarke, M. M. Bourne, S. A. Pozzi, Y. Xu, T. J. Downar, and P. Peerani, "Neutron spectroscopy of plutonium oxide using matrix unfolding approach," *Nuclear Instruments and Methods in Physics Research Section A: Accelerators, Spectrometers, Detectors and Associated Equipment*, vol. 622, no. 1, pp. 191–195, Oct. 2010, ISSN: 0168-9002. DOI: 10.1016/j.nima.2010.07.029. [Online]. Available: https://www.sciencedirect.com/science/article/pii/S0168900210016013 (visited on 02/03/2024).

[76] K. Ogren, J. Nattress, and I. Jovanovic, "Spectroscopic fast neutron transmission imaging in a treaty verification setting," *AIP Advances*, vol. 8, no. 1, p. 015 205, Jan. 2018, ISSN: 2158-3226. DOI: 10.1063/1.5004698. [Online]. Available: https://doi.org/10.1063/1.5004698 (visited on 02/03/2024).

[77] E. A. Klein, F. Naqvi, J. E. Bickus, H. Y. Lee, A. Danagoulian, and R. J. Goldston, "Neutron-Resonance Transmission Analysis with a Compact Deuterium-Tritium Neutron Generator," *Physical Review Applied*, vol. 15, no. 5, p. 054 026, May 2021, Publisher: American Physical Society. DOI: 10.1103/PhysRevApplied.15.054026. [Online]. Available: https://link.aps.org/doi/10.1103/PhysRevApplied.15.054026 (visited on 02/03/2024).

[78] D. L. Chichester and J. W. Sterbentz, "Neutron Resonance Transmission Analysis (NRTA): Initial Studies of a Method for Assaying Plutonium in Spent Fuel," Idaho National Lab. (INL), Idaho Falls, ID (United States), Tech. Rep. INL/CON-10-20684, May 2011. [Online]. Available: https://www.osti.gov/biblio/1023495 (visited on 02/03/2024).

[79] R. C. Runkle, D. L. Chichester, and S. J. Thompson, "Rattling nucleons: New developments in active interrogation of special nuclear material," *Nuclear Instruments and Methods in Physics Research Section A: Accelerators, Spectrometers, Detectors and Associated Equipment*, vol. 663, no. 1, pp. 75–95, Jan. 2012, ISSN: 0168-9002. DOI: 10.1016/j.nima.2011.09.052. [Online]. Available: https://www.sciencedirect.com/science/article/pii/S016890021101847X (visited on 12/05/2023).

[80] M. C. Hamel, J. K. Polack, M. L. Ruch, M. J. Marcath, S. D. Clarke, and S. A. Pozzi, "Active neutron and gamma-ray imaging of highly enriched uranium for treaty verification," *Scientific Reports*, vol. 7, no. 1, p. 7997, Aug. 2017, Number: 1 Publisher: Nature Publishing Group, ISSN: 2045-2322. DOI: 10.1038/s41598-017-08253-x. [Online]. Available: https://www.nature.com/articles/s41598-017-08253-x (visited on 12/05/2023).

[81] C. A. Miller, W. A. Peters, F. Y. Odeh, T. H. Shin, M. Mamtimin, S. D. Clarke, T. L. Grimm, and S. A. Pozzi, "Sub-critical assembly die-away analysis with organic scintillators," *Nuclear Instruments and Methods in Physics Research Section A: Accelerators, Spectrometers, Detectors and Associated Equipment*, vol. 959, p. 163 598, Apr. 2020, ISSN: 0168-9002. DOI: 10.1016/j.nima.2020.163598. [Online]. Available: https://www.sciencedirect.com/science/article/pii/S0168900220301649 (visited on 12/05/2023).

[82] G. R. Keepin, T. F. Wimett, and R. K. Zeigler, "Delayed Neutrons from Fissionable Isotopes of Uranium, Plutonium, and Thorium," *Physical Review*, vol. 107, no. 4, pp. 1044–1049, Aug. 1957, Publisher: American Physical Society. DOI: 10.1103/PhysRev.107.1044. [Online]. Available: https://link.aps.org/doi/10.1103/PhysRev.107.1044 (visited on 12/05/2023).

[83] J. Nattress, K. Ogren, A. Foster, A. Meddeb, Z. Ounaies, and I. Jovanovic, "Discriminating Uranium Isotopes Using the Time-Emission Profiles of Long-Lived Delayed Neutrons," *Physical Review Applied*, vol. 10, no. 2, p. 024 049, Aug. 2018, Publisher: American Physical Society. DOI: 10.1103/PhysRevApplied.10.024049. [Online]. Available: https://link.aps.org/doi/10.1103/PhysRevApplied.10.024049 (visited on 12/05/2023).

[84] K. Ogren, J. Nattress, and I. Jovanovic, "Discriminating Uranium Isotopes Based on Fission Signatures Induced by Delayed Neutrons," *Physical Review Applied*, vol. 14, no. 1, p. 014 033, Jul. 2020, Publisher: American Physical Society. DOI:

10.1103/PhysRevApplied.14.014033. [Online]. Available: https://link.aps.org/doi/10.1103/PhysRevApplied.14.014033 (visited on 12/05/2023).

[85] K. Ogren, T. Wu, J. Nattress, and I. Jovanovic, "The effects of low-Z shielding on uranium isotope discrimination using the time-emission profiles of long-lived delayed neutrons," *Nuclear Instruments and Methods in Physics Research Section A: Accelerators, Spectrometers, Detectors and Associated Equipment*, vol. 1019, p. 165 847, Dec. 2021, ISSN: 0168-9002. DOI: 10.1016/j.nima.2021.165847. [Online]. Available: https://www.sciencedirect.com/science/article/pii/S0168900221008329 (visited on 12/05/2023).

[86] H. F. Atwater, "Monte Carlo calculation of recoil spectra in He-4 proportional counters," *Nuclear Instruments and Methods*, vol. 100, no. 3, pp. 453–457, May 1972, ISSN: 0029-554X. DOI: 10.1016/0029-554X(72)90820-8. [Online]. Available: https://www.sciencedirect.com/science/article/pii/0029554X72908208 (visited on 12/05/2023).

[87] M. Manolopoulou, M. Fragopoulou, S. Stoulos, C. Koukorava, A. Spyrou, G. Perdikakis, S. R. Hashemi-Nezhad, and M. Zamani, "Studies on the response of 3He and 4He proportional counters to monoenergetic fast neutrons," *Nuclear Instruments and Methods in Physics Research Section A: Accelerators, Spectrometers, Detectors and Associated Equipment*, vol. 562, no. 1, pp. 371–379, Jun. 2006, ISSN: 0168-9002. DOI: 10.1016/j.nima.2006.02.040. [Online]. Available: https://www.sciencedirect.com/science/article/pii/S0168900206002774 (visited on 02/03/2024).

[88] S. A. Baldin, V. V. Gabrilovski, and F. E. Chukreev, "Scintillation in helium at high pressures due to alpha-particles," *Journal of Nuclear Energy (1954)*, vol. 8, no. 4, pp. 247–252, Jan. 1959, ISSN: 0891-3919. DOI: 10.1016/0891-3919(59)90011-7. [Online]. Available: https://www.sciencedirect.com/science/article/pii/0891391959900117 (visited on 12/05/2023).

[89] P. Guazzoni and M. Pignanelli, "On the performance of helium scintillation counters," *Nuclear Instruments and Methods*, vol. 72, no. 2, pp. 195–200, Jul. 1969, ISSN: 0029-554X. DOI: 10.1016/0029-554X(69)90156-6. [Online]. Available: https://www.sciencedirect.com/science/article/pii/0029554X69901566 (visited on 02/04/2024).

[90] D. Murer, R. Chandra, G. Davatz, H. Friederich, U. Gendotti, A. Howard, R. Lanza, P. Peerani, and A. Tomanin, "4He detectors for Mixed Oxide (MOX) fuel measurements," in *2011 IEEE Nuclear Science Symposium Conference Record*, ISSN: 1082-3654, Oct. 2011, pp. 4858–4864. DOI: 10.1109/NSSMIC.2011.6152485. [Online]. Available: https://ieeexplore.ieee.org/abstract/document/6152485 (visited on 02/04/2024).

[91] D. E. Murer, "He-4 fast neutron detectors in nuclear security applications," Accepted: 2017-06-13T22:25:05Z, Doctoral Thesis, ETH Zurich, 2014. DOI: 10.3929/ethz-a-010111172. [Online]. Available: https://www.research-collection.ethz.ch/handle/20.500.11850/154494 (visited on 12/05/2023).

[92] Y. Liang, T. Zhu, C. E. Parker, A. L. Richard, T. N. Massey, R. Chandra, H. Ray, K. A. Jordan, J. Baciak, and A. Enqvist, "Neutron spectroscopy and spectral unfolding with He-4 fast neutron scintillators," *Nuclear Instruments and Methods in Physics Research Section A: Accelerators, Spectrometers, Detectors and Associated Equipment*, vol. 922, pp. 1–7, Apr. 2019, ISSN: 0168-9002. DOI: 10.1016/j.nima.2018.10.098. [Online]. Available: https://www.sciencedirect.com/science/article/pii/S0168900218314128 (visited on 12/05/2023).

[93] J. M. Lewis, D. Raetz, D. Murer, and K. A. Jordan, "Analysis of In-Situ Fission Rate Measurements Using $^4{\rm He}$ Gas Scintillation Detectors," *IEEE Transactions on Nuclear Science*, vol. 61, no. 4, pp. 2217–2221, Aug. 2014, ISSN: 0018-9499, 1558-1578. DOI: 10.1109/TNS.2014.2321291. [Online]. Available: http://ieeexplore.ieee.org/document/6850091/ (visited on 01/10/2024).

[94] "S670: Fast Neutron Detector," Arktis Radiation Detectors Ltd., Zürich, Switzerland, Tech. Rep., 2022.

[95] K. T. Lim, S. Kim, M. Kim, J. Moon, G. Kim, and H. Chung, "The Feasibility of Passive Neutron Measurement for Dry Storage Safeguards Approach," *IEEE Transactions on Nuclear Science*, vol. 69, no. 6, pp. 1331–1335, Jun. 2022, Conference Name: IEEE Transactions on Nuclear Science, ISSN: 1558-1578. DOI: 10.1109/TNS.2022.3149322. [Online]. Available: https://ieeexplore.ieee.org/document/9705547 (visited on 01/10/2024).

[96] C. A. Meert, T. C. Wu, D. J. Trimas, C. A. Miller, I. Jovanovic, S. D. Clarke, and S. A. Pozzi, "Photoneutron Detection in a Pulsed High Photon Field using Helium-4 Scintillators," in *2020 IEEE Nuclear Science Symposium and Medical Imaging Conference (NSS/MIC)*, ISSN: 2577-0829, Oct. 2020, pp. 1–4. DOI: 10.1109/NSS/MIC42677.2020.9507952. [Online]. Available: https://ieeexplore.ieee.org/document/9507952 (visited on 12/05/2023).

[97] O. Searfus, K. Ogren, and I. Jovanovic, "Digital pulse analysis for fast neutron recoil spectroscopy with a 4He scintillation detector," *Nuclear Instruments and Methods in Physics Research Section A: Accelerators, Spectrometers, Detectors and Associated Equipment*, vol. 1046, p. 167 703, Jan. 2023, ISSN: 0168-9002. DOI: 10.1016/j.nima.2022.167703. [Online]. Available: https://www.sciencedirect.com/science/article/pii/S0168900222009950 (visited on 12/05/2023).

[98] G. F. Knoll, *Radiation Detection and Measurement*, 4th ed. Ann Arbor, MI: John Wiley & Sons, Aug. 2010, ISBN: 978-0-470-13148-0.

[99] R. C. Runkle, A. Bernstein, and P. E. Vanier, "Securing special nuclear material: Recent advances in neutron detection and their role in nonproliferation," *Journal of Applied Physics*, vol. 108, no. 11, p. 111 101, Dec. 2010, ISSN: 0021-8979. DOI: 10.1063/1.3503495. [Online]. Available: https://doi.org/10.1063/1.3503495 (visited on 12/05/2023).

[100] I. O. Andersson and S. Malmskog, "Investigation of the pulse-height distribution of boron trifluoride proportional counters," Aktiebolaget Atomenergi, Stockholm, Tech. Rep. AE-84, Aug. 1962. [Online]. Available: https://www.osti.gov/biblio/4779952 (visited on 12/05/2023).

[101] A. Biekert, S. A. Hertel, E. Huebler, J. Lin, H. D. Pinckney, R. K. Romani, A. Serafin, V. Velan, and D. N. McKinsey, "Nuclear recoil scintillation linearity of a high pressure He-4 gas detector," *Journal of Instrumentation*, vol. 14, no. 10, P10028, Oct. 2019, ISSN: 1748-0221. DOI: 10.1088/1748-0221/14/10/P10028. [Online]. Available: https://dx.doi.org/10.1088/1748-0221/14/10/P10028 (visited on 12/05/2023).

[102] *CoMPASS: Multiparametric DAQ Software for Physics Applications*, Viareggio, Italy, 2022.

[103] O. Searfus, P. Marleau, and I. Jovanovic, "Response of a high-pressure He-4 scintillation detector to nuclear recoils up to 9 MeV," under review, 2024.

[104] S. Woldegiorgis, A. Enqvist, and J. Baciak, "ResNet and CycleGAN for pulse shape discrimination of He-4 detector pulses: Recovering pulses conventional algorithms fail to label unanimously," *Applied Radiation and Isotopes*, vol. 176, p. 109 819, Oct. 2021, ISSN: 0969-8043. DOI: 10.1016/j.apradiso.2021.109819. [Online]. Available: https://www.sciencedirect.com/science/article/pii/S0969804321002220 (visited on 01/10/2024).

[105] O. Searfus, C. A. Meert, S. D. Clarke, S. A. Pozzi, and I. Jovanovic, "Rapid Detection of U-238 under Photon Active Interrogation with a He-4 Scintillation Detector," in *2022 IEEE Nuclear Science Symposium Conference Record*, Milan, Italy, Nov. 2022.

[106] O. Searfus, P. Marleau, E. Uribe, H. Reedy, and I. Jovanovic, "Passive and active neutron signatures of ^{233}U for nondestructive assay," *Physical Review Applied*, vol. 20, no. 6, p. 064 038, Dec. 2023, Publisher: American Physical Society. DOI: 10.1103/PhysRevApplied.20.064038. [Online]. Available: https://link.aps.org/doi/10.1103/PhysRevApplied.20.064038 (visited on 01/10/2024).

[107] R. A. Weldon, J. M. Mueller, P. Barbeau, and J. Mattingly, "Measurement of EJ-228 plastic scintillator proton light output using a coincident neutron scatter technique," *Nuclear Instruments and Methods in Physics Research Section A: Accelerators, Spectrometers, Detectors and Associated Equipment*, vol. 953, p. 163 192, Feb. 2020, ISSN: 0168-9002. DOI: 10.1016/j.nima.2019.163192. [Online]. Available: https://www.sciencedirect.com/science/article/pii/S0168900219314871 (visited on 01/15/2024).

[108] K. Oura, *Surface science : an introduction* (Advanced texts in physics, 1439-2674). Berlin ; New York: Springer, 2003, ISBN: 978-3-540-00545-2.

[109] A. Enqvist, C. C. Lawrence, B. M. Wieger, S. A. Pozzi, and T. N. Massey, "Neutron light output response and resolution functions in EJ-309 liquid scintillation detectors," *Nuclear Instruments and Methods in Physics Research Section A: Accelerators, Spectrometers, Detectors and Associated Equipment*, vol. 715, pp. 79–86, Jul. 2013, ISSN: 0168-9002. DOI: 10.1016/j.nima.2013.03.032. [Online]. Available: https://www.sciencedirect.com/science/article/pii/S0168900213003203 (visited on 01/19/2024).

[110] D. Pelowitz, "MCNPX User's Manual: Version 2.7.0," Los Alamos National Laboratory, Tech. Rep. LA-CP-11-00438, 2011.

[111] S. A. Pozzi, S. D. Clarke, W. J. Walsh, E. C. Miller, J. L. Dolan, M. Flaska, B. M. Wieger, A. Enqvist, E. Padovani, J. K. Mattingly, D. L. Chichester, and P. Peerani, "MCNPX-PoliMi for nuclear nonproliferation applications," *Nuclear Instruments and Methods in Physics Research Section A: Accelerators, Spectrometers, Detectors and Associated Equipment*, vol. 694, pp. 119–125, Dec. 2012, ISSN: 0168-9002. DOI: 10.1016/j.nima.2012.07.040. [Online]. Available: https://www.sciencedirect.com/science/article/pii/S0168900212008224 (visited on 12/05/2023).

[112] M. Berger, J. Coursey, M. Zucker, and J. Chang, *Stopping-Powers and Range Tables for Electrons, Protons, and Helium Ions, NIST Standard Reference Database 124*, 1993. DOI: 10.18434/T4NC7P. [Online]. Available: http://www.nist.gov/pml/data/star/index.cfm (visited on 01/26/2024).

[113] R. Brun and F. Rademakers, "ROOT — An object oriented data analysis framework," *Nuclear Instruments and Methods in Physics Research Section A: Accelerators, Spectrometers, Detectors and Associated Equipment*, New Computing Techniques in Physics Research V, vol. 389, no. 1, pp. 81–86, Apr. 1997, ISSN: 0168-9002. DOI: 10.1016/S0168-9002(97)00048-X. [Online]. Available: https://www.sciencedirect.com/science/article/pii/S016890029700048X (visited on 01/25/2024).

[114] J. H. Friedman, "Data Analysis Techniques for High Energy Particle Physics," Stanford Linear Accelerator Center, Stanford, CA, Tech. Rep., Sep. 1974.

[115] H. Schölermann and H. Klein, "Optimizing the energy resolution of scintillation counters at high energies," *Nuclear Instruments and Methods*, vol. 169, no. 1, pp. 25–31, Feb. 1980, ISSN: 0029-554X. DOI: 10.1016/0029-554X(80)90097-X. [Online]. Available: https://www.sciencedirect.com/science/article/pii/0029554X8090097X (visited on 01/27/2024).

[116] F. M. Penning, "Ein neues manometer für niedrige gasdrucke, insbesondere zwischen l0−3 und 10−5 mm," *Physica*, vol. 4, no. 2, pp. 71–75, Feb. 1937, ISSN: 0031-8914. DOI: 10.1016/S0031-8914(37)80123-8. [Online]. Available: https://www.sciencedirect.com/science/article/pii/S0031891437801238 (visited on 02/15/2024).

[117] J. H. Vainionpaa, C. K. Gary, J. L. Harris, M. A. Piestrup, R. H. Pantell, and G. Jones, "Technology and Applications of Neutron Generators Developed by Adelphi Technology, Inc," *Physics Procedia*, 3rd International Meeting of the Union for Compact Accelerator-driven Neutron Sources, UCANS III, 31 July–3 August 2012, Bilbao, Spain & the 4th International Meeting of the Union for Compact Accelerator-driven Neutron Sources, UCANS IV, 23-27 September 2013, Sapporo, Hokkaido, Japan, vol. 60, pp. 203–211, Jan. 2014, ISSN: 1875-3892. DOI: 10.1016/j.phpro.2014.11.029. [Online]. Available: https://www.sciencedirect.com/science/article/pii/S1875389214005768 (visited on 02/14/2024).

[118] M. Tanaka, S. Hara, T. Hae, T. Iga, K. Saitou, K. Amemiya, K. Hiramoto, and S. Kakiuchi, "Development of a high-current microwave ion source for proton linac application systems," *Review of Scientific Instruments*, vol. 75, no. 5, pp. 1894–1896, May 2004, ISSN: 0034-6748. DOI: 10.1063/1.1702106. [Online]. Available: https://doi.org/10.1063/1.1702106 (visited on 02/15/2024).

[119] R. Batchelor, W. B. Gilboy, J. B. Parker, and J. H. Towle, "The response of organic scintillators to fast neutrons," *Nuclear Instruments and Methods*, vol. 13, pp. 70–82, Aug. 1961, ISSN: 0029-554X. DOI: 10.1016/0029-554X(61)90171-9. [Online]. Available: https://www.sciencedirect.com/science/article/pii/0029554X61901719 (visited on 02/16/2024).

[120] O. Schwerer, M. Winkler-Rohatsch, H. Warhanek, and G. Winkler, "Measurement of cross sections for 14 MeV neutron capture," *Nuclear Physics A*, vol. 264, no. 1, pp. 105–114, Jun. 1976, ISSN: 0375-9474. DOI: 10.1016/0375-9474(76)90147-0. [Online]. Available: https://www.sciencedirect.com/science/article/pii/0375947476901470 (visited on 02/16/2024).

[121] K. Ogren, A. Kavner, S. Dazeley, and I. Jovanovic, "Development of 17N as a time-tagged neutron source for calibration of large antineutrino detectors," *Nuclear Instruments and Methods in Physics Research Section A: Accelerators, Spectrometers, Detectors and Associated Equipment*, vol. 1033, p. 166 654, Jun. 2022,

ISSN: 0168-9002. DOI: 10.1016/j.nima.2022.166654. [Online]. Available: https://www.sciencedirect.com/science/article/pii/S0168900222002133 (visited on 02/15/2024).

[122] E. Fermi, "Radioactivity Induced by Neutron Bombardment," en, *Nature*, vol. 133, no. 3368, pp. 757–757, May 1934, Number: 3368 Publisher: Nature Publishing Group, ISSN: 1476-4687. DOI: 10.1038/133757a0. [Online]. Available: https://www.nature.com/articles/133757a0 (visited on 02/16/2024).

[123] J. V. P. Long, "The estimation of tantalum in mixtures by neutron activation analysis," en, *The Analyst*, vol. 76, no. 908, p. 644, 1951, ISSN: 0003-2654, 1364-5528. DOI: 10.1039/an9517600644. [Online]. Available: http://xlink.rsc.org/?DOI=an9517600644 (visited on 02/16/2024).

[124] F. E. Senftle and A. F. Hoyte, "Mineral exploration and soil analysis using in situ neutron activation," *Nuclear Instruments and Methods*, vol. 42, no. 1, pp. 93–103, Jun. 1966, ISSN: 0029-554X. DOI: 10.1016/0029-554X(66)90275-8. [Online]. Available: https://www.sciencedirect.com/science/article/pii/0029554X66902758 (visited on 02/16/2024).

[125] A. A. Gordus, "Quantitative Non-Destructive Neutron Activation Analysis of Silver in Coins," en, *Archaeometry*, vol. 10, no. 1, pp. 78–86, 1967, _eprint: https://onlinelibrary.wiley.com/doi/pdf/10.1111/j.1475-4754.1967.tb00617.x, ISSN: 1475-4754. DOI: 10.1111/j.1475-4754.1967.tb00617.x. [Online]. Available: https://onlinelibrary.wiley.com/doi/abs/10.1111/j.1475-4754.1967.tb00617.x (visited on 02/16/2024).

[126] H.-G. Stosch, "Neutron Activation Analysis of the Rare Earth Elements (REE) – With Emphasis on Geological Materials," en, *Physical Sciences Reviews*, vol. 1, no. 8, Aug. 2016, Publisher: De Gruyter, ISSN: 2365-659X. DOI: 10.1515/psr-2016-0062. [Online]. Available: https://www.degruyter.com/document/doi/10.1515/psr-2016-0062/html (visited on 02/17/2024).

[127] Y. Eden, "Neutron activation analysis by combined capture and decay gamma-spectrum method," *Journal of Radioanalytical Chemistry*, vol. 6, no. 1, pp. 165–175, Sep. 1970, ISSN: 1588-2780. DOI: 10.1007/BF02513908. [Online]. Available: https://doi.org/10.1007/BF02513908.

[128] T. Gozani, "Novel applications of fast neutron interrogation methods," *Nuclear Instruments and Methods in Physics Research Section A: Accelerators, Spectrometers, Detectors and Associated Equipment*, vol. 353, no. 1, pp. 635–640, Dec. 1994, ISSN: 0168-9002. DOI: 10.1016/0168-9002(94)91740-X. [Online]. Available: https://www.sciencedirect.com/science/article/pii/016890029491740X (visited on 02/19/2024).

[129] L. A. Shope, R. S. Berg, M. L. O'Neal, and B. E. Barnaby, "Operation and Life of the Zetatron: A Small Neutron Generator for Borehole Logging," *IEEE Transactions on Nuclear Science*, vol. 28, no. 2, pp. 1696–1699, Apr. 1981, Conference Name: IEEE Transactions on Nuclear Science, ISSN: 1558-1578. DOI: 10.1109/TNS.1981.4331501. [Online]. Available: https://ieeexplore.ieee.org/document/4331501 (visited on 02/17/2024).

[130] R. S. Berg and E. L. Jacobs, "Factors Affecting the Operating Characteristic of the Zetatron: A Small Neutron Generator for Borehole Logging," *IEEE Transactions on Nuclear Science*, vol. 30, no. 2, pp. 1459–1462, Apr. 1983, Conference Name: IEEE Transactions on Nuclear Science, ISSN: 1558-1578. DOI: 10.1109/TNS.1983.4332560. [Online]. Available: https://ieeexplore.ieee.org/document/4332560 (visited on 02/17/2024).

[131] *Thermo Scientific P 211 Neutron Generator*, 2008. [Online]. Available: https://www.thermofisher.com/document-connect/document-connect.html?url=https://assets.thermofisher.com/TFS-Assets%2FCAD%2FSpecification-Sheets%2FD10500~.pdf.

[132] "Safeguards Techniques and Equipment:" International Atomic Energy Agency, Text, 2011, ISBN: 9789201189103 Publication Title: Safeguards Techniques and Equipment: pp. 1–146. [Online]. Available: https://www.iaea.org/publications/8695/safeguards-techniques-and-equipment (visited on 12/05/2023).

[133] L. G. Worrall, A. Worrall, G. F. Flanagan, S. Croft, A. M. Krichinsky, C. A. Pickett, R. D. McElroy, S. L. Cleveland, D. N. Kovacic, J. M. Whitaker, and J. L. White-Horton, "Safeguards Considerations for Thorium Fuel Cycles," *Nuclear Technology*, vol. 194, no. 2, pp. 281–293, May 2016, Publisher: Taylor & Francis _eprint: https://doi.org/10.13182/NT15-103, ISSN: 0029-5450. DOI: 10.13182/NT15-103. [Online]. Available: https://doi.org/10.13182/NT15-103 (visited on 12/05/2023).

[134] L. G. Worrall, V. Henzl, A. Swift, N. Luciano, E. Cervi, J. Cooley, B. Davies, J. S. Denton, A. Favalli, B. Grogan, A. Krichinsky, K. Hogue, M. L. Lockhart, D. J. Mercer, A. Milojevich, J. Stinnett, R. Reed, and A. Worrall, "Safeguards Technology for Thorium Fuel Cycles: Research and Development Needs Assessment and Recommendations," Oak Ridge National Laboratory (ORNL), Oak Ridge, TN (United States), Tech. Rep. ORNL/TM-2020/1866, May 2021. DOI: 10.2172/1818724. [Online]. Available: https://www.osti.gov/biblio/1818724 (visited on 12/05/2023).

[135] "IAEA Safeguards Glossary," International Atomic Energy Agency, Text, 2022, ISBN: 9789201221223 Publication Title: IAEA Safeguards Glossary, pp. 1–300.

[Online]. Available: https://www.iaea.org/publications/15176/iaea-safeguards-glossary (visited on 12/05/2023).

[136] U. E. Humphrey and M. U. Khandaker, "Viability of thorium-based nuclear fuel cycle for the next generation nuclear reactor: Issues and prospects," *Renewable and Sustainable Energy Reviews*, vol. 97, pp. 259–275, Dec. 2018, ISSN: 1364-0321. DOI: 10.1016/j.rser.2018.08.019. [Online]. Available: https://www.sciencedirect.com/science/article/pii/S1364032118305951 (visited on 12/05/2023).

[137] R. J. Gehrke, V. J. Novick, and J. D. Baker, "Γ-ray emission probabilities for the U-232 decay chain," *The International Journal of Applied Radiation and Isotopes*, vol. 35, no. 7, pp. 581–589, Jul. 1984, ISSN: 0020-708X. DOI: 10.1016/0020-708X(84)90100-5. [Online]. Available: https://www.sciencedirect.com/science/article/pii/0020708X84901005 (visited on 12/05/2023).

[138] J. E. Turner, *Atoms, Radiation, and Radiation Protection*. John Wiley & Sons, Jan. 2008, ISBN: 978-3-527-61698-5.

[139] G. N. Vlaskin and Y. S. Khomyakov, "(, n) Neutron Spectra on Thick Light Targets," *Atomic Energy*, vol. 130, no. 2, pp. 104–118, Jun. 2021, ISSN: 1573-8205. DOI: 10.1007/s10512-021-00781-0. [Online]. Available: https://doi.org/10.1007/s10512-021-00781-0.

[140] T. Murata, H. Matsunobu, and K. Shibata, "Evaluation of the (, xn) reaction data for JENDL/AN-2005," Japan, Tech. Rep., 2006, JAEA-Research–2006-052 INIS Reference Number: 38021268, p. 77.

[141] D. L. Chichester and E. H. Seabury, "Using electronic neutron generators in active interrogation to detect shielded fissionable material," in *2008 IEEE Nuclear Science Symposium Conference Record*, ISSN: 1082-3654, Oct. 2008, pp. 3361–3367. DOI: 10.1109/NSSMIC.2008.4775063. [Online]. Available: https://ieeexplore.ieee.org/document/4775063 (visited on 12/05/2023).

[142] R. B. Roberts, L. R. Hafstad, R. C. Meyer, and P. Wang, "The Delayed Neutron Emission which Accompanies Fission of Uranium and Thorium," *Physical Review*, vol. 55, no. 7, pp. 664–664, Apr. 1939, Publisher: American Physical Society. DOI: 10.1103/PhysRev.55.664. [Online]. Available: https://link.aps.org/doi/10.1103/PhysRev.55.664 (visited on 12/05/2023).

[143] R. B. Roberts, R. C. Meyer, and P. Wang, "Further Observations on the Splitting of Uranium and Thorium," *Physical Review*, vol. 55, no. 5, pp. 510–511, Mar. 1939, Publisher: American Physical Society. DOI: 10.1103/PhysRev.55.510.2. [Online]. Available: https://link.aps.org/doi/10.1103/PhysRev.55.510.2 (visited on 12/05/2023).

[144] D. J. Hughes, J. Dabbs, A. Cahn, and D. Hall, "Delayed Neutrons from Fission of U-235," *Physical Review*, vol. 73, no. 2, pp. 111–124, Jan. 1948, Publisher: American Physical Society. DOI: 10.1103/PhysRev.73.111. [Online]. Available: https://link.aps.org/doi/10.1103/PhysRev.73.111 (visited on 12/05/2023).

[145] P. Dimitriou, I. Dillmann, B. Singh, V. Piksaikin, K. P. Rykaczewski, J. L. Tain, A. Algora, K. Banerjee, I. N. Borzov, D. Cano-Ott, S. Chiba, M. Fallot, D. Foligno, R. Grzywacz, X. Huang, T. Marketin, F. Minato, G. Mukherjee, B. C. Rasco, A. Sonzogni, M. Verpelli, A. Egorov, M. Estienne, L. Giot, D. Gremyachkin, M. Madurga, E. A. McCutchan, E. Mendoza, K. V. Mitrofanov, M. Narbonne, P. Romojaro, A. Sanchez-Caballero, and N. D. Scielzo, "Development of a Reference Database for Beta-Delayed Neutron Emission," *Nuclear Data Sheets*, Special Issue on Nuclear Reaction Data, vol. 173, pp. 144–238, Mar. 2021, ISSN: 0090-3752. DOI: 10.1016/j.nds.2021.04.006. [Online]. Available: https://www.sciencedirect.com/science/article/pii/S0090375221000168 (visited on 12/05/2023).

[146] L. V. East, R. H. Augustson, H. O. Menlove, and C. F. Masters, "Delayed-neutron abundances and half-lives from 14.7-MeV fission," *Trans. Amer. Nucl. Soc. 13: 760-1(Nov 1970).*, Jan. 1970. [Online]. Available: https://www.osti.gov/biblio/4095358 (visited on 12/05/2023).

[147] R. Nicol, J. Parrott, A. Krichinsky, W. Box, C. Martin, and W. Whitson, "Fabrication of Zero Power Reactor Fuel Elements Containing U-233," Oak Ridge National Laboratory, Tech. Rep., 1982.

[148] C. E. Moss, M. A. Nelson, R. B. Rothrock, and E. B. Sorensen, "MC-15 Users Manual," Los Alamos National Lab. (LANL), Los Alamos, NM (United States), Tech. Rep. LA-UR-18-29563, Oct. 2018. DOI: 10.2172/1477606. [Online]. Available: https://www.osti.gov/biblio/1477606 (visited on 12/05/2023).

[149] R. Glass, "AT-400R Affirmation Summary," Sandia National Laboratories, Tech. Rep. SAND98-1231/1, 1996.

[150] K. Schwinkendorf, "Criticality Safety Index Determination for ORNL U-233 ZPR Fuels in AT-400R Containers," National Security Technologies LLC, Tech. Rep. NCSE-CSID-2011-001, 2011.

[151] V. M. Piksaikin, V. A. Roshchenko, and G. G. Korolev, "Relative yield of delayed neutrons and half-life of their precursor nuclei from U-238 fission by 14.2–17.9 MeV neutrons," *Atomic Energy*, vol. 102, no. 2, pp. 151–159, Feb. 2007, ISSN: 1573-8205. DOI: 10.1007/s10512-007-0023-1. [Online]. Available: https://doi.org/10.1007/s10512-007-0023-1 (visited on 12/05/2023).

[152] V. A. Roshchenko, V. M. Piksaikin, L. E. Kazakov, and G. G. Korolev, "Relative yield of delayed neutrons and half-life of their precursor nuclei with fissioning of Pu-239 by 14.2–17.9 MeV neutrons," *Atomic Energy*, vol. 101, no. 6, pp. 897–900, Dec. 2006, ISSN: 1573-8205. DOI: 10.1007/s10512-006-0188-z. [Online]. Available: https://doi.org/10.1007/s10512-006-0188-z (visited on 12/05/2023).

[153] V. A. Roshchenko, V. M. Piksaikin, G. G. Korolev, and A. S. Egorov, "Time features of delayed neutrons and partial emissive-fission cross sections for the neutron-induced fission of Th-232 nuclei in the energy range 3.2–17.9 MeV," *Physics of Atomic Nuclei*, vol. 73, no. 6, pp. 913–921, Jun. 2010, ISSN: 1562-692X. DOI: 10.1134/S1063778810060013. [Online]. Available: https://doi.org/10.1134/S1063778810060013 (visited on 12/05/2023).

[154] O. Searfus, C. A. Meert, S. Clarke, S. Pozzi, and I. Jovanovic, "Detection of uranium photofission neutrons with a He-4 scintillation detector," under review, 2024.

[155] B. J. Micklich, D. L. Smith, T. N. Massey, C. L. Fink, and D. Ingram, "FIGARO: Detecting nuclear materials using high-energy gamma-rays," *Nuclear Instruments and Methods in Physics Research Section A: Accelerators, Spectrometers, Detectors and Associated Equipment*, Proceedings of the tenth Symposium on Radiation Measurements and Applications, vol. 505, no. 1, pp. 466–469, Jun. 2003, ISSN: 0168-9002. DOI: 10.1016/S0168-9002(03)01122-7. [Online]. Available: https://www.sciencedirect.com/science/article/pii/S0168900203011227 (visited on 02/05/2024).

[156] T. Gozani, "Fission Signatures for Nuclear Material Detection," *IEEE Transactions on Nuclear Science*, vol. 56, no. 3, pp. 736–741, Jun. 2009, Conference Name: IEEE Transactions on Nuclear Science, ISSN: 1558-1578. DOI: 10.1109/TNS.2009.2015309. [Online]. Available: https://ieeexplore.ieee.org/document/5076103 (visited on 02/05/2024).

[157] B. Boyer, "Chapter 9 - International Safeguards Inspections," in *Nuclear Safeguards, Security, and Nonproliferation (Second Edition)*, J. E. Doyle, Ed., Boston: Butterworth-Heinemann, Jan. 2019, pp. 255–292, ISBN: 978-0-12-803271-8. DOI: 10.1016/B978-0-12-803271-8.00009-6. [Online]. Available: https://www.sciencedirect.com/science/article/pii/B9780128032718000096 (visited on 02/05/2024).

[158] R. Berndt, E. Franke, and P. Mortreau, "235U enrichment or UF6 mass determination on UF6 cylinders with non-destructive analysis methods," *Nuclear Instruments and Methods in Physics Research Section A: Accelerators, Spectrometers, Detectors and Associated Equipment*, vol. 612, no. 2, pp. 309–319, Jan. 2010, ISSN: 0168-9002. DOI: 10.1016/j.nima.2009.10.060. [Online]. Available: https:

//www.sciencedirect.com/science/article/pii/S0168900209019846 (visited on 02/07/2024).

[159] R. T. Kouzes, E. R. Siciliano, J. H. Ely, P. E. Keller, and R. J. McConn, "Passive neutron detection for interdiction of nuclear material at borders," *Nuclear Instruments and Methods in Physics Research Section A: Accelerators, Spectrometers, Detectors and Associated Equipment*, vol. 584, no. 2, pp. 383–400, Jan. 2008, ISSN: 0168-9002. DOI: 10.1016/j.nima.2007.10.026. [Online]. Available: https://www.sciencedirect.com/science/article/pii/S0168900207022085 (visited on 02/07/2024).

[160] E. Lepowsky, J. Jeon, and A. Glaser, "Confirming the absence of nuclear warheads via passive gamma-ray measurements," *Nuclear Instruments and Methods in Physics Research Section A: Accelerators, Spectrometers, Detectors and Associated Equipment*, vol. 990, p. 164 983, Feb. 2021, ISSN: 0168-9002. DOI: 10.1016/j.nima.2020.164983. [Online]. Available: https://www.sciencedirect.com/science/article/pii/S0168900220313802 (visited on 02/07/2024).

[161] S. Kluter, "Technical design and concept of a 0.35 T MR-Linac," *Clinical and Translational Radiation Oncology*, vol. 18, pp. 98–101, Sep. 2019, ISSN: 2405-6308. DOI: 10.1016/j.ctro.2019.04.007. [Online]. Available: https://www.sciencedirect.com/science/article/pii/S2405630819300692 (visited on 02/07/2024).

[162] S. Boucher, P. Frigola, A. Murokh, M. Ruelas, I. Jovanovic, J. B. Rosenzweig, and G. Travish, "Inverse compton scattering gamma ray source," *Nuclear Instruments and Methods in Physics Research Section A: Accelerators, Spectrometers, Detectors and Associated Equipment*, Compton sources for X/ rays: Physics and applications, vol. 608, no. 1, Supplement, S54–S56, Sep. 2009, ISSN: 0168-9002. DOI: 10.1016/j.nima.2009.05.035. [Online]. Available: https://www.sciencedirect.com/science/article/pii/S0168900209009681 (visited on 02/09/2024).

[163] C. A. Meert, A. T. MacDonald, A. J. Jinia, W. M. Steinberger, S. D. Clarke, and S. A. Pozzi, "Photoneutron Detection in Active Interrogation Scenarios Using Small Organic Scintillators," *IEEE Transactions on Nuclear Science*, vol. 69, no. 6, pp. 1397–1402, Jun. 2022, Conference Name: IEEE Transactions on Nuclear Science, ISSN: 1558-1578. DOI: 10.1109/TNS.2022.3164601. [Online]. Available: https://ieeexplore.ieee.org/document/9772086 (visited on 02/08/2024).

[164] A. J. Jinia, T. E. Maurer, C. A. Meert, M. Y. Hua, S. D. Clarke, H.-S. Kim, D. D. Wentzloff, and S. A. Pozzi, "An Artificial Neural Network System for Photon-Based Active Interrogation Applications," *IEEE Access*, vol. 9, pp. 119 871–119 880, 2021, Conference Name: IEEE Access, ISSN: 2169-3536. DOI: 10.1109/

ACCESS.2021.3108406. [Online]. Available: https://ieeexplore.ieee.org/document/9524625 (visited on 02/08/2024).

[165] A. Zilges, D. L. Balabanski, J. Isaak, and N. Pietralla, "Photonuclear reactions—From basic research to applications," *Progress in Particle and Nuclear Physics*, vol. 122, p. 103 903, Jan. 2022, ISSN: 0146-6410. DOI: 10.1016/j.ppnp.2021.103903. [Online]. Available: https://www.sciencedirect.com/science/article/pii/S0146641021000624 (visited on 02/05/2024).

[166] R. T. Kouzes, J. H. Ely, A. T. Lintereur, E. K. Mace, D. L. Stephens, and M. L. Woodring, "Neutron detection gamma ray sensitivity criteria," *Nuclear Instruments and Methods in Physics Research Section A: Accelerators, Spectrometers, Detectors and Associated Equipment*, vol. 654, no. 1, pp. 412–416, Oct. 2011, ISSN: 0168-9002. DOI: 10.1016/j.nima.2011.07.030. [Online]. Available: https://www.sciencedirect.com/science/article/pii/S0168900211014628 (visited on 02/05/2024).

[167] Varex Imaging, *High energy linear accelerators*, 2023. [Online]. Available: https://www.vareximaging.com/products/security-industrial/linear-accelerators/linatron-m/linatron-m9.

[168] C. A. Miller, C. A. Meert, S. D. Clarke, and S. A. Pozzi, "Mitigation of photon active interrogation background for fast neutron detection," *AIP Conference Proceedings*, vol. 2160, no. 1, p. 050 015, Oct. 2019, ISSN: 0094-243X. DOI: 10.1063/1.5127707. [Online]. Available: https://doi.org/10.1063/1.5127707 (visited on 02/05/2024).

[169] T. W. Burrows, *Q-value calculator (qcalc)*, 2023. [Online]. Available: https://www.nndc.bnl.gov/qcalc/.